VALORIZATION OF RICE-HUSK FOR OPTIMAL PRODUCTION OF BIO-OIL, BIO-CHAR, AND SILICA NANOPARTICLES

A thesis submitted
in partial fulfillment of the requirements
for the degree of

Doctor of Philosophy

by

Sutapa Das

Roll No. 166107009

Department of Chemical Engineering

Indian Institute of Technology Guwahati

Guwahati–781039

Assam, India

November 2022

भारतीय प्रौद्योगिकी संस्थान गुवाहाटी • Indian Institute of Technology Guwahati •

DEDICATED

TO

MY PARENTS

भारतीय प्रौद्योगिकी संस्थान गुवाहाटी • Indian Institute of Technology Guwahati •

भारतीय प्रौद्योगिकी संस्थान गुवाहाटी
Indian Institute of Technology Guwahati

STATEMENT

I do hereby declare that the content embodied in this thesis entitled **“VALORIZATION OF RICE-HUSK FOR OPTIMAL PRODUCTION OF BIO-OIL, BIO-CHAR, AND SILICA NANOPARTICLES”** is the result of investigations carried out by me at Department of Chemical Engineering, Indian Institute of Technology Guwahati, Guwahati, India, under the guidance of Prof. Vaibhav V. Goud. In keeping with the general practice of reporting scientific observations, due acknowledgements have been made wherever the work described is based on the findings of other investigators.

Sutapa Das

Date : 07/11/2022

Sutapa Das

Indian Institute of Technology Guwahati

CERTIFICATE

This is to certify that the thesis entitled **"VALORIZATION OF RICE-HUSK FOR OPTIMAL PRODUCTION OF BIO-OIL, BIO-CHAR, AND SILICA NANOPARTICLES"** submitted by **Mrs. Sutapa Das (Roll No.: 166107009)**, a research scholar in the Department of Chemical Engineering, Indian Institute of Technology Guwahati, for the award of the degree of Doctor of Philosophy, is a record of the original research work carried out by her under my supervision and guidance. The thesis has fulfilled all requirements as per the regulations of the institute and in my opinion has reached the standard needed for submission. The work documented in this thesis have not been submitted to any other University or Institute for the award of any degree.

7.11.22

Prof. Vaibhav V. Goud

Professor

Department of Chemical Engineering

Indian Institute of Technology Guwahati

Guwahati - 781039, Assam, India.

Acknowledgements

The entire duration of this doctoral program has been full of memorable and enriching experiences for me. Not only have I been fortunate enough to understand my limitations and improve upon them on a professional front but I have also learned valuable lessons that have made me a better person. As I near the tenure of my PhD study, I would like to express my earnest and heartfelt gratitude to the people who have supported me throughout the journey. First and foremost, I would like to thank my thesis supervisor Prof. Vaibhav V. Goud for his patience, wisdom and guidance which aided me to endure and resolve challenges that I encountered during my PhD tenure. I sincerely thank him for allowing me the latitude to explore scientific pursuits and provide a guiding light throughout this study. I am grateful to the members of my doctoral committee, Prof. Mahuya De, Prof. Ajay Kalamdhad and Prof. Animes Kumar Golder, for accepting to evaluate my thesis and provide insightful comments.

During my PhD study, I had the wonderful experience of learning from my lab seniors Dr. Venu Babu Borugadda, Dr. Garima Srivastava, Dr. Robinson Timung, Dr. Dipshikha Kalita (Institute Post-Doctoral Fellow), Dr. Dipesh Kumar (Research Associate) and Mr. Chitta Ranjan Barik who not only assisted me in developing technical knowledge but also provided constant encouragement. I would also like to particularly thank Dr. Atanu Kumar Paul, Dr. Mood Mohan and Mr. Sukumar Purohit for the stimulating discussions.

I am thankful to the members of our research group Ms. Nongmaithem Debeni Devi, Mr. Abebe Moges, Mr. Ravichandran Patil, Mr. Rahul Tiwari, Mr. Pravin Suryawanshi, Ms. Kakali Borah, Mr. Dalvir Singh, Mr. Mangal, Ms. Angana for providing a collaborative research environment. I earnestly appreciate the help, support and guidance from each of them.

I would be grateful to all the faculty members and staff of the Department of Chemical Engineering, and Central Instruments Facility, IIT Guwahati.

Most importantly I would like to thank my support system which includes Ms. Anushree Ghosh, Ms. Shreya Mukherjee, Ms. Surabhi Patel, Dr. Sushma Chakraborty, Ms. Kajal Ingtipi, Mr. Jinesh Machale, Ms. Shivani Gupta, Ms. Jenasree Hazarika Mrs. Nilanjana Chakraborty and Dr. Piyal Mondal for their constant faith and patience.

Last but not the least, this thesis would not have been complete without the endless trust and support of my parents, my husband Dr. Siddharth Thakur, my grandparents-in- law and parents-in-law.

Sutapa Das

Indian Institute of Technology Guwahati

Abstract

Employing renewable sources for developing energy feedstocks and a gamut of value-added products presents an attractive route towards fostering a sustainable future. In this regard, biomass-based resources offer ample scope in terms of availability, processing-ability, and product generation. Prior art suggests the utilization of various thermochemical techniques for the effective conversion of biomass. Pyrolysis, in particular, has been widely utilized in different research settings owing to its ability to process a wide range of feedstocks while generating an array of products. Given that India is one of the leading rice producers, the amount of agricultural waste, i.e., rice husk (RH) generated, is significant. Commonly prevailing ineffective measures of transforming this biomass, such as incineration, often result in material loss while causing environmental pollution. Hence, considering the above situation, this thesis is constructed towards the objective of employing RH as a potential source for the generation of valuable products such as bio-oil, bio-char, and silica nano particles, while using slow pyrolysis under different process environments (inert–N_2 and reactive–CO_2).

The introductory section of the thesis highlights the different characteristics of pyrolytic products such as bio-oil, bio-char, non-condensable gases, and nano particles. An extensive literature survey discussing the involvement and modifications of pyrolysis methodology towards biomass conversion has been presented. The next section highlights the various processing conditions enforced, optimization tools employed, characterization techniques utilized, and procedures followed to generate, optimize, analyze and enrich the pyrolytic products obtained in this study. Thereafter, individual

TH-3101_166107009

subsections present the different works of this thesis concerning the generation of bio-oil, bio-char, and silica.

RH initially undergoes acidic pretreatment to remove the inorganics, which otherwise would degrade the bio-oil quality. The processed precursor was subjected to a slow pyrolysis process in an N_2 environment and optimized using a CCD model-dependent RSM technique. The model highlighted the relationship and operating ranges of the three vital process parameters: temperature, holding time, and inert gas flow rate. The optimum conditions identified for the process to produce maximum bio-oil yield (35.5 wt %) were temperature, 427 °C; time, 45 min; and flow rate, 0.8 L/min. The bio-oil obtained was treated using a solvent extraction technique to improve its calorific value and reduce the water content. The upgraded bio-oil was characterized, and its compositional analysis revealed it to be a mixture of phenols, esters, and aromatics.

Moreover, utilization of one of the pyrolytic gases, CO_2, as a carrier gas also improved the carbon footprint of the process while introducing a reactive environment. The RSM optimized the slow-pyrolysis of RH to achieve the maximum bio-oil yield of 31.7 wt% at the optimal condition of 551 °C, 1.1 L/min, and 53 min. The subsequent characterization of by-product, i.e. bio-char, prompted its use as a catalyst and showed enriched bio-oil yield conforming to the ASTM standards when added in different proportions to the feedstock before the thermochemical conversion.

As observed in the previous sub-section, bio-char is a versatile material that can be tailored to different applications or precursors for other valuable products. Thus, there is a need to understand the effect of varying reaction environments on structural and physico-chemical characteristics of bio-char so that its final properties could be modified accordingly. RH was subjected to an RSM-optimized slow pyrolysis technique under two different environments – N_2 and CO_2 to obtain bio-char. The optimal conditions of the process parameters under N_2 environment were 521 °C, 48 min, 0.87 L/min, and under CO_2 environment were 545 °C, 0.87 L/min, and 43 min, respectively. Characterization studies of the obtained bio-char revealed that the bio-char generated under a reactive environment had a higher porosity, surface area, and pH. At the same time, the bio-char generated under the inert environment had a higher carbon content. Therefore, the former could be potentially used as an adsorbent, and the latter could be involved in soil conditioning application. Hence, to highlight the effectiveness of the bio-char as an adsorbent, a study was undertaken to determine its efficacy towards removing the ranitidine pollutant.

Initially, the RH was pyrolyzed under a reactive environment to generate highly porous bio-char. Further improvement in the bio-char textural properties was realized, as it was exposed to an alkali-mediated activation process, rendering it with a high surface area of 440 m^2/g. In the presence of aqueous ranitidine solution, the upgraded bio-char was analyzed for its adsorption capabilities. The adsorption of 50 ppm ranitidine on the activated bio-char at pH 9 resulted in the removal of 88.3% reactant at 100 mg adsorbent dosage. Moreover, the adsorption kinetics followed a pseudo-second-order pathway, while the Langmuir model described the adsorption isotherm.

After pyrolysis, as the volatiles get converted to liquids and gases, the bio-char mainly contains inorganics i.e. silica. This work highlighted an alternative methodology for producing silica nanoparticles, utilizing renewable precursor material (bio-char) and employing a relatively facile operation protocol. The bio-char produced under various temperatures under a reactive environment subsequently subjected to different pH conditions. The modified bio-char was then calcined to generate the silica nanoparticles. The produced silica nanoparticles were further characterized to determine their surface properties, zeta potential, and roughness. A proof-of-concept was established wherein the obtained silica nanoparticles were functionalized to be involved in an oil/water separation application. The silica nanoparticles were primarily silanized, adsorbed on a cotton substrate, and used as a membrane. The membrane showed significant hydrophobic and oleophilic capabilities, as it separated oil from an oil/water mixture.

Table of Contents

Chapter I

Introduction and literature review

TH-3101_166107009

Chapter II

Materials and methods

Chapter III

Optimal production of bio-oil using slow pyrolysis process under inert environment and its upgradation using solvent extraction method

Chapter IV

Catalytic upgradation of bio-oil using slow pyrolysis process under reactive environment

TH-3101_166107009

Chapter V

Optimal production of bio-char with maximum carbon content under both inert (N_2) and reactive (CO_2) environment

Chapter VI

Utilization of bio-char produced under reactive environment for the separation of ranitidine from synthetic wastewater

Chapter VII

Optimal synthesis of silica nanoparticle from bio-char produced during the pyrolysis process under reactive environment and its application towards the preparation of superhydrophobic coatings

Chapter VIII

Conclusions and future scope

Indian Institute of Technology Guwahati

List of Tables

Table No. **Table Caption** **Page No.**

Chapter I

Chapter II

Chapter III

Chapter IV

Chapter V

Chapter VI

Chapter VII

Indian Institute of Technology Guwahati

भारतीय प्रौद्योगिकी संस्थान गुवाहाटी • Indian Institute of Technology Guwahati •

List of Figures

Figure No. **Table Caption** **Page No.**

Chapter I

Chapter II

Chapter III

Chapter IV

TH-3101_166107009

Chapter V

TH-3101_166107009

Chapter VI

Chapter VII

Indian Institute of Technology Guwahati

Nomenclature

Abbreviations

ATR – Attenuated Total Reflectance

ARHB – Activated Rice-Husk Bio-char

ANOVA – Analysis of Variance

CCD – Central Composite Design

CC – Corn Cob

CS – Cotton Stalk

CV – Calorific Value

DOE – Design of Experiments

DSC – Differential Scanning Calorimetry

DTG – Differential Thermogravimetric

FT-IR – Fourier Transform Infrared Spectroscopy

HHV – Higher Heating Value

RH – Rice Husk

RSM – Response Surface Methodology

TGA – Thermogravimetric Analysis

TSP – Two Step Pyrolysis

WS - Walnut Shell

TH-3101_166107009

Units

% – Percentage

°C – Degree Centigrade

°C/min – Degree Centigrade per Minute

cP – Centipoise

g – Gram

min – Minute

h – Hour

kg – Kilogram

kg/m^3 – Kilogram Per Cubic Meter

m^3 – Cubic Meter

kJ/mol – Kilo Joule Per Mole

mg KOH/g – Milligrams of KOH Per Gram

MJ/kg – Mega Joule Per Kilogram

wt% – Weight Percentage

vol% – Volume Percentage

µL – Microlitre

CHAPTER I

Introduction and literature review

Motivation

Current Scenario

Objectives

Thesis Organization

भारतीय प्रौद्योगिकी संस्थान गुवाहाटी • Indian Institute of Technology Guwahati •

Chapter I

Introduction and literature review

This chapter briefly discusses alternative energy resources for meeting the growing energy demands. The focus is also towards sustainable utilization of rice husk (RH) to produce bio-oil, bio-char, non-condensable gases, and other value-added products. The chapter covers the current state of the art on utilization of agro residue as well as its conversion to biofuels. In addition, the review also focuses on different experimental techniques utilized for biomass conversion to produce valuable products like bio-oil, bio-char, silica nanoparticles etc. The literature review also discusses various physico-chemical properties of bio-oil, bio-char, silica nanoparticles obtained from slow pyrolysis using RH. Based on the research lacunae, the knowledge gap has been addressed, followed by the formulation of the research objectives of the thesis and its organization.

1.1 Introduction

Energy is a vital driving force for sustaining the global evolution of economies [1]. Industries ranging from marine engineering [2], earth excavation [3] to gadgets and healthcare [4], all require energy in one form or another for their operation. In the present scenario, most of the energy requirements are met by exploring fossil-fuel reserves and utilizing their derivatives [5]. The burgeoning population, technological revolution, and improved living standards have led to the excessive utilization of energy. As a result of the anthropogenic activities, supplies of oil-based products have been dwindling with their usage leading towards the generation of greenhouse gases

TH-3101_166107009

that have caused significant and irreversible damage to the environment [6,7]. This has stimulated global research towards identifying a cleaner, and reliable energy source. Among the renewable technologies adapted so far, biomass-derived energy (bioenergy) presents an attractive alternative as it is an economically viable energy source employing a feedstock that not only is abundant in environment, but also is a precursor for different value-added products like bio-char, bio-oil

Presently, biomass-based energy sources contribute ~12% of the world's energy supply; however, they are theoretically capable of producing 100% of the world's energy supply [6,8]. In this regard, different countries, particularly the European Union (European Environment Agency), had formulated a plan for a 20% contribution from bioenergy to global supply by 2020 and 27% by 2030 [9]. The Government of India (Ministry of New and Renewable Energy) has also laid significant policies regarding the inclusion of biomass to generate energy. A physical target of 740 MW supply was estimated by the end of 2020 [10]. Such strategies adopted by governments would encourage sustainable production of energy and lead towards establishing carbon-neutral economies.

Over the decades, different types of biomass have been explored depending on their availability, product outlook, and affordability [11]. They have been categorized into three generations with varying crop characteristics. The first generation of feedstocks relied upon accessible and edible food crop fractions such as sugarcane, sorghum with their main product profile being biofuel. Oil seed crops such as soybean, oil palm, and sunflower are also utilized mainly for producing biodiesel [12,13]. However, the search for alternate biomass sources emerged due to the limitation of fertile land availability and conflict over incentivizing energy crops over food crops. This led to the

TH-3101_166107009

identification of the second generation of non-edible crops, which have a low lifetime (plantation to harvest), high yield, high energy density, high harvest index (most parts of the plant are used), and are adaptable towards the different climate. Examples include eucalyptus, alfalfa, switchgrass, agricultural residues (sugarcane bagasse, RH, wheat straw), and agro-industrial wastes (potato peel, apple pomace, soybean cake) [14]. These are mainly lignocellulosic biomass, i.e. plant based materials which are not edible and hence can be exploited for energy generation. Besides the utilization of terrestrial plants, reports in the literature have also explored non-edible marine biomass as the third-generation feedstock. These include seaweed and microalgae [15]. However, this feedstock category requires further exploration as they suffer from high production costs, limited scale-up opportunities due to technical challenges, and varying efficiency of conversion technologies [16].

Plant biomass itself is a rich source of valuable products besides utility for energy generation. Degradation of different biomass through pyrolysis primarily leads to the production of bio-oil, bio-char, and non-condensable gases [17]. These products find diverse applications in areas such as boiler fuel (bio-oil) [18], soil conditioner [19], adsorbent (bio-char), formation of catalysts [20], industrial chemicals (gases) [21]. Furthermore, specific bio-char conversion also leads to the generation of silica [21], a multi-functional material with utility ranging from preparation of superhydrophobic coatings for self-cleaning windows, filters, and anti icers to smart materials and biocompatible layers for biosensing [22–24]. Deng et al., prepared a superhydrophobic (SiO_2-TiO_2/PDMS) cloth, which can be used as a filter for selectively adsorbing oil from an oil-water mixture [25]. Hence, effective biomass utilization would promote the generation of diverse products and, on a larger scale, would facilitate the growth of a circular economy.

Biomass has been considered as a potential alternative energy source to conventional fossil fuels [26]. They have been exploited to produce various chemicals and fuels as they have very low sulfur and nitrogen (N_2) content, resulting in less SO_x and NO_x generation [27]. Agricultural wastes or residues are lignocellulosic biomass that is still not fully exploited and is widely available at a cheaper cost [26]. Agricultural wastes consist of RH, rice straw, corn stalk, corncob, pinewood, beech wood, wheat straw, bagasse etc., to name a few. The composition of these wastes is different as presented in Table 1.1; hardwood biomass like beech wood, poplar, and cherry wood has a negligible amount of ash, whereas RH, corn leaves, and rice straw have a high amount of ash content. So, based on the composition, the conversion techniques are selected. These wastes could be converted to useful products via physical, thermo-chemical, or biological methods [28,29]. It is evident that lignocellulosic biomass act as feedstock for renewable biofuels such as bio-oil, bio-char, gases, other value-added products, and bio-ethanol. For example, India is a rice-producing country and generates a huge amount of RH in turn. It may be noted that rice is predominantly used as a staple food in many South Asian countries, including India (28% global rice production in 2020), which further generates a considerable amount of usable biomass. It may be noted that the biomass usability, feasibility, and product profile are analyzed for downstream processing by primarily considering the availability of biomass. Among the other types of biomass (wheat husk, wheat straw, corn cob, bagasse, poplar, hazelnut shell etc.), RH is predominantly available in northeastern India and, thus, will assist in improving the economic feasibility and carbon footprint of the process [33].

Moreover, the silica content in RH is exceptionally high, which will also help us widen the obtained products' applicability [34]. Rice production by different Asian countries has been represented in a pie chart depicted in Figure 1.1. Out of India's 28% global rice production, the country also deals with the waste management of 24000 tonnes of RH (waste generated after rice milling) [35].

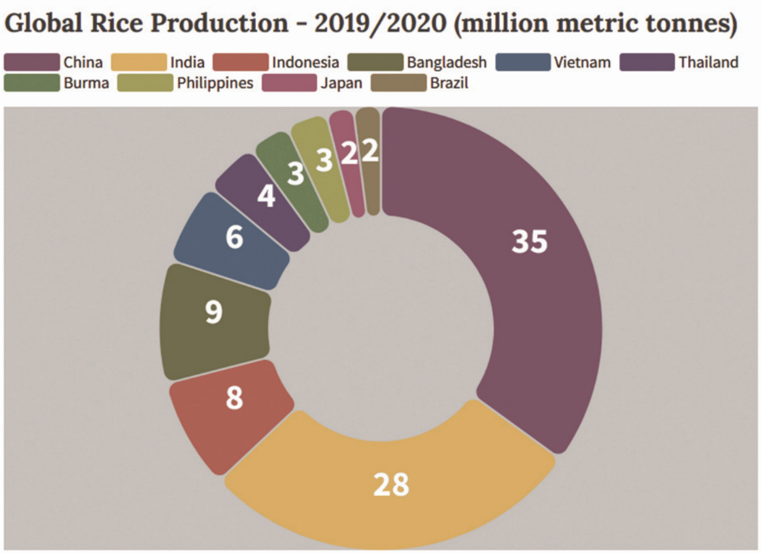

Figure 1.1. Worldwide production of rice in the year 2020.

The collection and proper disposal of these wastes are complex owing to their volume, and the process is also not financially viable [36]. Hence, these are either dumped or burnt in the fields, causing a detrimental effect on the environment. As RH contains a huge amount of silica, multifunctional products could be derived from it via alternative and more efficient conversion techniques [26].

Table 1.1. Lignocellulosic composition of various biomass [37].

Biomass	Cellulose (wt%)	Hemicellulose (wt%)	Lignin (wt%)	Ash (wt%)
Rice husk	25–35	18–21	26–31	18
Rice straw	28–36	23–28	12–14	20
Wheat straw	33–38	26–32	17-19	4
Corn cob	42–45	35–39	14–15	3.5
Corn leaves	~27	~13	~15	10.9
Switch grass	5–20	30–50	10–40	5–6
Bamboo	~40	~20	~20	~2
Sugarcane bagasse	42–48	19–25	20–42	–
Beech	45	33	20	–
Poplar	49	24	20	1
Cherry wood	46	29	18	0.5
Oat straw	31–37	27–38	16–19	–
Hazelnut shell	~25	~28	~42	~1

Different techniques are developed to scale up the utilization of biomass as an energy source; however, these are mostly in the nascent phase. For example, gasification plants in India use RH to generate about 20-400 kW of power [38]. However, lack of awareness and technical complexity leads to a significant loss in terms of energy production as well as recovering value-added material every year [39]. Thus, the need of the hour is to develop different techniques that lead to the wholesome conversion of this biomass.

1.2 Pretreatment of biomass

Biomass consists of cellulose, hemicellulose, lignin, ash, extractives and inorganics [40]. The lignocellulosic matrix becomes the barrier for biomass valorization for value-added products or biofuel generation. Thus, characterization for the degree of lignification, cellulose crystalline structure, and cell wall constituents' complexity need to be addressed before breaking down the biomass for obtaining valuable products [41]. In this regard, the pretreatment process of biomass effectively aids in disrupting the recalcitrant lignocellulosic structure, reduces the degree of crystallinity of cellulose, and removes the inorganics. Different types of pretreatment processes (physical, biological, and chemical) have been developed depending upon the composition of the biomass and desired outcome in terms of product profile [42]. The physical pretreatment process includes milling and grinding the biomass for their size reduction, which can further be utilized in conversion processes. On the contrary, the biological pretreatment is carried out using microorganisms (bacteria, fungi and etc.) for biomass degradation before enzymatic saccharification. In contrast, the chemical treatment includes pretreatment by alkali and acids [42,43]. The alkali pretreatment is mostly done to solubilize the lignin, making the carbohydrates more available for enzymatic hydrolysis to produce bio-ethanol [42]. The acid pretreatment can be done using both concentrated and dilute acids. The corrosive nature, high maintenance, operational cost, and formation of inhibitory compounds like furfural and 5HMF make the concentrated acid pretreatment outdated. However, dilute acid treatment is more feasible, which does not alter the basic structure of biomass and further leaches out the inorganics, thereby making the biomass more accessible for conversion [17].

This work mostly focuses on chemical treatment methodologies like dilute acid pretreatment for leaching out the inorganics. Inorganic acids such as H_2SO_4, HCl, and HNO_3 are mainly utilized to break down the lignocellulosic structure. This method helps to solubilize the hemicellulose content and disrupt the cell wall structure releasing sugars and soluble oligomers. This also enhances biomass porosity and assists in degradation [44]. It may be noted that acidic pretreatment helps to remove alkali (Na, K) and alkaline earth salts (Mg, Ca) that are known to act as catalysts during the pyrolysis process. For instance, the presence of K in the biomass promotes the formation of low-molecular-weight substances and prevents the formation of levoglucosan [45]. The cations primarily lower the bio-oil yield and increase bio-char production by inducing fragmentation of monomers during the pyrolysis process [46]. Higher ash content in bio-oil promotes rapid aging, and therefore, pretreatment is needed to retain the bio-oil properties for a longer duration by slowing down the aging process [47].

1.3 Conversion technologies

Different biomass conversion processes such as thermochemical and biochemical methods are shown in Figure 1.2. The thermochemical technique utilizes heat and/or catalysts to transform biomass to biofuel and other valuable products [48]. This technique is not feedstock-specific and can quickly process multiple feedstocks (a few h). In comparison, the biochemical approach utilizes enzymes and microorganisms to convert biomass. This process is relatively slow (days) [49]. Although employing biological agents to decompose lignocellulosic material is attractive economically, their stability is a significant issue. These organic components are susceptible to change in the reaction environment, such as pH and temperature, so they require proper attention for optimal usage. Since industrial processes may not always provide mild, sterile conditions, it becomes imperative to identify robust organisms that are not only capable of performing the reactions but can also withstand the environment [50]. Hence, thermochemical processes have an edge and are mostly preferred for large-scale processing of biomass. Thus, the thermochemical methodology has been further explored in recent years in different forms such as combustion, gasification, and pyrolysis.

Combustion refers to the thermal degradation of biomass in the presence of oxygen. Herein, heat is generated during the conversion process, which can be utilized for other purposes [51]. However, the efficiency of the process is low (~10%). Gasification is related to the oxidation process of biomass, wherein the conversion of solid fuel to gaseous fuel occurs [52]. On the other hand, pyrolysis refers to the degradation of biomass in the absence of oxygen and leads to the generation of different fuels (solid, liquid, and gas). Compared to the other processes, its efficiency is high as it produces multiple products, thereby making the process more economical. Hence, it has been extensively investigated over the last few decades [53].

Pyrolysis is a complex process that deals with the thermal decomposition of biomass in an oxygen-free environment. The biomass conversion begins at ~300 °C and goes up to 800 °C. The long-chain compounds present in the biomass get converted to short-chain compounds, resulting in tar, bio-char, bio-oil, and gaseous components (non-condensable) [54]. These components' formation rate depends on many process variables such as feedstock characteristics, reactor configuration, heating rate, temperature, and pressure, which eventually produces bio-oil, bio-char, non-condensable gases, and other valuable compounds (bio-adsorbent and silica nanoparticles) [55].

The pyrolysis process can be classified into slow pyrolysis and fast pyrolysis, based on the heating rate of the process. In slow pyrolysis heating rate is varied in the range of 1–10 °C/min, and the process temperature is varied between 300 °C–800 °C with a variation in holding time from minutes to hours. This process is also called carbonization, as solid carbon is its primary product. The heating rate and the residence time affect the end product composition as the feedstock inside the reactor undergoes different primary and secondary reactions. Traditionally, the process was used for charcoal production. However, this process led to the generation of harmful gases like carbon mono-oxide and therefore was termed an inefficient energy process. However, slow pyrolysis is preferred to obtain the optimum quality of both solid and liquid products. Bio-oil and bio-char obtained from slow pyrolysis are of good quality and quantity (25–45 wt% bio-oil recovery), and thus could further be employed for various sustainable applications.

On the other hand, fast pyrolysis primarily reduces the secondary cracking reactions, thereby producing a high amount of bio-oil. In this process, the heating rate is varied between 20–200 °C/min with a very short holding time of 0.5–10 s. Hence, bio-oil is the primary product of this, and the bio-char yield is too low in the case of fast pyrolysis. Pyrolysis is an endothermic process requiring an external heating source, making the process energy-intensive. Hence, to increase the thermal efficiency of the process, the non-condensable gases are recycled as carrier gas. To understand the effect of these gases pyrolysis has been carried out under carbon-monooxide (CO) [56], carbon-dioxide (CO_2) [57], hydrogen (H_2) [58], and methane (CH_4) [59] environments by various researchers.

Indian Institute of Technology Guwahati

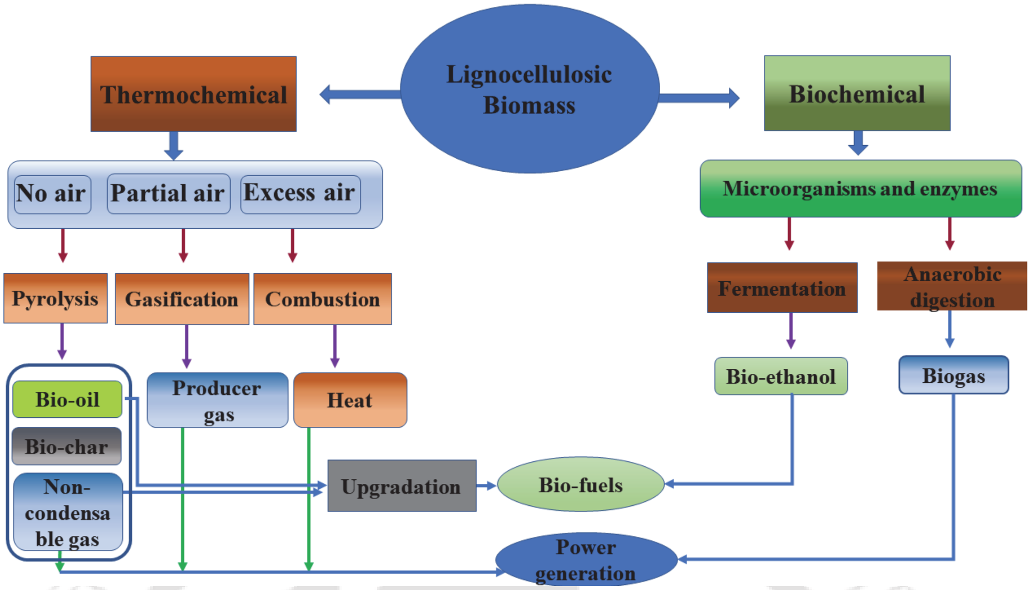

Figure 1.2. Conversion technologies of lignocellulosic biomass to different products.

1.3.1 Bio-oil

Bio-oil is more advantageous with respect to conventional fossil fuels as it possesses lower sulfur, ash, and N_2 content, thereby releasing lower amounts of SO_2, soot, and N_2 [60]. Furthermore, the plants take up the CO_2 released during bio-oil production from biomass or utilized as a carrier gas in processing plants, thereby balancing the amount of overall CO_2 [61]. The typical characteristic range of different parameters for bio-oil and conventional fuel has been provided in Table 1.2. It is also referred to as the bio-oil or wood distillate. It is produced by a rapid/controlled degradation of lignocellulosic biomass and separated from the gaseous constituents by employing a condenser. It is a dark brown organic liquid mixture that comprises a significant fraction of water and many organic compounds such as acids, ketones, phenols, ether, sugar, furans, alkenes, and miscellaneous solid particles [62]. The water content in the final composition depends on the initial moisture content of the feedstock and water formed during the pyrolysis process. The bio-oil's higher heating value (HHV) ranges between 15 to 20 MJ/kg, less than half of conventional fuels HHV. This is ascertained to the presence of considerable oxygen content (35–40 wt%) on a dry weight basis. The carboxylic acid content of bio-oil is responsible for its low-pH value that causes corrosion in engines. So, various techniques (solvent extraction, hydrodeoxygenation, and catalytic pyrolysis) are followed to upgrade the bio-oil properties and diminish such unwanted (carboxylic acids, formic acid, acetic acid, esters and etc.) organics [17,63–65]. The upgraded bio-oil can be achieved by solvent extraction. Based on the polarity of the solvent, various unwanted organics can be separated from the bio-oil, which makes it suitable for fossil fuel substitution. In the hydrodeoxygenation process, high pressure (345 atm) with temperature in the range of 100–500 °C using H_2 and catalyst is followed for bio-oil production. In this technique, the oxygen is removed in H_2O, CO, or CO_2 so that carbon remains intact in the organic phase [63]. In catalytic pyrolysis, the biomass gets converted to aromatics via deoxygenation reactions in the presence of a catalyst [64]. Primarily commercial zeolite-based catalysts have been studied; however, there are few studies on the effective utilization of biomass-derived catalysts. Considering the rich diversity of biofuels that can be generated because of the pyrolysis process, this work explores the different facets of biomass-derived products via a slow pyrolysis technique under inert (N_2) and reactive (CO_2) environments utilizing RH as the primary biomass source.

Table 1.2. The typical range of parameters observed in bio-oil and conventional fuel [66].

Properties	Bio-oil	Fuel oil
Water content (wt%)	15–30	0.1
pH	2–3	Neutral
C (wt%)	54–58	85
H (wt%)	5.5–7	11
O (wt%)	35–40	1
N (wt%)	0–0.2	0.3
S (wt%)	Trace	0.5–3
Ash (wt%)	0–0.2	0.1
Higher heating value (MJ/kg)	16–19	40
Specific gravity	1.2	0.94
Viscosity at 500 °C (cP)	40–100	180
Pour point (°C)	-33	-18

1.3.2 Bio-char

In addition to bio-oil, the other prominent biomass-derived product is bio-char. The solid by-product of the biomass pyrolysis process contains unconverted organic solids and carbonaceous residues along with some mineral fractions [67]. Depending on the feedstock composition, process conditions, and reactor configuration, bio-char's physico-chemical characteristics and structural morphology can vary. The bio-char yield greatly depends on the pyrolysis temperature and also on the composition of biomass. For example, the carbon content of bio-char can vary from 53 wt%–96 wt%, while the heating value can vary from 20–36 MJ/kg [68]. Conventional carbonization or slow pyrolysis utilizes lower heating rates (working temperature does not go beyond 700 °C), with longer vapor residence time [69]. This technique develops bio-char with high carbon content (low bio-oil content), which can be utilized in agro-industry products as soil supplements. This grade of bio-char helps enhance soil fertility and contain pollution by providing a route for carbon sequestration [70]. Slow pyrolysis changes the chemical composition of bio-char by varying the C/H and O/H ratios and significantly contributes to its physical characteristics by making it highly porous. The porous morphology of bio-char formed during the pyrolysis process due to volatiles removal at the high temperatures equips it with a honeycomb-like structure with a high surface area (100–500 m^2/g), ideal for contaminant adsorption and filtration applications [67,71]. Another facet of bio-char is its high HHV, which endows it to be a high-energy supplement. Utilizing it for combustion is considered more environmentally friendly than using coal [72].

1.3.3 Non-condensable gases

Biomass pyrolysis also leads to gaseous products, such as hydrogen (H_2), methane (CH_4), propane (C_3H_7), ethylene (C_2H_2), carbon monoxide (CO), and carbon dioxide (CO_2) [73]. Higher inherent moisture content can also contribute towards higher H_2 content compared to a dried feedstock [74]. Gases like CH_4 and CO_2 generally originate after methylene and methoxy bonds break, while CO and CO_2 are produced from carboxyl and carbonyl groups [75]. Variation in several parameters such as initial moisture content, feedstock particle size, and process temperature can significantly affect the gas composition. As already highlighted, high moisture content feedstock (more than 10%) generally releases higher H_2 content in gases. Also, this kind of feedstock usually results in higher extraction of water-soluble components in gases, thereby reducing gas yield [76]. Higher reaction temperatures lead to higher thermal degradation rates, which results in increased volatile products. The gaseous products undergo various reactions such as decarbonylation and dehydrogenation at these conditions [77]. As mentioned earlier, the feedstock size also plays a vital role in determining the overall gas composition. Smaller particles favor the cracking of hydrocarbons, thereby producing more H_2 gas. Larger-sized particles lead to lower heating rates, which results in increased bio-char yield and decreases gas production due to low residence time of volatiles in the reactor [54]. Pyrolytic gas finds application in various fields, including utilization in combustion engines for transportation purposes [78] or production of liquid biofuels.

1.3.4 Silica nanoparticles

Silica is a functional material that finds application across different fields. Its chemical structure allows it to be suitably functionalized such that it can be used in catalysis, sorption, and insulation applications. In particular, the porous form of silica or silica nanoparticles is highly sought after as they can be tailored accordingly. Over the past decades, different approaches have been pursued to synthesize silica nanoparticles chemically. The utilization of silicon tetraethoxysilane to produce silica nanoparticles is widely followed. This hydrothermal technique can obtain silica nanoparticles with modulated size and porosity. However, scaling up is economically not feasible, as generation of the precursor involves a multi-step procedure that is energy-intensive and requires a harsh environment in terms of high acidity, high temperature, and high pressure. In light of this and considering the increasing demand for silica nanoparticles, biogenic silica or biomass-derived silica offers an attractive route. Considering the enormous proportions of waste biomass, its utilization to produce silica has been touted as a cost-effective, scalable approach [79]. Thus, one of the goals of this thesis is related to the synthesis, characterization, and application of biomass-derived silica nanoparticles.

1.4 Literature review

The present section compiles the state-of-the-art research and experimental biomass conversion techniques related to biofuels, their upgradation, and utilization.

1.5 Current scenario of rice husk

Globally, India contributes to 28% of rice production, which generates a considerable amount (~24000 tonnes) of by-product i.e. RH [35]. This type of biomass has a considerable fraction of cellulose and hemicellulose that can produce different valuable products. However, managing this huge amount of waste becomes a problem for the farmer [80]. Moreover, its high fiber content can not be used as animal feed [81]. Hence, the widely practiced method of discarding this RH waste is either by openly dumping it for further usage as manure or incinerating it, which causes severe environmental pollution. The capital of India, New Delhi, faces the wrath of this problem every year, wherein rice husks along with rice straws are openly burnt. This causes increase in the air quality index reaches to 370–400, as reported by the central pollution control board (CPCB) [80,82]. Hence, to address this burning issue, the current thesis uses this waste to generate valuable products.

TH-3101_166107009

1.6 Pyrolysis processes

Pyrolysis is classified as slow or fast based on the heating rate. Slow pyrolysis is preferred to obtain the optimum quality of both solid and liquid products. Also, through slow pyrolysis, bio-oil obtained is in the range of 25–45% along with the excellent quality of bio-char, which could be further activated to be used as adsorbents or to derive other value-added products. On the other hand, fast pyrolysis primarily reduces the secondary cracking reactions, producing a high bio-oil yield. Pyrolysis is an endothermic process that requires an external heating source, making the process energy-intensive. Hence, to increase the thermal efficiency of the process, the non-condensable gases are recycled as carrier gas. The following paragraphs are incorporated to highlight the role of pyrolysis environment on the physico-chemical characteristics of the derived pyrolytic products.

1.7 Pretreatment process

The RH feedstock contains a significant amount of lignocellulosic matter (i.e., cellulose (25-35 wt%), hemicellulose (18-21 wt%), and lignin (26-31 wt%)). The feedstock can be transformed into value-added products via pyrolysis. However, they are known to contain inorganics, making it difficult to convert them into biofuels. Hence various pretreatment processes (alkali, acid, torrefaction etc.) are carried out to leach out the inorganics so that the volatile content present in the biomass becomes more accessible during the conversion processes. The biomass in its crude form is recalcitrant, making it difficult for energy production; therefore, pretreatment makes it more accessible for thermo-chemical conversions. Compared to the alkaline pretreatment process, acid pretreatment is relatively faster, does not require a neutralizing step, prevents the

TH-3101_166107009

formation of caustic salts that lead to corrosion of containers, and helps in the recovery of silica as a valuable product [83].

Hence, for the present study, a dilute acid pretreatment process was used so that it only leached out the inorganics without disturbing the original framework of the biomass. In a related study, Cen et al., reported the dilute acid (aq. HCl) based pretreatment of rice straw at 50 °C for 2 h followed by its pyrolysis. They reported an increase in bio-oil yield from 20.5 wt% to 31.8 wt%, while the calorific value increased from 15.2 to 16.7 MJ/kg [84]. Similarly, Kumagai et al., in their study, carried out acid pretreatment at varying H_2SO_4 concentrations (1, 3, 6, and 9 M) followed by pyrolysis of pretreated wood samples and reported a maximum bio-oil yield of 46.8 wt% at 3M H_2SO_4 concentration [85].

1.8 Pyrolysis under inert (N_2) environment

Various reports in the literature have utilized slow pyrolysis to produce different products by varying other variables such as process temperature, holding time, and gas flow rate. These studies are mainly carried out under an inert N_2 environment, Zhang et al., studied two-step pyrolysis (TSP) of different feedstocks- walnut shell (WS), cotton stalk (CS), and corn cob (CC) to understand its effect on the yield of acids, furans, ketones, and sugars. The sample was first pyrolyzed at 400 °C for the 20 s and then pyrolyzed at 650 °C for 20 s. They reported that CC and CS released most of the volatiles in the first step, whereas WS produced more phenolics in the second step. Different value-added compounds could be selectively targeted using this technique as it fractionally converted the components of the respective biomass [86].

In another study by Zhang et al., on the fast pyrolysis of RH using both one-step pyrolysis (OSP) and two-step pyrolysis (TSP). They found that TSP improved bio-oil quality in terms of lower acidic value and higher phenolics but decreased the overall bio-oil yield. However, it increased both bio-char and non-condensable gas yield. In case of OSP, the temperature was kept at 550 °C, and for TSP, the first set of temperatures was held at 400 °C and the second at 550 °C. The results obtained in the TSP showed the improved composition of non-condensable gases, like H_2 and CH_4 content increased by more than 70% and 35%, respectively [87].

Zhang et al., initially torrified the biomass (sawdust) and then used it for studying a fast pyrolysis process. They studied the effect of torrefaction and the pyrolysis temperature on the products, i.e., CO_2, CO, CH_4, and H_2. The torrefaction temperature (from 240 °C to 300 °C) increased the bio-char yield from 19.80% to 22.09%, however gas yield decreased from 25.78% to 17.18%. They reported that the CO content increased with the torrefaction severity; however, CO_2 content decreased. Also, they found that the activation energy of the gaseous products obtained from the torrefied biomass was higher than crude biomass. Hence, it could be well established that torrefaction has a significant effect on the conversion of biomass [88].

Biswas et al., carried out the slow pyrolysis of corn cob, wheat, rice straw, and RH in order to obtain maximum bio-oil yield. The effect of pyrolysis temperature and the type of feedstock on the bio-oil yield was studied. It was observed that for each particular biomass, there was an optimal pyrolysis temperature for obtaining maximum bio-oil yield. Pyrolysis temperature of 450 °C was sufficient to get the maximum bio-oil yield in the case of RH (38%) and corn cob (47.3%). However, in the case of wheat (36.7%) and rice straw (28.4%), the optimum temperature was found to be 400 °C. The results revealed that the raw biomass conversion was maximum in the case of RH (56.62%), which indicates that the nature of feedstock also affects the bio-oil yield. The bio-oil produced using corn-cob as feedstock was reported to have the highest phenolic content compared to other feedstocks. Hence, it was clear from this study that the bio-oil composition, yield, and characteristics depend on the feedstock characteristics and pyrolysis temperature [89].

Lin et al., utilized crofton weed to produce bio-oil and bio-char. They investigated adding a catalyst (ZnO and Na_2CO_3) to the product yield. The addition of catalyst increased the bio-oil yield and decreased the carboxylic acid content in the bio-oil. The study revealed that 3 wt% ZnO gave a maximum bio-oil yield of 28.8%, and the formation of noncondensable gases, particularly CO, was higher during catalytic pyrolysis. Also, the bio-char obtained can be used as a potential photocatalyst for dye degradation in wastewater as it has a high surface area (185.86 m^2/g) [90].

Casoni et al., studied various agro-industrial wastes, i.e., corn cob, sugarcane bagasse, and sunflower seed hull to produce bio-oil and bio-char using a fast pyrolysis process. The study revealed that the acid pretreatment increased the bio-char yield and decreased bio-oil yield. The study concluded that bio-oil produced could be used as a feedstock for furfural production. The obtained bio-char could be used as a potential adsorbent, soil conditioner, and pollution remediation as they had a high surface area and were microporous in nature [91].

Zhang et al., investigated slow pyrolysis of pine saw dust in the temperature range 400–800 °C in a fixed bed reactor. They reported that pyrolysis temperature did not affect the bio-oil yield; however, the increase in temperature increased the yield of non-condensable gases while reducing the bio-char yield. They found that the temperature also greatly affects the composition of non-condensable gases. As the temperature was ramped up, the yield of CO_2 decreased (15.14% at 800 °C), whereas the yield of combustible gases (H_2 (47.44%) and CO (29.52%) increased. They found that the decomposition of lignin (which starts around 500 °C) and other higher molecular weight hydrocarbons promoted the formation of H_2 gas. Also, the secondary reactions at the higher temperature favor the H_2 formation. The obtained bio-char was further characterized and used as an adsorbent to remove Ag^+ ions from an aqueous solution as its content beyond a permissible limit is designated as harmful by World Health Organization [92].

Kumar et al., pyrolyzed peanut shells at different heating rates of 10, 15, and 20 °C/min in a fixed bed pyrolyzer. They studied the iso-conversional models to calculate the activation energy which was found to be in the range of 186 kJ/mol–226.97 kJ/mol. They investigated the effect of three variables, i.e., heating rate, temperature, and N_2 flowrate. They employed box-behenken design of RSM for optimizing the individual variables for the optimum yield of bio-oil. The study reported the optimum conditions to be 650 °C, 20 °C/min, and 0.1 L/min to achieve an optimum bio-oil yield of 43.24%, with a bio-char yield of 28.25%. Hence, the study established that slow pyrolysis with high temperature and low N_2 flowrate should be maintained to obtain a high bio-oil yield. Also, the obtained bio-char contained micronutrients; thus, it could be used as a soil enhancer [93].

Tripathy et al., studied a new type of pyrolysis, i.e., microwave pyrolysis to degrade oil palm shells to produce bio-char. The experimental methodology was optimized via response surface methodology (RSM) with a central composite design (CCD). The objective was to maximize the bio-char yield and its specific surface area by varying three variables- microwave power, radiation time, and N_2 flowrate. The established optimum conditions were 1080.81 W, 29.95 min, and 133.48 cm^3/min to produce ~61% bio-char yield with BET surface area of 250 m^2/g [94].

Laouge et al., studied the fast pyrolysis of Pearl Millet (PM) and *Sida cordifolia* L. (Sida) to obtain maximum bio-oil. They used the RSM tool to optimize the process variables, i.e., particle size, temperature, and N_2 gas flow rate. The maximum bio-oil yield in PM (~48%) and Sida (48%) were obtained at optimum 1.5 mm, 400 °C, and 0.2 L/min conditions. The study reported that temperature had the maximum effect on the system, followed by particle size and N_2 flowrate [95].

1.9 Pyrolysis under reactive (CO_2) environment

During pyrolysis, the generated non-condensable gases can be recycled and used as a carrier gas to make it economically more viable. However, this type of pyrolysis environment has been reported to affect the yield and composition of the obtained products. For example, Pilon et al., pyrolyzed switchgrass in the temperature range of 300–500 °C under N_2 and CO_2. They reported that the liquid yield was less under the CO_2 environment at 300, 400, and 500 °C as compared to the N_2 environment. Also, the composition of non-condensable gases was affected by the pyrolysis environment. The amount of CO was higher than CO_2 and CH_4 in the 500 °C–CO_2 environment compared to the 500 °C–N_2 environment. The ash content at 500 °C–CO_2 was significantly lower than the raw feedstock. This confirmed that the CO_2 reacts with biomass, affecting the biomass conversion process [96].

Another study by Zhang et al., on pyrolysis of corncob was carried out at 550 °C under different environments (CO_2, CO, CH_4, H_2, and N_2). They reported that the highest liquid yield (58.7%) was obtained in the case of a CH_4 environment and the lowest (49.6%) in CO. The compositional analysis of the liquid product suggested that in the case of CO and CO_2, methoxy-containing groups were reduced and phenolics' content enhanced. They reported that more oxygenated compounds present in the liquid fraction were converted to CO_2 and H_2O in the case of CO and H_2 environments. Also, the calorific value of the liquid improved in the case of CO and H_2 environments. The bio-char yield was found to be lowest in the case of CO_2, which suggests that CO_2 could react with the bio-char at a high temperature. This was confirmed by higher CO yield under the CO_2 environment [56].

Mo et al., studied the pyrolysis of microalgae under N_2 and CO_2 environments with (MgO and ZSM-5) and without catalyst. They reported that maximum bio-oil yield (~44%) was obtained at 450 °C under an N_2 environment. However, the maximum bio-oil yield (~39%) was reported in the case of CO_2 at 400 °C. The non-condensable gas yield was higher in the case of CO_2 environment as compared to N_2, suggesting that cracking was faster under CO_2. Hence, 450 °C and 400 °C were considered optimal temperatures for N_2 and CO_2 environments to maximize liquid yield, respectively. In the case of N_2, MgO catalyst showed better results; the bio-oil yield increased to 46.2%; however, ZSM-5 (bio-oil yield–44.8%) did not have much impact. While, in the case of CO_2, both the catalyst showed adverse effects as the bio-oil yield dropped to 35% (MgO) and 37% (ZSM-5) [97].

Biswas et al., studied slow pyrolysis of rice straw under a CO_2 environment in a fixed bed reactor. The process temperature varied from 300 to 450 °C, while the maximum liquid yield was obtained at 400 °C. The primary compounds present in the bio-oil were phenols, ketones, aldehydes, and alkanes, as identified by GC-MS and ^1H NMR analysis. Compared to the N_2 environment, more bio-oil was produced under the CO_2 environment. Moreover, the CO_2 environment was observed to affect the bio-oil characteristics as there was an enhancement in the oxygenated compounds and reduction in the aliphatic compounds. In the case of bio-char, the carbon content and the overall yield was higher under the CO_2 environment, owing to the high degree of carbonization [98].

Another study concerning slow pyrolysis of the feedstock, i.e., pinewood, was reported by Biswas et al. They analyzed the biomass conversion, bio-oil yield, and composition under N_2 and CO_2 environment. The maximum bio-oil yield achieved was ~54% at 400 °C under the CO_2 and ~58% at 500 °C under the N_2 environment. The biomass conversion and non-condensable gas content increased with increasing the process temperature. GC-MS analysis revealed that the phenolic content under the CO_2 environment was lower than under the N_2 environment for the bio-oil produced in the fixed bed reactor. From XRD analysis, it was observed that the cellulose content in the bio-char was significantly less in the CO_2 environment than N_2 environment [99].

The effect of employing alternate heating modes on the pyrolysis product distribution was investigated by Chen et al. The group reported the pyrolysis of sugarcane bagasse under a CO_2 environment and in the presence of conventional heating and microwave-assisted heating. Charcoal was utilized as the absorber for the pyrolysis performed under microwave-assisted heating conditions. Significant differences in the product distribution were observed between the two heating modes. In conventional heating, the primary product was bio-oil, having a yield of 51%–54%. Increasing the temperature reduced the bio-oil yield, possibly due to secondary cracking of bio-oil. In microwave-assisted heating, the primary product was bio-char, with a yield in the range of 61%–84%. Reducing the charcoal blending ratio reduces the bio-char yield and increases the latter heating mode's gas and liquid yield. This was reported due to higher energy consumption at a lower absorber ratio. Moreover, H_2 was detected, and its content also varied from 2%–12%, as the secondary decomposition of bio-char and cracking of vapors was relatively easier than conventional heating [100].

1.10 Upgradation of bio-oil

The obtained bio-oil cannot directly be used as an engine or transportation fuel due to its high water content, low calorific value, and high acid value. The compositional analysis of bio-oil revealed that the presence of higher oxygenated compounds are responsible for their poor properties. Thus, to improve these properties, upgradation techniques (catalytic pyrolysis or hydrotreatment) are employed [101]. The catalysts utilized in catalytic pyrolysis are mainly metal oxides which are not cost-effective. Another concern associated with these catalysts is their reusability, which is susceptible to deactivation after a few cycles [102]. Hence, to address these issues, economically viable alternatives have been researched that influence the physico-chemical characteristics of the bio-oil. Utilization of the generated bio-char as a catalyst has been performed of late, and the results show that increasing the catalyst to biomass ratio enhances phenolic compounds in the bio-oil, thereby making the bio-oil more stable [71].

Another similar instance was reported by Ren et al. They investigated the catalytic pyrolysis of sawdust pellets at 650 °C in a microwave pyrolysis setup in the presence of corn stover bio-char as the catalyst. The results obtained indicated that the usage of the catalyst enhanced the syngas yield while improving the phenol and other aromatic content fraction in the bio-oil. The syngas yield increased upon increasing the catalyst ratio. The group also proposed a reaction mechanism that indicated that the aromatics were derived from lignin decomposition while aliphatics were obtained from cellulose and hemicellulose degradation. Anhydrosugars and furans were present as intermediate compounds. Bio-char produced from lignin had various functional groups on its surface, such as carboxylic acids, ketones, etc. These groups aided in the cracking and upgrading reactions of bio-oil, thereby regulating the biomass product distribution within the reactor [103].

Chan et al., studied the utility of catalytic bio-char in the pyrolysis process employing hardwood chips and switchgrass as the feedstock. The thermochemical reactions took place in a cylindrical fixed-bed reactor at 500 °C. Compared to a non-catalytic pyrolysis system, the bio-char influenced the bio-oil yield, pH value, and moisture content. However, the carbon content in the bio-oil had reduced, probably owing to its conversion into CO and CO_2 [104].

Owing to its porous nature and high surface area, bio-char has also been used to support different catalysts used in the pyrolysis process. Shen et al., utilized silica-based nickel nanoparticles incorporated bio-char as the catalyst for RH pyrolysis. It was observed that by increasing the catalyst content, the yield of non-condensable gases increased while the bio-oil content reduced. The gas content increased due to the further devolatilization of bio-char along with the occurrence of other tar reforming reactions.

TH-3101_166107009

Moreover, by changing the composition of the catalyst, the product distribution also varied. It was also observed that the catalyst underwent poisoning as it reacted with the acidic groups present on the tar surface [105].

In another study, Nguyen et al., explored the utility of Ni/bio-char catalyst towards bio-oil upgradation via a hydrotreatment process. The results indicated that the hydrotreated bio-oil was mainly composed of light hydrocarbons such as *n*-heptadecane, making it readily miscible with diesel for potential use as fuel. Moreover, a significant reduction in the N_2 and O_2 content in the bio-oil was observed. Thereby, the presence of the composite catalyst aided in improving the fuel characteristics of the obtained bio-oil [106].

1.11 Valorization of byproducts

1.11.1 Bio-char as adsorbent

Over the last few decades, the research fraternity has actively explored different avenues to optimize biomass conversion to bio-char, as it is a multi-functional compound that also undergoes physico-chemical transformation via relatively simple procedures. Su et al. utilized RH as feedstock and developed a green catalytic pyrolysis process, resulting in minimal waste generation. Before the pyrolysis process, the feedstock was washed with acid to eliminate the inorganic content. This step ensured improvement in the bio-char quality and promoted volatiles released from the feedstock. The group prepared the catalyst by pyrolyzing pine sawdust and then activated it to increase its reactive sites and specific surface area. The bio-char obtained via the catalytic process was further utilized as an adsorbent for phenol adsorption, and its adsorption capacity was found to be around 400 mg/g. Moreover, the highest bio-oil yield was obtained in acid-washed RH without catalyst. The bio-oil obtained after catalytic pyrolysis had a lower yield but improved quality [107].

Gao et al., pyrolyzed jujube pit at 800 °C for 2 h to produce bio-char. The obtained bio-char was characterized and found suitable to be used as a potential adsorbent. The specific surface area was found to be 246.9 m^2/g with an average pore diameter of 3.38 nm. Then, the bio-char was used for lead adsorption (Pb II) from an aqueous solution. The kinetics of Pb (II) adsorption process suggested that it reached equilibrium in 30 min and the maximum adsorption capacity was determined to be 137.1 mg/g at pH 6. Also, the reusability of the adsorbent was studied, and it was found that even after 5 cycles, it retained 70% of its initial adsorption capacity. The study concluded that jujube pit-based bio-char could act as an adsorbent for wastewater purification [108].

Another study by Thangagari et al., used bio-char derived from *Azadirachta indica* leaves to remove chromium (Cr (VI)). The feedstock was pyrolyzed at 450 °C for 4 h, which led to the generation of the bio-char. The adsorption experiments were carried out at different pH, with the highest Cr (VI) removal of 58.54 mg/g reported at pH 2. Also, the adsorption process fitted the Langmuir type adsorption isotherm, and the bio-char usage rate was found to be 4630 mg/L. The bio-char was reactivated using NaOH and again utilized for Cr (VI) removal; however, after six cycles, the adsorption efficiency dropped from 96% to 57% [109].

Barman et al., carbonized *Sterculia foetida* waste at 500 °C for 2 h to obtain bio-char. The obtained product was further activated using KOH, and after activation, the specific area was observed to be 161.4 m^2/g. The study was conducted to remove two pollutants, i.e., acenaphthene and naphthalene present in wastewater. It was reported that the maximum removal efficiency of 92% and 94% for acenaphthene and naphthalene, was obtained, respectively. The adsorption process followed Langmuir and Temkin adsorption isotherms with pseudo-second-order kinetics. Also, the activated bio-char was reported to maintain its high removal efficiency for 6 continuous adsorption-desorption cycles [110].

Torrellas et al., studied the adsorption of ibuprofen and tetracycline from synthetic aqueous solution onto commercial and synthesized adsorbents. From the experimental analysis, it was verified that the adsorption of the contaminants followed pseudo-second-order kinetics. The adsorption isotherm was classified as S-type, indicating the occurrence of multilayer adsorption. At the adsorbents surface, π-π EDA interactions with the formation of –COOH and C=O bonds facilitated tetracycline adsorption. For ibuprofen adsorption, acidic groups on the surface also provided the ideal textural properties. Moreover, the equilibrium data were analyzed using different models, and strong correlation between experimental and predicted data followed Weber and Morris's model. Among the other adsorbents, activated carbon derived from RH proved to be the most effective, with an adsorption capacity for ibuprofen of 239.8 mg/g and tetracycline of 845.9 mg/g. A fixed-bed setup also demonstrated significant removal efficiencies of adsorbents at the breakthrough time – 96% for tetracycline and 97% for ibuprofen, respectively.

1.11.2 Production of silica nanoparticles

Conversion of biomass to value-added products such as silica nanoparticles offers a great alternative to the chemical-intensive processes followed at a commercial scale that generates this product while releasing different toxic by-products. Silica nanoparticles find wide-ranging applications in the semi-conductor industry, pharmaceuticals, and adsorbents. From the viewpoint of biomass-derived silica nanoparticles, various reports in the literature have presented methods for generating, extracting, and purifying silica nanoparticles. These methods provide different avenues for overcoming common problems associated with silica production, such as size control, harsh acids usage, and complex extraction techniques.

Sharifian et al., utilized RH, rice straw and prepared a comparative analysis involving different steps for obtaining silica nanoparticles and activated carbon. A multi-stage operation involving K_2CO_3 impregnation, carbonization, chemical activation, acid extraction, washing, and separation led to the generation of activated carbon and silica nanoparticles. Among the two feedstocks, rice straw gave activated carbon of higher surface area (2229 m^2/g) and pore volume, along with a silica yield of (25%). At the same time, RH gave activated carbon of area 1941 m^2/g and silica yield of 40%. The silica obtained was mainly in the amorphous phase, with the rice straw-derived silica having a more-powdery nature. The average particle size of silica was less than 50 nm [111].

Another technique to synthesize silica nanoparticles from RH involved utilizing the alkaline treatment method. In work by J. H. Lee et al., a two-stage continuous process (i.e., ball milling and alkaline leaching) was developed to transform RH. Different alkaline solutions such as NaOH, KOH were utilized to determine the efficacy of the process. The use of NaOH provided a faster response and fine powdery texture. The extraction process was operated for 80 h with an 89% extraction efficiency and a solid content of ~6%. The silica obtained revealed a 98.5% purity and was further characterized using XRD and BET techniques. The overall configuration of silica nanoparticles included utilizing a ball mill-operated equipment with an attrition ball mill for improving the sample texture [112].

Zedin et al., generated high-quality amorphous silica while utilizing RH as the feedstock. The feedstock was pretreated using an acid treatment to remove the impurities, subjected to burning at 700 °C for 4 h, and then made to undergo leaching in the presence of varying concentrations of NaOH. The purity of the silica nanoparticles generated using 3 N NaOH concentration was ~99.7% having an average diameter in the range of 87–114 nm. The generated particles were of almost uniform size while present in the agglomerated state. Increasing the NaOH concentration led to the generation of larger size extracted silica particles. Also, the silica surfaces became rough, and particle distribution became more non-uniform as the particles began to agglomerate due to van der Waal's forces [113].

El-Sakhawy et al., presented a work wherein the production of silica particles was realized through 4 different routes. These included, (i) burning of feedstock in a muffle furnace at 850 °C, (ii) initial reduction in RH volume by burning at 450 °C followed by mixing the obtained ash with 1N HCl such that after washing, it was subjected to burning at 700 °C for 3h (iii) un-grinded RH initially soaked in water, mixed with 1N HCl, and then burned at 700 °C (iv) grinded RH was initially soaked in water and subjected to same steps as mentioned in the previous route. The mesoporous silica obtained from the process was found to have a purity of > 99% and an average particle size in the range 41.3–71.3 nm. Acid pretreatment in the earlier mentioned routes removed almost 56–74% metallic impurities, as confirmed by XRF analysis [114].

TH-3101_166107009

Chun et al., devised a facile, environmental-friendly technique for obtaining silica nanoparticles from RH. The group proposed a route of alkali extraction under mild conditions followed by acetic acid addition for silica precipitation. The process was studied under varying NaOH concentrations at 80 °C to determine the optimal NaOH concentration. Polyethylene glycol was added during the precipitation step to control the morphology of spherical silica particles. As polyethylene glycol has sufficient number of ethylene oxide chains to stabilize the silicate species, its presence aided in maintaining the overall morphology of the silica particles. This also allowed the silica particles to have a surface area of ~250 m^2/g due to micropores' presence. The purity of these particles was around 98%. The group also demonstrated that the silica particles' size could be altered by varying the precipitation reaction temperature. At 5 °C, the average size was 1.4 μm, whereas, at 60 °C, the average size was around 0.25 μm. With increasing temperature, more nuclei formed, resulting in a higher number of smaller-sized particles in the presence of polyethylene glycol [115].

1.11.3 Functionalization of silica nanoparticles

Silica nanoparticles find utility in a wide array of applications such as drug delivery, self-cleaning, superhydrophobic, oleophobic, and oleophilic coating, owing to their versatile nature, robustness, biocompatibility, and ease of functionalization. Terrell et al., utilized commercial silica (Aerosil R 202) and functionalized silica to obtain a superhydrophobic and oleophobic coating on stainless steel and aluminum coupons. They functionalized the silica particles using 1% fluoro alkylsilane. Then, they applied a silane coupling agent on the coupon surfaces, and then the functionalized solution was spray-coated and cured at 100 °C for 1 h. They also studied the thermal stability of these coatings. The study concluded that the functionalized particles had both high water (≥ 150°) and oil (≥ 140°) contact angle at 100 °C, and the contact angle decreased by 10–13° at 400 °C. Hence, it could be well established that these coatings are thermally stable and could be used as coatings in industries [116].

The use of superhydrophobic substances to improve the waterproofing and thermal insulation property of building materials is a promising approach towards developing stable structures. In a related study by Song et al., perfluorosilane compound was mixed with ultrafine fly ash to create a superhydrophobic composite coating. This was later applied to a concrete block, and its surface was analyzed. The composite coating adhered onto the concrete surface and formed a "Lotus leaf-like" texture that imparted superhydrophobicity to the concrete block with the asperities present on the block. A contact angle of ~155° and a sliding angle of 2.5° was obtained. A high contact angle was obtained as the surface energy of the self-assembled monomolecular layer of the perfluorosilane compound was low due to the low polarizability of C–F bond. Moreover, due to the high bond energy of the C–F bond and short bond length, its interaction with hydroxyl groups was limited. Overall, the coating provided a high waterproofing capability with ~97% reduction in water uptake after 4 days compared to an uncoated block [117].

Design of smart surfaces capable of distinguishing liquids based on their inherent properties finds usage primarily in liquid handling and liquid sequestration applications such as controlling oil spills. The coatings on these surfaces need to be robust, withstand pressure and facilitate oil adsorption while retaining water. Li et al., prepared a superhydrophobic (contact angle of 159°) and superoleophilic cotton (contact angle of

0°) fabric by coating the cotton with octadecyltrimethoxysilane (ODTMS). Silica layer had formed on the fabric's surface after its precursor underwent hydrolysis. ODTMS underwent hydrolysis and condensed on the silica particle surface. The silica particles permeated the cotton fabric such that it adhered onto its surface via surface functional groups. After ODTMS hydrolysis, long-chain alkyl groups were introduced onto the silica surface. This chemical functionalization combined with the nanoscale roughness imparted a highly hydrophobic nature to the fabric surface coated with functionalized silica particles. The coated surface showed excellent hydrophobicity towards different solutions such as acidic, basic, and salt-laden solutions. The hydrophobic silica coating thus displayed high separation efficiency, fast oil capture kinetics, and good recycling efficiency [118].

Silica nanoparticles have also been utilized in the toxic metal adsorption, as reported by Chung et. al. The group employed a hydrothermal route for preparing monodisperse amorphous silica nanoparticles and mesoporous silica nanoparticles in the range 15–60 nm. The experimental analysis determined the surface area of the mesoporous silica nanoparticles to be almost 4 times that of amorphous silica nanoparticles, and more than 70% of it was attributed to the nanopores within mesoporous silica nanoparticles. Amino functionalized surfaces of nanoparticles were employed to adsorb Cr(VI) ions, and it was observed that the rapid adsorption followed pseudo-second-order kinetics. The adsorption kinetics exhibited rapid adsorption of almost 90% Cr(VI) within 1 min. The analysis suggested that the rapid uptake of the metallic ion was partially due to the mixed adsorption-partial reduction system. The amino-functionalized mesoporous silica nanoparticles and amorphous silica nanoparticles displayed a high adsorption capacity of 34 mg/g and 42 mg/g and a high removal efficiency of 62% and 77%, respectively unfunctionalized counterparts. Langmuir model was adapted to elucidate the adsorption isotherm. Thus, this could be an alternative to clean marine pollutants [119].

The development of superhydrophobic coatings also finds utility in marine engineering as they actively participate as coatings for protecting machinery and equipment from getting damaged due to marine biofouling. Philip et al. developed a silica nanoparticles-graphene oxide composite coating for layering titanium surfaces in a related study. The anodized titanium substrate was first electrophoretically coated with the graphene oxide layer. After that, this substrate was immersed in a solution containing silica nanoparticles dispersed in perfluorooctyltriethoxy silane. The silanized silica nanoparticles interact with the hydroxyl and carboxyl groups of the graphene oxide sheet. At higher pH, electrostatic interactions between these two compounds lead to the formation of a superhydrophobic layer on the titanium surface that is more uniform compared to the case wherein the graphene oxide layer is absent. After the coating, the average roughness of the surface went up to 200 nm. These physicochemical characteristics imparted a water contact angle of 173° and a tilting angle of 0°. Experiments conducted in the presence of gram-positive and gram-negative bacteria indicated 3–5 orders of magnitude reduction in bacterial adhesion on the composite coated surface compared to a bare, control sample [120].

Composite silica nanoparticles have also been utilized in pharmaceutical studies involving in vivo analysis. A study by Chen et al., investigated the utility of amino functionalized mesoporous silica nanoparticles as carrier for the drug vancomycin. For in vivo studies, the drug embedded mesoporous silica nanoparticles was attached to thioketal functionalized methoxy polyethylene glycol, which is a reactive oxygen species responsive material. Under physiological conditions, the release rate of the drug can be controlled, and only ~21% drug could released after 36 h. In the absence of any thioketal group, the drug release rate was 10 times higher; thereby, the risk of improper release was high. The group reported that in vivo studies incorporating the composite, the multi-layered drug resulted in a 14–day period for infection treatment. After this time, the tissue was free of disease [121].

1.12 Knowledge gap

As per the world scenario, it is essential to adopt alternative approaches to solve major issues like fossil fuel dependency for energy production and organic waste management. Measures taken will alleviate the severe environmental burden regarding air/water/land pollution generated during their utilization. Moreover, they will also aid in the economic uplifting of many societies as encouragement of non-conventional energy feedstocks will promote grid-parity and a cleaner environment. Considering the above situation, one of the promising approaches being extensively researched in the last few decades concerns biomass technology. On the one hand, effective biomass utilization can significantly aid in waste management, while on the other, it offers a route towards a circular economy. Moreover, it can also generate versatile products like bio-oil (potential energy source), bio-char (adsorbent, soil conditioner), and silica.

The first critical step towards forming a sustainable methodology for the looming problem is the scientifically sound and conscious identification of biomass for further downstream processing. One of the largest rice producers, India generates a huge amount of RH classified as waste. The husk is primarily degraded in the open environment, leading to severe air pollution in many geographical regions [122]. In light of this, the present thesis focuses on the sustainable utilization of waste RH for the production of valuable products like bio-oil, bio-char, and biogenic silica. Reports in the literature highlight the effectiveness of pyrolysis for biomass conversion as it retains an advantage in terms of broad feedstock compatibility and efficient generation of multiple products.

In terms of experimental operation, limited studies employing pyrolysis have utilized optimization tools to maximize their product output. Few have incorporated response surface methodology (RSM) optimization tools in their work. For instance,Singh et al., have studied the pyrolysis of *Acacia nilotica*, under nitrogen environement and designed the pyrolysis process usng RSM coupled with central composite design method. The temperature was found to have maximum effect followed by heating rate, holding time and nitrogen flowrate. Maximum bio-oil yield (33.59 wt %) was obtained at optimal condition of 507.04 °C, 58.25 min, 38 °C/min and 40.52 mL/min [123]. Another study was reported by Te et al., on optimization of pyrolysis process for the production of bio-char from banana peels. The optimum condition for obtaining maximum bio-char yield of 58.8 % was found to be 356.1 °C, 180 min, 14.7 °C/min [124]. A study on fast pyrolysis of barks (forest industry) for the production of phenol rich bio-oil was reported by Ren et al. They found the optimal conditions to be 485 °C, 28 L/min and 0.35 mm particle size for maximum bio-oil yield of 30.42 %. Particle size was found to have the maximum effect followed by gas flow rate and temperature [125]. Hence, it could be inferred that the utilization of an optimization tool eliminates the drawbacks associated with conventional optimization method with a limited number of experiments. Therefore, this thesis focuses on employing RSM with the central composite design (CCD) method to make the process more economical from an industrial perspective. The produced pyrolytic bio-oil may be used for heat/thermal application in industrial burners and process heating. However, prior-art studies reveal that the characteristics of pyrolytic bio-oil are not suitable for use in internal combustion engines. It has high water content (>30%) and a low calorific value of 10–12 MJ/kg with the presence of acids and oxygenated compounds. Therefore, upgradation of bio-oil is necessary to improve the aforementioned characteristics. The upgradation techniques such as hydrodeoxygenation, desulphurization or catalytic pyrolysis are not economically viable and use commercial catalysts that eventually lead to low hydrocarbon and high coke content in the bio-oil. Therefore, catalytic pyrolysis using the bio-char as a catalyst is preferred.This technique addresses the above-mentioned shortcomings and lowers the overall pyrolysis temperature [126]. Therefore, the bio-char produced from slow pyrolysis has been used as an alternative to commercial catalysts. Along with its utility as a catalyst, the bio-char obtained under CO_2 could also be used to obtain functional silica nanoparticles as it finds utility in diverse applications ranging from coating to drug delivery. Optimization of the process variables involved in the generation of silica nanoparticles from biomass can thus aid in providing an economically sustainable, scalable, and environmentally friendly approach.

1.13 Scope and objectives of the thesis

Thus, based on the literature review and knowledge gap, it seems that there is considerable scope for utilizing agro-residual waste, i.e., RH, to produce bio-oil, bio-char, non-condensable gases, and silica nanoparticles through slow pyrolysis. Hence the present study focuses on utilizing this waste to produce value-added compounds. Therefore, this Ph.D. thesis with the title '**Valorization of rice husk for optimal production of bio-oil, bio-char, and silica nanoparticles**' targets the fulfillment of the following primary objectives.

1. Optimal bio-oil production using slow pyrolysis process under inert environment and its upgradation using solvent extraction method.

    i. Physico-chemical characterization of biomass.

    ii. Optimization of process variables such as pyrolysis temperature, holding time, and nitrogen flow rate.

    iii. Upgradation of bio-oil using solvent extraction method and its characterization.

2. Catalytic upgradation of bio-oil using slow pyrolysis process under reactive environment (CO_2).

    i. Optimization of process variables such as pyrolysis temperature, holding time, and carbon-dioxide flow rate.

    ii. Characterization of bio-char.

    iii. Upgradation of bio-oil using catalytic pyrolysis and its characterization.

3. Optimal bio-char production with higher carbon content under both inert (N_2) and reactive (CO_2) environments.

    i. Optimization of process variables such as pyrolysis temperature, holding time, and *nitrogen* flow rate.

    ii. Optimization of process variables such as pyrolysis temperature, holding time, and *carbon-dioxide* flow rate.

iii. Physico-chemical characterization of the produced bio-char under both the environment.

4. Utilization of bio-char produced under a reactive environment to separate ranitidine from synthetic wastewater.

    i. Activation of bio-char using KOH.

    ii. Adsorption kinetics and adsorption isotherm study of the ranitidine adsorption process.

5. Optimal synthesis of silica nanoparticles from bio-char produced during the pyrolysis process under reactive environment and its application towards the preparation of superhydrophobic coatings.

    i. pH optimization of bio-char for producing lower average particle size of silica nanoparticles

    ii. Functionalization of silica nanoparticles to make it superhydrophobic and superoleophilic for cleaning oil spills.

1.14 Organization of thesis

The content of the thesis has been divided into seven different chapters.

Chapter I provides an overview of the current scenario of RH generation and its utilization for bio-oil, bio-char, and other value-added products with state-of-the-art literature. This chapter also contains the formulation of objectives and the thesis layout.

Chapter II discusses details of the materials and methodology employed in this thesis. This chapter provides details of the pretreatment process undertaken before the pyrolysis process. This chapter also contains all the characterization techniques used to estimate RH's physicochemical properties and composition, bio-oil, bio-char, non-condensable gases, and silica nanoparticles. The methodology of the slow pyrolysis process for bio-oil and bio-char from RH is explained in detail in this chapter.

Chapter III focuses on the slow pyrolysis of rice husk for producing bio-oil under an inert environment. The effect of temperature, holding time, N_2 flowrate on the bio-oil yield has been discussed. The upgradation of bio-oil via solvent extraction method has been presented. Also, the physico-chemical properties and the composition of the bio-oil have been elaborated.

Chapter IV focuses on the slow pyrolysis of rice husk under a reactive environment to obtain optimal bio-oil yield. Variation and optimization of different process variables such as temperature, holding time, and CO_2 flow rate regarding optimal bio-oil yield are elaborated. The chapter also contains a catalytic pyrolysis technique to upgrade the bio-oil. Extensive characterization of the upgraded bio-oil has been carried out.

Chapter V highlights the optimization of slow pyrolysis of RH to obtain a significant amount of bio-char with maximum carbon content under inert and reactive environments. The effect of environment on the structural characteristics of bio-char has been discussed with the help of different characterization methods.

Chapter VI deliberates on the utilization of bio-char produced under a reactive environment as an adsorbent to remove pharmaceutical pollutants (ranitidine) from synthetic wastewater. In brief, the chapter discusses the activation of bio-char and its adsorption kinetics. The influence of pH and adsorbent dosage on the pollutant adsorption process has also been presented.

TH-3101_166107009

Chapter VII focuses on producing silica nanoparticles from bio-char obtained under a reactive environment. The chapter also discusses the application of the functionalization particles for selective adsorption of oil from an oil-water mixture.

Chapter VIII summarizes the overall work of the thesis and presents the conclusions drawn from the overall work. It also provides recommendations for future work based on the output of this thesis.

Indian Institute of Technology Guwahati

CHAPTER II

Materials and methods

Materials and methods

Experimental procedures

Physico-chemical pharacterizations of peedstocks and products

Applications

Indian Institute of Technology Guwahati

Chapter II

Materials and methods

In this chapter, the details of experimental procedures for (i) slow pyrolysis of rice husk for the production of bio-oil, bio-char, and non-condensable gases (ii) production of silica nanoparticles (iii) functionalization of silica nanoparticles (iv) application of superhydrophobic and oleophilic silica nanoparticles have been discussed. Response surface methodology (RSM) with central composite design (CCD) was employed to optimize the process variables such as pyrolysis temperature, N_2/CO_2 flowrate, and holding time. This chapter presents details about characterization techniques such as proximate analysis, ultimate analysis, XRD, XRF, TGA, FTIR. The upgradation methodology for improving the bio-oil properties i.e., solvent extraction and catalytic pyrolysis, was elaborately discussed. The procedure for activating bio-char followed by its usage as an adsorbent was also presented in this chapter.

2.1 Materials

The RH of ijong rice cultivar was collected from Six Mile Mill, Assam, India. The collected RH was then washed, dried, and grounded to powder form and sieved (BSS 52 mesh) to obtain a homogeneous particle size of ≤300 µm. Sulfuric acid (≥98%), *n*-hexane (≥99%), ethanol (≥99%), sodium hydroxide pellets, and potassium hydroxide were obtained from Sigma–Aldrich, India. Ranitidine was purchased from MP Biomedicals, 1H, 1H, 2H, 2H-Perfluorodecyltriethoxy silane (PFDS), Tricholorododecyl silane (TCDS), and Stearic acid (SA) of analytical grade with more than 95% purity was purchased from Sigma Aldrich, India. Dichlorodimethyl silane

TH-3101_166107009

(DCMS), and Toluene were obtained from Merck India Pvt. Ltd., and Ethanol (99.9%) was purchased from an analytical reagent. Octadecyltrimethoxysilane (ODTMS) was procured from the Tokyo chemical industry.

2.2 Methods

2.2.1 Compositional analysis of rice husk

The biochemical composition of untreated RH was determined by following the analytical procedures of the National Renewable Energy Laboratory (NREL), namely LAP–002 and LAP–005. The cellulose, hemicellulose, acid-soluble, and insoluble lignin contents were assessed following the NREL/TP–510–42618 protocol [127,128].

2.2.2 Ultimate analysis

The elemental compositions such as carbon, oxygen, hydrogen, N_2, and sulfur in RH samples were determined using CHNS Elemental Analyzer (Eurovector/EA3000). Approximately 1 mg sample was completely combusted in pure oxygen, resulting in different gases such as CO_2, H_2O, N_2, and SO_2. The analysis of these gases (mole counts) provides elemental compositions. The percentage of oxygen was calculated by difference (i.e., O = 100– (C+H+N+S+ash)).

2.2.3 Proximate analysis

This analysis is the most widely used method for solid and liquid fuels characterization, such as moisture content (MC), ash content (AC), volatile matter (VM), and fixed carbon content (FC). For each analysis, the crucible was dried at respective operating temperature (i.e., for moisture content at 105±1 °C for 6 h, ash content at 810±25 °C for 4 h, and volatile matter at 910±25 °C for 10 min) and placed in a desiccator.

2.2.4 Calorific value

A Toshniwal bomb calorimeter was used to measure the biomass's calorific value (CV) (IS 1350-1, India). The biomass sample pellets weighing 1 g each were put in contact with the platinum wire attached with cotton thread placed in the ignition port. 1 L of millipore water was added to the bomb and then filled with 20 bar oxygen. The bomb calorimeter was submerged in the Millipore water, and the calorimeter jacket was maintained at 25 °C by circulating water. In the isothermal jacket, a calorimeter was placed with a 10 mm air gap between surfaces. The ignition energy when discharged from about 40 V platinum wire was evaluated from the variation in potential throughout a 1256 or 2900 μF capacitor.

2.2.5 Thermogravimetric (TG) analysis

TG technique provides a measurement of weight loss of the sample as a function of temperature and time. This technique is used continuously to monitor the physical and chemical changes of a sample that occur with an increase or decrease in the temperature of the sample. Mass loss observed in the TGA can be directly related to the thermal stability and volatility of the sample. TGA experiments were performed from ambient temperature to 1000 °C at a heating rate of 10 °C/min, and an inert gas (N_2) was used as a purge gas.

2.2.6 X-ray fluorescence (XRF) analysis

The XRF analysis of RH and bio-char was conducted at National Centre for Earth Science Studies (NCESS), Thrissur using Bruker (Model-S8 Tiger and S4 Pioneer) sequential wavelength dispersive X-ray spectrometers.

2.2.7 X-ray diffraction (XRD) analysis

XRD analysis of the sample was recorded by Bruker D8 (Model-D8- Advance) advance diffractometer with Cu-Kα radiation at 45 kV and 40 mA. The substrate holder along with the sample, underwent a tilt in the range 5°–90° (2θ angle) with 0.04° step size as it was subjected to X-ray radiation. The scanning speed employed for measurement was 2°/min. The crystallinity index (CrI (%)) of the raw and acid-treated RHs was determined using the following equation:

$$CrI(\%) = \frac{I_{002} - I_{am}}{I_{002}}, \qquad 2.1$$

where, I_{002} corresponds to the maximum intensity of the diffraction plane (0 0 2) at θ=22° and I_{am} indicates the minimum intensity of the amorphous region at θ=18°.

2.2.8 Fourier transform infrared (FT-IR) spectroscopy

Infrared spectra of the samples were measured using FT-IR analyzer (Shimandzu: IR Affinity) with attenuated total reflection (ATR) using air as background to identify the characteristic functional groups. All the ATR spectra of the samples were recorded in the scanning range of 5000–600 cm^{-1} for 30 repeated scans at a spectral resolution of 4 cm^{-1}. The spectra were recorded in transmittance mode.

2.2.9 Field emission scanning electron microscopy (FESEM) analysis

The morphology of different samples was characterized with FESEM (Zeiss, Sigma, Germany). The sample was deposited on the carbon tape and attached to the metallic stub, mounted on a sample holder. The samples were subjected to gold coating to reduce charging. Thereafter, the image analysis was performed on the gold-coated samples to understand the morphology and surface characteristics of the deposited material.

2.2.10 Energy dispersive X-ray (EDX)

The powder samples were spread on the conductive carbon tape attached to the sample holder (stub). It was thereafter coated with gold to reduce sample charging. Once the sample was loaded into the instrument, its imaging as well as elemental analysis was carried out using FESEM-EDX Zeiss (Model: Sigma). The elemental analysis aided in the identification of the different elements present close to the sample surface.

2.2.11 Atomic force microscopy (AFM)

The functionalized silica nanoparticles sample in ethanol was drop casted on 1 cm × 1 cm glass substrate and then dried. The AFM spectra of the coated glass substrate were recorded using a Bruker AFM system (Model: Innova). The AFM scan revealed the texture of the coated functionalized silica nanoparticles surface along with its roughness.

2.2.12 Brunauer-Emmer-Teller (BET) surface area analysis

The sample's total surface area, pore size, and pore size distribution were calculated via Quantachrome (Model: Autosorb-IQ MP) using N_2 adsorption. BET analysis was carried out for the feedstock, and bio-char was obtained at different temperatures to analyze their BET surface area and pore size.

2.2.13 Pretreatment procedure

The biomass was treated using dilute sulfuric acid to leach out the inorganics. The washed, dried and sieved RH was loaded in an autoclave reactor at 1:20 (w/v) solid to liquid ratio. Sulfuric acid with molarity of 0.4M was prepared and utilized for pretreatment. The pretreatment process was carried out at 121 °C for 2 h. After the pretreatment, the biomass was filtered and then oven-dried at 40–50 °C for 8 h to obtain the acid-treated biomass.

2.2.14 Rice husk pyrolysis

20 g of acid-treated biomass was loaded in a 100 mL batch pyrolysis reactor (3.8 cm i.d. × 8.1 cm length). Experiments were performed by varying the process variables such as temperature, gas flow rate, and holding time. N_2 gas was selected to maintain an inert environment inside the reactor. The N_2 gas flow rate was controlled using a rotameter while a PI controller maintained the temperature and holding time at the desired levels. All the experiments were carried out in the batch pyrolysis reactor with a total heating rate of 10 °C/min. The thermocouple was deployed to detect the temperature changes inside the reactor. The vapors generated from the reactor were passed onto the condenser to trap the liquid (bio-oil). The schematic diagram of the experimental setup is shown in Figure 2.1. After every experiment, the reactor was washed with distilled water before the next run-in to avoid choking.

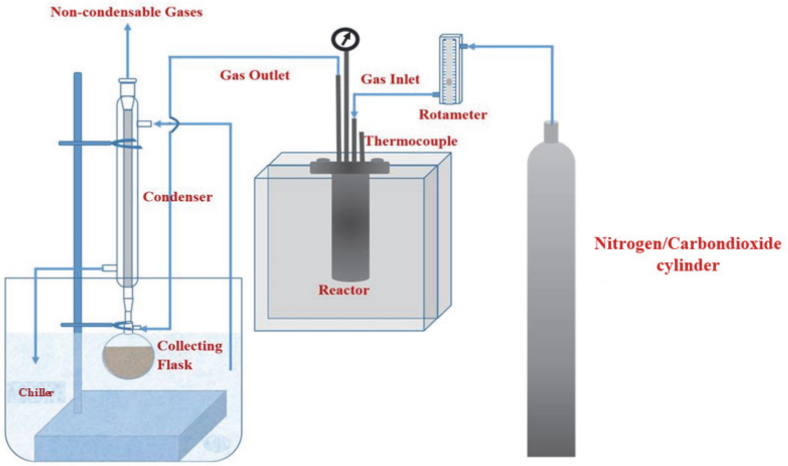

Figure 2.1. Experimental setup of slow pyrolysis of biomass under inert and reactive environment.

The yield of bio-oil, bio-char, non-condensable gas, and biomass conversion (into oil and gas) [129] has been calculated using the following equations:

$$Bio-oil\ yield\ (\%) = \frac{mass\ of\ bio-oil}{mass\ of\ biomass} \times 100 \qquad 2.2$$

$$Bio-char\ yield\ (\%) = \frac{mass\ of\ residue}{mass\ of\ biomass} \times 100 \qquad 2.3$$

$$Biomass\ conversion\ (\%) = \frac{decrease\ in\ weight\ of\ reaction\ mixture}{mass\ of\ biomass} \times 100 \qquad 2.4$$

$$Non-condensable\ gas\ (\%) = 100-(bio-oil+bio-char)\ yield \qquad 2.5$$

2.2.15 Design of experiments (DOE) using RSM

The preliminary experiments were carried out to find the operating range of independent variables; for that reason, a few initial experiments were conducted by

TH-3101_166107009

varying one variable at a time and keeping others at a constant value. The selection of variables and their efficiency for bio-oil yield was considered after an extensive review of the literature. The RSM technique was used to analyze the preliminary experimental data obtained from the pyrolysis process. Design expert software® trial version 7 (Stat–Ease, inc., Minneapolis, MN, USA) was used for regression and graphical analysis of the results obtained from the pyrolysis process. The statistical analysis was carried out based on the relationship between the coded (Z_i) and the real (X_i) values according to the following equation [130].

$$Z_i = \frac{X_i - X_o}{\Delta X_i}, \qquad i = 1,\ 2\ and\ 3 \tag{2.6}$$

Where, Z_i: the dimensionless coded value of an independent variable,

X_i: corresponding real value of the independent variable,

X_o: the real value of an independent variable (X_i) at the center point,

ΔX_i: step change of uncoded variable i.

Each variable was varied over three points. The system can be explained by a second-order polynomial model, which represents the response as a function of independent variables [130].

$$Y = \beta_o + \sum_{i=1}^{n} \beta_i X_i + \sum_{i=1}^{n} \beta_{ii} X_i^2 + \sum_{i=1, i<j}^{n} \sum_{j=1, i\le j}^{n} \beta_{ij} X_i X_j + \varepsilon \tag{2.7}$$

Where, Y is the predicted response,

β_o: constant intercept

β_i: coefficient of the linear term

β_{ii}: coefficient of quadratic term

β_{ij}: coefficient of the interaction term

X_i and X_j: uncoded independent variable

ε : experimental error.

The variables *i, j, k,* and *n* are integers. When $i<j$, β_{ij} represents the interaction effects of the variables X_i and X_j. Model's statistical significance was evaluated by ANOVA test using probability value ($p<0.05$ and Fisher's Satirical test (F–test)). Also, the regression coefficient (R^2) value pointed towards the competence of fitting between the predicted and experimental responses.

Based on the preliminary experiments, the specific range of each variable was fixed for the three different objectives.

2.2.16 Upgradation techniques

2.2.16.1 Solvent extraction

A single-stage solvent extraction procedure was employed to enrich bio-oil quality by using different organic solvents (OS) – hexane, ethyl acetate, and acetone. Equal volumes of as-obtained bio-oil and OS were mixed in a flask by keeping it in a shaker rotating at 120 RPM for 12 h. After that, the mixture was filtered, and OS-extracted bio-oil was then transferred to a rotavapor unit (Buchi-300, Switzerland) to remove the solvent from the bio-oil. The percentage of extraction was calculated using the following equation.

$$\%\,Extraction = \frac{mass\ of\ recovered\ bio\text{-}oil}{mass\ of\ optimized\ bio\text{-}oil} \times 100 \qquad 2.8$$

2.2.16.2 Catalytic pyrolysis

The in-situ catalytic upgradation procedure included the addition of the bio-char to the RH in three different proportions i.e., 25 wt% (C_1), 33 wt% (C_2), and 50 wt% (C_3). These mixtures were then pyrolysed at the optimal conditions to achieve maximum bio-oil yield. The obtained upgraded bio-oil was thereafter subjected to extensive characterization to understand the effect of adding catalyst on upgraded bio-oil properties.

2.2.17 Kinematic viscosity

Rheological analysis of all the samples was performed using Interfacial Rheometer (Anton-Paar Model: MCR 301) at 40 °C and a constant shear rate of 5/s. The thermostatic water bath was used to control the working temperature within the set range of 40–100±0.1 °C. Approximately 0.6 mL sample volume was used for the rheology study. The sample was analyzed using a plate (PP 50, Dia.: 50 mm) and plate (INSET I-PP 80/SS, Dia.: 80 mm) system. The sample temperature was maintained constant within ±0.1 °C. The measurements were triplicated, and the average values were reported.

2.2.18 Cold flow properties by differential scanning calorimetry (DSC)

Pour point (PP) was measured to determine the low-temperature flow properties, and it was a rough indication of the lowest temperature at which the sample could be pumped. The present study determined PP by adopting the DSC technique (Model: 201 F1 Phonix; Make: Netzsch, Germany). 3 to 5 mg sample was taken in a 40 µL sealed pan under the N_2 flowrate of 0.04 L/min. A temperature program with four sequential active steps was used, in which the sample was heated from room temperature (RT) to 50 °C at 5 °C/min at a constant heating rate. Then it was held at 50 °C for 5 min (isothermal condition) to homogenize the sample. After that, it was cooled from 50 °C to (–30 °C) at 5 °C/min and continued at the same temperature for 5 min in order to complete the crystallization process. After that, the sample was heated from (–30 °C) to 50 °C at a heating rate of 5 °C/min, DSC measurements were repeated twice, and the average values were reported.

2.2.19 pH, water content and acid value

The pH of the bio-oil was detected using a digital meter (Eutech pH 700). To determine the bio-char's pH, the bio-char sample in 1:20 w/v ratio was dispersed in distilled water. The sample was kept in a shaker for 12 h at 120 RPM, and pH was measured using pH strips. The water content in bio-oil was determined by a Karl Fischer titrator (KF-878, Metrohm, Switzerland). The sample was dissolved in KF methanol, and iodine was added to the KF reagent. The endpoint was determined potentiometrically. The acid value of bio-oil was determined by ASTM D974 method.

2.2.20 GC and GC–MS analysis

GC analysis was carried out to identify the composition of non-condensable gases. Perkin Elmer Clarus 590 GC equipped with a TCD was used. The oven temperature was initially kept at 50 °C for 2 min, thereafter it was raised to 100 °C at 10 °C/min. The final temperature was maintained for 25 min. The injector and detector temperature was maintained at 200 °C with N_2 flowrate of 0.03 L/min.

Perkin Elmer Clarus 680 GC equipped with a MS detector 600C was used to identify the compositions of bio-oil. The column temperature was heated from RT to 40 °C. The temperature was maintained for 4 min. Then, the temperature was ramped to 280 °C at a rate of 50 °C/min. The final temperature was maintained for 15 min. Helium was used as carrier gas at a flow rate of 0.01 L/min. The ion source temperature was set at 270 °C; MS detector was operated in the full scan mode in the range 45 to 400 M/Z. The constituents present were identified by comparing the mass spectra with the research library.

2.2.21 Bio-char activation

Initially, 2 g of bio-char produced under reactive environment was mixed with 500 mL 2 N KOH solution and stirred for 1 h. After that, it was filtered using Whatman filter paper-1. In a washing step, the retentate was mixed with deionized water, and the solution was stirred, followed by the addition of 0.1 N HCl to neutralize the mixture. Then, it was again filtered, and the obtained bio-char was dried at 105 °C for 24 h [131].

2.2.22 Batch adsorption studies

Based on the initial characterization (surface area) the activated bio-char prepared at 500 °C ($ARHB_{500}$) was chosen as the preliminary adsorbent for the adsorption studies. Batch adsorption of ranitidine was carried out in a shaker wherein 100 mg of the activated bio-char was mixed with 100 mL ranitidine solution of concentration 50 mg/L (for each case study). The study investigated the effect of various process variables like adsorption time (2–140 min), solution pH (3, 5, 7, 9, and 11), and pyrolysis temperature ($ARHB_{300}$, $ARHB_{500}$ and $ARHB_{700}$) on the adsorption capacity of the prepared activated bio-char. The ranitidine removal (R%), adsorption capacities (mg/g) at equilibrium, and at a time ‘t’ were calculated using Equations (2.9), (2.10), and (2.11), respectively [132].

$$R(\%) = \frac{C_o - C_e}{C_o} \times 100 \tag{2.9}$$

$$q_e = \frac{V}{m}(C_o - C_e) \tag{2.10}$$

$$q_t = \frac{V}{m}(C_o - C_t) \tag{2.11}$$

Here, C_o (mg/L) and C_e (mg/L) are ranitidine's initial and equilibrium concentrations in the solution, respectively. q_e (mg/g) is the equilibrium adsorption capacity. C_t (mg/L) and q_t (mg/g) are the concentration of ranitidine in solution and adsorption capacity at time t, respectively. V (L) is the volume of solution taken for each adsorption experiment, and m (g) is the adsorbent dosage.

Table 2.1. Kinetic models.

Model [133][134]	Equation
Pseudo first order	$\log(q_e - q_t) = \log q_e - \frac{k_1 t}{2.303}$
Pseudo second order	$\frac{t}{q_t} = \frac{1}{k_2 q_e^{\ 2}} + \frac{t}{q_e}$
Elovich	$q_t = \frac{\ln(a_e b_e)}{b_e} + \frac{1}{b_e}\ln(t)$
Intra particle diffusion	$q_t = k_{id}(t)^{0.5} + c$

Table 2.2. Adsorption isotherm models.

Model	Equation
Langmuir [133][134]	$\frac{C_e}{q_e}=\frac{1}{bQ_m}+\frac{C_e}{Q_m}$
Freundlich [133][134]	$\log q_e=\log k_f+\frac{1}{n}\log C_e$
Temkin [133][134]	$q_e=B\ln k_t+B\ln C_e$
Sip's [135]	$\frac{1}{q_e}=\frac{1}{Q_{\max}K_s}(\frac{1}{C_e})^{\frac{1}{n}}$

2.2.23 Ultraviolet (UV) spectroscopy

The ranitidine concentration was measured by a UV-Vis spectrophotometer (Shimadzu UV 2600). The measurements were carried out at a wavelength of 313 nm [132], utilizing an established calibration curve of ranitidine in the concentration range of 5–100 mg/L.

2.2.24 Preparation of silica precursor

Rice husk was pretreated with dilute sulfuric acid (0.1 M) to leach out the inorganics. The pretreated RH was then pyrolyzed under a carbon dioxide (CO_2) environment at three different temperatures, i.e., 300, 500, and 700 °C at a constant holding time of 45 min and CO_2 flowrate 1.1 L/min. The obtained bio-char was further utilized to prepare silica nanoparticles.

2.2.25 Preparation of silica nanoparticles at different pH

The obtained bio-char was adjusted to different pH 3, 5, 7, and 9. Bio-char was treated with 0.1M H_2SO_4 with the loading of 1:20 (w/v) and was kept in an incubator shaker

Indian Institute of Technology Guwahati

for 24 h at 30 °C and 120 RPM to adjust the pH. Then, the respective bio-char was heated in a muffle furnace (oxygen-free environment) at a rate of at 10 °C/min, from room temperature to 610 °C for 4 h. The calcination process was performed to remove the carbon content and other volatiles to obtain silica nanoparticles.

2.2.26 Functionalization of silica nanoparticles

The silica nanoparticles were further modified using PFDS, TCDS, ODTMS, DCMS, and SA. Ethanol was used as the solvent for each of the modifiers. 40 mg of silica nanoparticles was added to modifier/ ethanol mixture (volume ratio: 2:100 mL) and stirred for 1 h at 1200 RPM at 80 °C. The modified silica nanoparticles was further coated on glass side and cotton fabrics and characterized to understand the functionalities of the modified particles.

2.2.27 Separation efficiency of the coated substrate

The functionalized silica nanoparticles were coated on the cotton fabric. The cotton was utilized as a membrane to separate oil from oil-water mixture. The separation efficiency of the cotton membrane was calculated according to the following equation

$$Separation\ efficiency\ (\eta)\% = \frac{Final\ volume\ of\ \ oil\ separated\ (ml)}{Initial\ volume\ of\ \ oil\ (ml)} \qquad 2.12$$

CHAPTER III

Optimal production of bio-oil using slow pyrolysis process under inert environment and its upgradation using solvent extraction method

---

Effect of process variables on bio-oil production

Optimization of slow pyrolysis process using RSM

Bio-oil upgradation using solvent extraction

Physico-chemical characterization of upgraded bio-oil

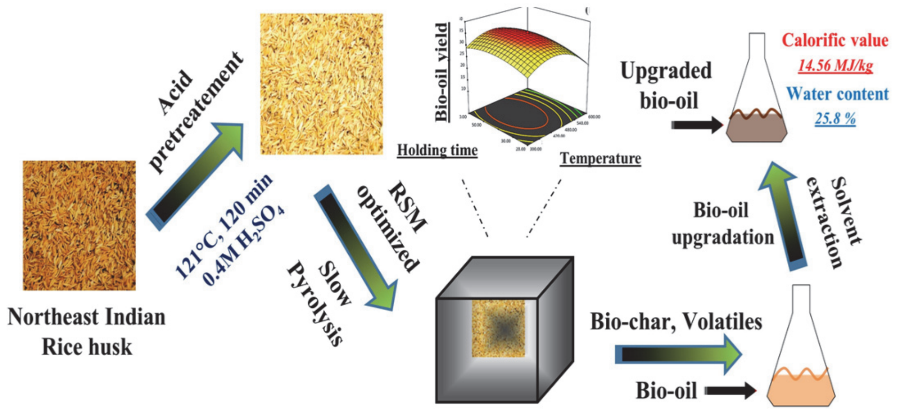

भारतीय प्रौद्योगिकी संस्थान गुवाहाटी • Indian Institute of Technology Guwahati •

Chapter III

Optimal production of bio-oil using slow pyrolysis process under inert environment and its upgradation using solvent extraction method

The present work highlights the thermal decomposition of acid pretreated RH using slow pyrolysis to produce useful and valuable products. At first, the biomass sample was systematically characterized. The sample with higher volatile matter content and reduced metallic contaminants was pyrolyzed, and the process was optimized using CCD followed by RSM to achieve maximum bio-oil yield. A quadratic model was developed based on the analysis of variance (ANOVA) to determine the trend and relationship between the experimental responses and the process variables, mainly temperature, N_2 flowrate, and holding time. Temperature showed the maximum effect, followed by holding time and N_2 flowrate. Optimum conditions for the process were found to be 427 °C, 0.8 L/min, and 45 min, which resulted in the maximum bio-oil yield of 35.5 wt% with biomass conversion of 50.8 wt%. Acid pretreatment was carried out to remove inorganics, which otherwise would have led to the formation of low molecular weight compounds in the bio-oil. The optimized bio-oil was further subjected to solvent extraction to improve its quality in terms of low water content (25.8 wt%) and high calorific value (14.56 MJ/kg). The upgraded bio-oil was thoroughly characterized and contained a complex mixture of acids, phenols, aromatics, esters, and other substances.

3.1 Characterization of rice husk

The biomass sample (i.e., RH) used in the present study was characterized by performing proximate and ultimate analysis. It is an efficient conventional way to evaluate the quality of agricultural residues for biofuel and biochemical production. Before conducting the proximate and ultimate analysis, RH was acid-treated in an autoclave (0.4 M H_2SO_4, 121 °C, 1.03 bar, 120 min). The untreated and acid-treated samples were analyzed for their inherent moisture content (8.8% and 9.4%, respectively), as they are directly related to water content in the bio-oil and its calorific value. The volatile matter, which is another critical parameter to consider, was present mainly in gas and hydrocarbons form, which could be devolatilized readily than solid fuel. The acid-treated sample contained higher volatile matter (57.8%) than the untreated one, indicating the positive effect of acid treatment on biomass composition. This also favored the bio-mass to bio-oil conversion%, as biomass containing higher volatile matter and lower fixed carbon produces a significant quantity of bio-oil. The bulk density of acid-treated RH improved to 210 kg/m^3 from 160 kg/m^3. The comparative evaluation of elemental analysis of both the sample by atomic absorption spectroscopy (AAS) revealed a substantial decrease in the mineral concentration after the acid-treatment, i.e., 33 ppm of K, 36 ppm of Fe, 27.6 ppm of Zn, 15.3 ppm of Pb and 58.3 ppm of Cd (Table 3.1). During the acid-treatment process, this can be attributed to substantial leaching of inorganics, particularly Fe, K, and Ni metal ions. Hong *et al*., have reported that acid pretreatment reduces the concentration of metal ions which subsequently enhances the volatile matter content. This also improved the bio-oil yield and reduced the extent of secondary reactions [136].

The acid treatment mainly leached out the metal ions but did not affect the silica, which is the main component of the ash and can be evidenced from the ash component of RH before and after pretreatment. The composition of metal oxides was determined by XRF analysis, as shown in Table 3.1. It could be observed that the pretreatment increased the silica content from 84.8 wt% to 96.5 wt% as a result of the reduced inorganic content in the acid-treated sample.

The detailed results of the proximate, ultimate analysis and the metal compositions (detected by atomic absorption spectroscopy (AAS)) are shown in Table 3.1. The conversion efficiency of RH to bio-oil or other value-added chemicals was related to the presence of chemical constituents such as cellulose, hemicellulose, and lignin. The RH sample used in the present study contained 32 wt% cellulose, 15 wt% hemicelluloses, and 23.5 wt% lignin. Higher cellulose and hemicellulose content as compared to other biomasses such as corn leaves, switch grass and hazelnut shells, make RH a potential source for the production of bio-oil or other value-added products. The acid-treatment of the sample mainly degraded the hemicellulose content to 9.8 wt%. Apart from the proximate and ultimate analysis, it was also necessary to characterize the samples using other techniques such as TGA, FT–IR, and XRD analysis.

TH-3101_166107009

Table 3.1. Characteristics of rice husk.

	Rice husk	**Acid-treated rice husk**
Proximate analysis		
Moisture (%)	8.8±1.3	9.4±1.3
Volatile matter (%)	52.7±1.5	57.8±1.3
Ash (%)	18±2	17±1
Fixed carbon (%)	20.5±1.8	17.7±3.1
Ultimate analysis		
C (%)	40.6	41.4
H (%)	4.2	4.4
O (%)	54	53.2
N (%)	1.2	0.9
S (%)	–	–
HHV (MJ/kg)	12.2	12.8
Inorganic metal concentration (ppm)		
Fe	178.7±6	36±6
K	357±5.8	33±3.8
Zn	55.7±5.5	27.7±2.5
Ni	25±3.6	0
Pb	26.7±4.1	15.3±3.5
Cd	81.7±5	58.3±6.1
XRF analysis (wt%)		
SiO_2	84.8	96.5
Na_2O	0.6	0.19
MgO	0.9	0.15
Al_2O_3	1.16	0.6
P_2O_5	2.7	0.17
SO_3	2.5	1.6
Cl	0.7	0.1
K_2O	3.8	0.1
CaO	0.9	0.08
TiO_2	0.08	0.07
Fe_2O_3	1.7	0.2

3.1.1 TGA analysis

TGA analysis was carried out to study the thermal degradation behavior of acid-treated biomass, and the obtained results are shown in Figure. 3.1. The efficacy of biomass conversion to bio-oil depends on the degradation of these individual components. The initial weight loss from ambient temperature to 110 °C could be due to the removal of physically adsorbed water and lower molecular weight volatiles. The hemicellulose and cellulose degraded in the temperature range 200–350 °C and 300–375 °C, respectively, and lignin being thermally more stable, continued to degrade up to 500 °C [137][138]. The active thermal region depicts that decomposition and volatilization occur in a single stage. The higher molecular weight constituents decomposed to lower molecular weight constituents, which underwent volatilization. Approximately 38 wt% of biomass was left as residue even at 800 °C. This shows that the biomass contained a high amount of ash. Also, in case of acid-treated biomass, it can be observed that the degradation started slightly at a lower temperature, contributing to the economy of the process [139]. Thus, TGA analysis aided in determining the operating range for the preliminary experiments that were performed for the pyrolysis process and suggested the temperature range required for RSM designing. The onset temperature values for RH was found to be 350 °C, which is similar to results reported for wheat straw (350 °C) [140], corn stover (325 °C) [141].

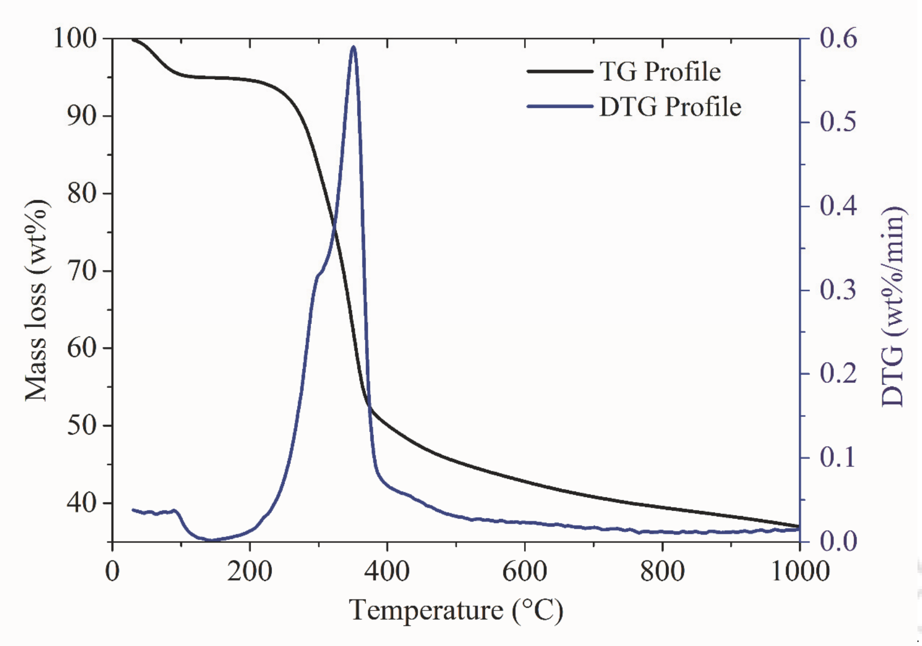

Figure 3.1. TG and DTG profile of acid-treated rice husk.

3.1.2 FT-IR analysis

FT-IR analysis of the untreated and acid-treated biomass was performed to compare the distribution of functional groups, and the results have been shown in Figure. 3.2. Initial water content is confirmed by the presence of a stretching band between 4000–3400 cm^{-1} (O–H group stretching). This broad peak also confirms the O–H stretching band of the silanol Si–OH groups present on the silica surface [138]. The peak at 1640 cm^{-1} confirms the presence of cellulose, which can be ascribed to the bending of the hydroxyl group and stretching of hydrogen bonds associated with cellulose structure. The peak at 1380 cm^{-1} in the acid-treated biomass could be due to the change in the C–H group after acid treatment. The absorption band at around 800 cm^{-1} is present in both raw and acid-treated biomass, which corresponds to the typical cristobalite phase of silica [138]. This indicates that acid pretreatment did not affect the silica structure of RH [142].

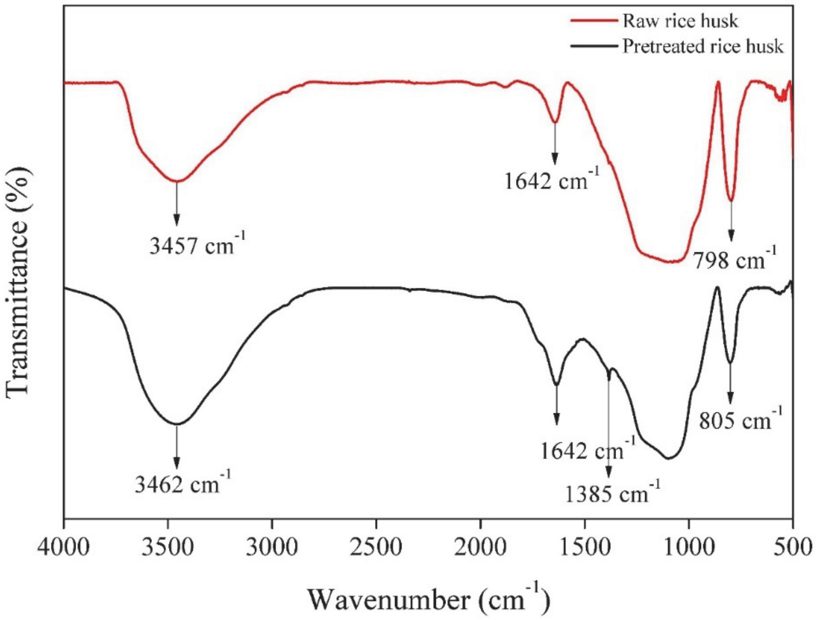

Figure 3.2. FT–IR spectra of raw (untreated) and acid-treated rice husk.

3.1.3 XRD analysis

The sample was also analyzed using XRD, and the results have been shown in Figure. 3.3. The analyzed sample exhibited an increase in crystallinity from 31.87% to 40.83% after acid treatment, which attributes to the decomposition of the amorphous part of the biomass (hemicelluloses) to simple reducing sugars [143]. The pretreatment results also showed a positive effect on the calorific value, as it increased from 12.1 to 12.7 MJ/kg [144]. Comparable results were also reported by Cen et al., [84] and Zhang et al., [145] on the rice straw and RH, respectively. According to the literature, although metal content in the biomass is limited, it displays catalytic activity upon interaction with the vapors during pyrolysis. Subsequently, it increases the overall bio-char and gas yield, respectively [146]. This could probably explain the enhancement in bio-oil yield by separating inorganics after the acid-treatment process. A similar trend was noticed in the present work as the bio-oil yield increased from 32 to 35.5 wt% after the pretreatment.

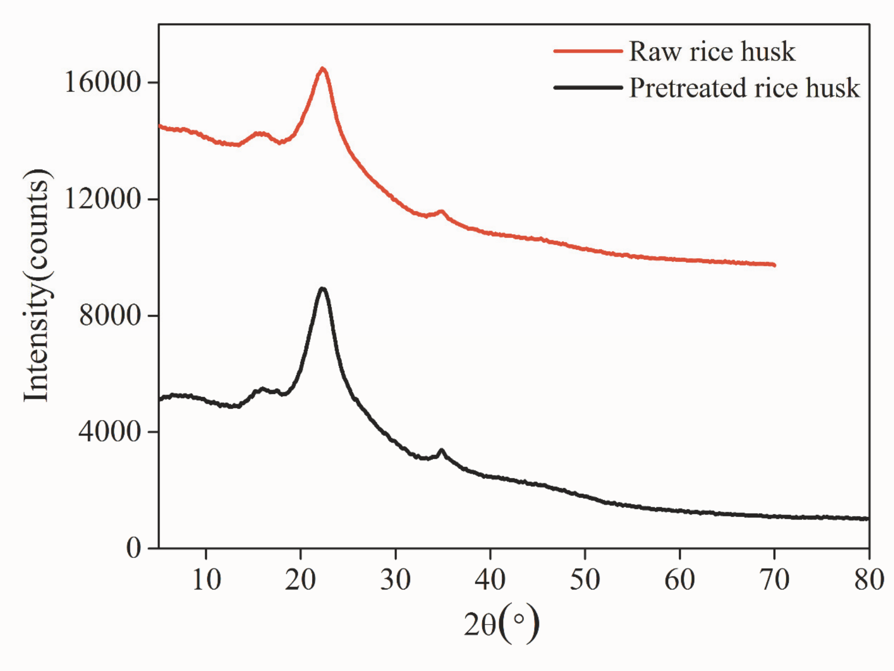

Figure 3.3. XRD spectra for raw (untreated) and acid-treated rice husk.

3.2 Selection of process variables

Pyrolysis of lignocellulosic biomass is a complex process that depends on many factors such as temperature, pressure, holding time, heating rate, condensate temperature, flow rate of inert gas, etc. Some of these process variables show significant effects, while others may not significantly impact the pyrolysis process. However, based on the literature [141,147], temperature, holding time, N_2 flowrate, and heating rate played a significant role in the slow pyrolysis of biomass to maximize the bio-oil yield. The present study employed a slow pyrolysis process with a fixed heating rate of 10 °C/min to maximize the bio-oil yield using acid-treated biomass. To analyze the effect of thermal degradation on the acid-treated rice husk, TGA was carried out, and the results obtained have been presented in Figure. 3.1. The result showed that the onset temperature, i.e. the temperature at which the conversion of volatiles began, was 350 °C. It also confirmed that the decomposition was not significant beyond 600 °C, but the analysis continued up to 800 °C. Based on the above analysis, the operating range of temperature and holding time was fixed as 300−600 °C and 20−60 min, respectively. Similarly, based on the earlier published literature [145,148], the N_2 flowrate range was fixed as 0.8−1.5 L/min. Therefore, to cover the significant range of biomass degradation, the above-mentioned process variables were chosen for further experimentation and the preliminary results are reported in the section below.

3.3 Preliminary experimental data

3.3.1 Effect of temperature

To determine the effect of temperature on the bio-oil yield, preliminary experiments were carried out at a constant N_2 flowrate of 0.8 L/min and holding time of 60 min, respectively. Figure. 3.4 (a) shows the effect of the temperature on the product yield. From Figure. 3.4 (a), it can be seen that the bio-oil yield increased with an increase in the temperature up to a specific range and decreased thereafter. A significant change was noticed in the bio-oil yield (27% to 34%) when the reaction temperature increased from 300 to 400 °C, while bio-char yield decreased from 55 to 48%, respectively. Further, an increase in the temperature to 500 °C reduces both the bio-oil (32%) and bio-char yield (45%), which can be attributed to secondary cracking reactions of the

TH-3101_166107009

pyrolysis gases at elevated temperatures. As the decrease in bio-oil yield was not significant at 500 °C, hence another experiment was performed at a higher temperature, i.e., 600 °C wherein a considerable drop in bio-oil (24.8 wt%) was observed confirming the conversion of all the volatiles, which is consistent with the literature [141,149]. The increase in bio-oil yield up to 400 °C was attributed to the generation of the maximum amount of volatiles; however, the further increase resulted in secondary cracking reactions, which reduced the bio-oil yield and subsequently increased the gas yield to 40.3 wt% at 600 °C. Also, the highest bio-char yield at 300 °C was due to the insufficient decomposition of the pretreated biomass as its onset temperature was found to be 350 °C (Figure. 3.1). The reduction in bio-char yield at 600 °C (35 wt%) was mainly due to the initiation of secondary cracking reactions. Hence, 400 °C was set as the fixed operating temperature for further pyrolysis experiments.

3.3.2 Effect of holding time

The effect of holding time on bio-oil yield was investigated at 400 °C and a constant N_2 flow rate of 0.8 L/min. The minimum bio-oil yield of 21 wt% with a corresponding bio-char yield of 55 wt% was observed at 20 min holding time (Figure. 3.4 (b)). Further increase in the holding time to 40 min resulted in 32.8 wt% of bio-oil and 49 wt% of bio-char yield. After that, both the bio-oil and bio-char yield decreased to 27 wt% and 47.7 wt% at 60 min pyrolysis time, whereas the gas yield increased by 7 wt%. This could be because of the initiation of secondary cracking, which increased the gas yield. Also, since most of the volatiles would have converted to bio-oil at around 40 min, the reaction time period would have favored the secondary cracking reactions resulting in decreased bio-char yield. These results were in accordance with the reports documented by Acikalin et al. They varied the holding time from 10 to 50 min and obtained the maximum bio-oil yield of 53.08 wt% at 20 min interval [147].

3.3.3 Effect of nitrogen flowrate

A pyrolysis experiment was set up to check the effect of N_2 flowrate on the bio-oil yield by keeping temperature and holding time fixed at 400 °C and 40 min, respectively. The yield of bio-oil with respect to the flow rate is depicted in Figure. 3.4 (c). Figure. 3.4 (c) shows the marginal difference in the bio-oil yield when the N_2 flow rate was increased from 0.8 to 1.5 L/min, with the maximum bio-oil yield (32 wt%) attained at 1.2 L/min. The slight reduction in the bio-oil yield and subsequent increase in the gas yield with increasing N_2 flowrate could be due to the insufficient quenching of the volatiles [150]. In the case of bio-char, the maximum yield of 49.8 wt% was observed at 0.8 L/min. The bio-char yield was found to decrease (i.e., 47.3 wt%) with an increase in the N_2 flowrate to 1.5 L/min, which is consistent with the literature [150]. The pyrolysis gas concentration becomes relatively low with an increase of N_2 flowrate in the pyrolysis chamber. The vapors are rapidly pushed out to the condensing zone, reducing the vapor residence time. Thus, it restricts the initiation of repolymerization and hence lowers the bio-char yield [149].

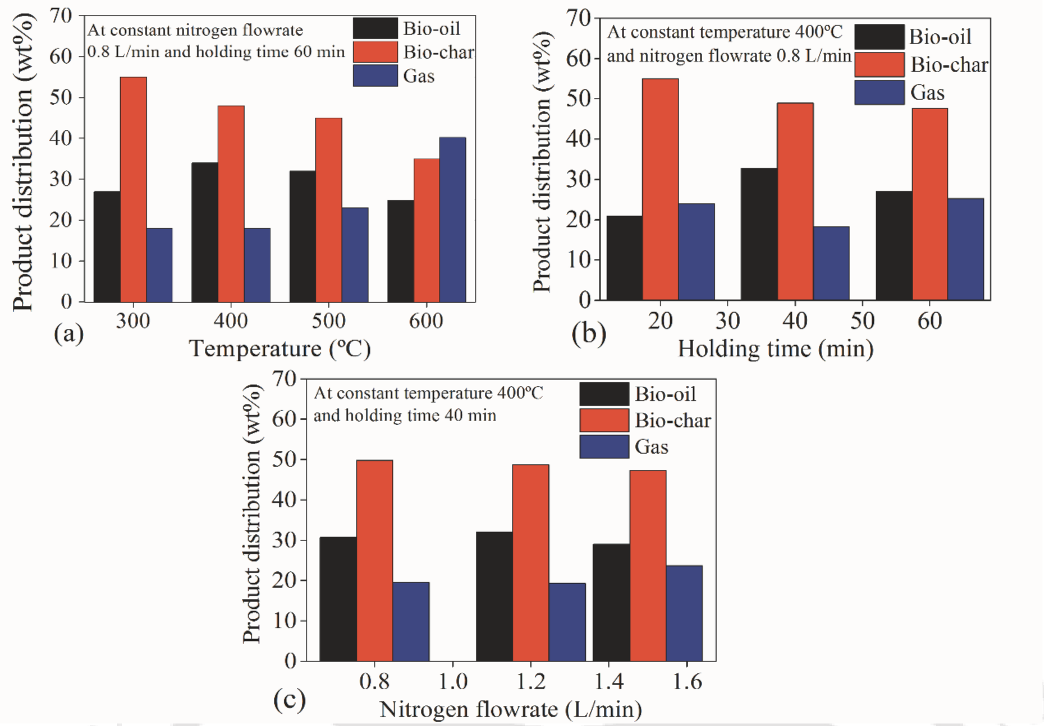

Figure 3.4. The individual effect of process variables (a) temperature, (b) holding time, and (c) nitrogen flowrate on the bio-oil yield during slow pyrolysis of pretreated rice husk.

3.4 Optimization of process variables by RSM

3.4.1 ANOVA and fitting quadratic model

The experimental and model-predicted data are shown in Table 3.2. The effect of independent variables on the bio-oil yield during biomass pyrolysis can be evaluated from the F-test of ANOVA as represented in Table 3.3. From the table, it can be inferred that the experimental and predicted (Figure 3.5) values of bio-oil yield are in good agreement. In the 20 sets of experiments, the bio-oil yield varied in the range of 11.5 to 35.6%. The significance of the model and each process variable was evaluated on the basis of p-value and F-value. The importance of factors was based on the F or p-value, i.e., the greater the magnitude of F-value and correspondingly smaller the “prob>F” value, the more significant is the corresponding coefficient [151]. The ANOVA of the suggested model was analyzed and shown in Table 3.3. From the table, it can be observed that the F-value of the model was 123.46, and the corresponding p-value was < 0.0001, which suggests that the model is highly significant. The temperature was the most influential variable among the process variables with F– value of 103.49 and p–value <0.0001, followed by holding time (F– value of 31 and p–value <0.0002). It could be observed from Table 3.3 that based on the F and p–value of 4.2 and 0.0675, respectively, the N_2 flow rate found to have a negligible effect on the bio-oil yield. Also, the squared term of process variables temperature (A^2) and holding time (C^2) were found to be significant, and interaction terms (AB, AC, and BC) were insignificant. In order to ensure the reliability of the model, lack of fit test was performed. The lack of fit was found to be insignificant with an F–value of 2 (p=0.2320), which implied that there was no evidence of the model not fitting the data. Moreover, the adequacy of the model fit was confirmed by estimating the regression coefficient (R^2), which was found to be equal to 0.99 (Figure. 3.5). The value of the adjusted regression coefficient (R^2 = 0.99) also confirmed the model to be highly significant. The higher value of the predicted regression coefficient (R^2 = 0.98) suggested that the model can be used to predict response for a given set of independent variables (within the range of model operation). The low value of the coefficient of variation (C.V. = 3.02%) indicated good accuracy and reliability of the experiments. The RSM developed model (based on sequential square model sum) was a quadratic equation to predict the bio-oil yield in terms of coded variables (Equation 3.1). It was observed that there was a good agreement between the experimental output and model-predicted data, which is shown in Figure. 3.5.

$$\begin{aligned} Bio-oil\ yield\ (Coded) &= +34.92-(2.35\times A)-(0.47\times B)+(1.29\times C)-(0.29\times A\times B) \\ &+(0.15\times A\times C)+(0.104\times \mathrm{B}\times \mathrm{C})-(6.7\times A^2)-(0.26\times B^2)-(2.67\times C^2) \end{aligned} \quad 3.1$$

In Equation 3.1, A (temperature (°C)), B (flowrate (L/min)), and C (holding time (min)) were variables in coded terms.

Table 3.2. Central composite design matrix with corresponding experimental and predicted response.

Sl. No.	Actual Value			Bio–oil yield (%)	
	Temperature (°C)	**Flowrate (L/min)**	**Holding time (min)**	**Experimental**	**RSM predicted**
1	300	0.8	20	27.00	26.59
2	600	0.8	20	22.24	22.15
3	300	1.5	20	27.07	26.42
4	600	1.5	20	21.70	20.83
5	300	0.8	60	29.00	29.06
6	600	0.8	60	25.40	25.24
7	300	1.5	60	29.20	28.48
8	600	1.5	60	23.90	23.51
9	197.73	1.15	40	19.30	19.93
10	702.26	1.15	40	11.50	12.01
11	450	0.56	40	35.00	34.97
12	450	1.73	40	32.20	33.37
13	450	1.15	6.36	24.38	25.20
14	450	1.15	73.63	29.20	29.53
15	450	1.15	40	33.70	34.92
16	450	1.15	40	35.00	34.92
17	450	1.15	40	34.80	34.92
18	450	1.15	40	35.60	34.92
19	450	1.15	40	35.00	34.92
20	450	1.15	40	35.60	34.92

TH-3101_166107009

Table 3.3. Analysis of variance (ANOVA) for the experimental design to obtain maximum bio-oil yield by the suggested quadratic model.

Source	Sum of squares	Df	Mean square	F–value	p–value Prob> F
Model	812.50	9	90.28	123.46	< 0.0001
A–Temperature	75.68	1	75.68	103.49	< 0.0001
B–Flowrate	3.07	1	0.15	4.20	0.0675
C–Holding time	22.67	1	22.67	31	0.0002
AB	0.66	1	0.66	0.91	0.3621
AC	0.18	1	0.18	0.25	0.6221
BC	0.05	1	0.05	0.12	0.7386
A^2	646.58	1	646.58	884.22	< 0.0001
B^2	1	1	1	1.37	0.2692
C^2	102.83	1	102.83	140.63	<0.0001
Residual	7.31	10	0.7312	–	–
Lack of fit	4.88	5	0.9755	2	0.2320
Pure error	2.43	5	0.49	–	–
Cor total	819.81	19	–	–	–
R^2					**0.9911**

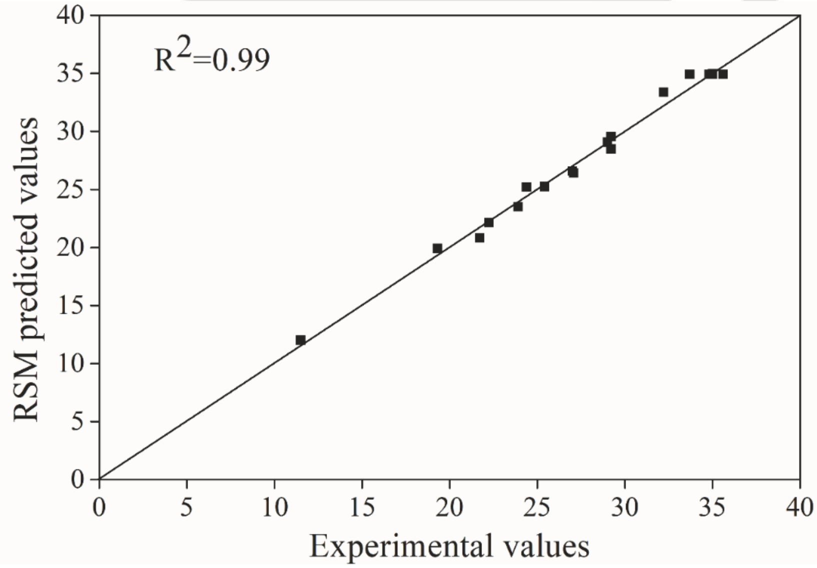

Figure 3.5. The plot of actual and model-predicted values for bio-oil yield.

The relationship between the selected process variables and the resulting response function is shown in Figure. 3.6 (a–c). Figures show that the temperature had a

TH-3101_166107009

maximum effect on bio-oil yield, followed by holding time. At the same time, N_2 flowrate had the least effect on the bio-oil yield, which was evident from the higher p-values. Figure. 3.6 (a) represents the 3D response surface and contour plots for the combined effect of temperature and holding time at a constant N_2 flowrate of 1.15 L/min. From the figure, it can be seen that the bio-oil yield increased from 28 wt% at 300 °C, reached a maximum at 430 °C, and decreased thereafter. The maximum achievable bio-oil yield at 430 °C was 35.2 wt% with a corresponding bio-char yield of 48 wt%. The increase in bio-oil yield up to 430 °C was due to the maximum volatiles conversion. After that, a decrease in the yield could be due to the initiation of secondary cracking reactions at around 430–440 °C. A similar observation was reported by Acikalin et al., [147], wherein they varied the reaction temperature from 350–650 °C and reported the maximum bio-oil yield of 52.73 wt% at 500 °C. Another study on neem press seed by Dhanavath et al., [139] reported temperature as the most significant process variable among the other studied variables, i.e., N_2 flowrate, holding time, and temperature. Another study conducted by Mushtaq et al., [136] reported that final pyrolysis temperature decreased with the N_2 flow rate. In the current work, an almost similar trend was noticed, in which the bio-oil yield remains unchanged with the increasing N_2 flow rate up to 1.5 L/min at the optimum temperature of 430 °C (Figure. 3.6 (a) and (c)). Moreover, the increased holding time (40 min) and temperature (430 °C) resulted in the maximum bio-oil yield of 35.2 wt%. Further, an increase in the holding time and pyrolysis temperature beyond the optimal value decreased the bio-oil yield, which could be due to the initiation of repolymerization reactions (Figure. (3.6 b)). All the different profiles in Figure. 3.6 (a–c) are found to be analogous with the preliminary data (Figure. 3.4).

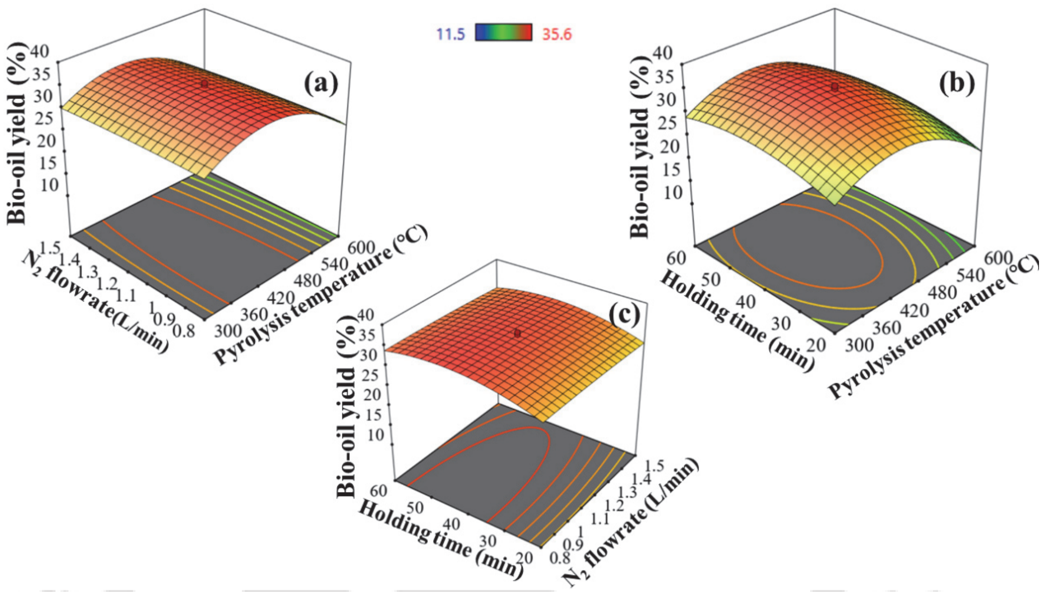

Figure 3.6. Response surface plot presenting the effect of (a): temperature (°C) and holding time (min) (b): temperature (°C) and flowrate (L/min) on bio-oil yield (c): holding time (min) and flowrate (L/min).

3.5 Optimization of process variables

The desirability function tool, i.e., Design expert software, was used to predict the optimum set of process variables within the chosen operating range to maximize the bio-oil yield. The maximum predicted bio-oil yield was 35.5 wt% at 427 °C, 0.9 L/min, and 45 min with the maximum desirability of 0.99. Actual experiments performed at the suggested condition resulted in 34.2 wt% bio-oil yield, which is within a range of 1.3% deviation from the RSM predicted yield. This indicates that the developed model could accurately predict the bio-oil yield within the chosen range of the process variables. Moreover, the corresponding bio-char, non-condensable gas yield, and biomass conversion were found to be 49.2, 15.3, and 50.8 wt%, respectively.

Indian Institute of Technology Guwahati

3.6 Bio-oil characterization at the optimized condition

3.6.1 Solvent extraction

The water content in the bio-oil was determined using a Karl Fischer titrator. The bio-oil with a high water content of ~55% had a low calorific value of 9–10 MJ/kg [152]. Thus, the solvent extraction technique was selected to improve the bio-oil characteristics so that its possibility as a potential boiler fuel supplement could enhance. Three solvents—hexane, ethyl acetate, and acetone—were chosen to represent a diverse range of polarity values. The bio-oil yield obtained was highest for ethyl acetate (~30%) and lowest for hexane (~4%) [153]. Ethyl acetate recovered the highest bio-oil from the pyrolyzed sample due to its favorable characteristics (polarity). GC–MS analysis of upgraded bio-oil later revealed that most chemical species present in the upgraded bio-oil had a mid-polar nature and thus supported the choice of ethyl acetate as the preferred solvent for bio-oil extraction.

3.6.2 Properties and composition of upgraded bio-oil at optimized conditions

Tables 3.4 and 3.5 represent the bio-oil properties and bio-oil constituents identified using GC–MS. The analysis shows that the bio-oil density of untreated raw rice husk was much higher than the acid-treated RH (feedstock) [152]. The water content in the upgraded bio-oil decreased from 55 wt% to ~26 wt% [81]. The lower water content indicates that the obtained bio-oil can be used as a transportation fuel. The calorific value of the upgraded bio-oil was found to comply with the ASTM standards. The acid value (determined by the ASTM D974 method) reduced from 152 mg KOH/g to

71.2 mg KOH/g (upgraded bio-oil), thereby making the upgraded bio-oil less corrosive [154].

The detailed composition of upgraded bio-oil determined using the GC-MS analysis is presented in Table 3.5. The major peaks representing the components in a considerable fraction within the bio-oil were identified using the available library. It mainly consists of acids, esters, aromatics, phenols, and ketones. Also, the other compounds in bio-oil were combustible and formed during lignin degradation. The FT-IR results also complemented the GC-MS composition (Figure. 3.7). The O–H stretching vibration from 3300–2500 cm^{-1} centered at 3000 cm^{-1} confirms the presence of carboxylic acid [155]. Also, the peak around 3500 cm^{-1} represents the O–H stretching of water and phenols [156]. The bands at 2860 cm^{-1} and 2950 cm^{-1} confirms the presence of octadecanoic acid butyl ester, and the peak in the range 2100 cm^{-1} to 2250 cm^{-1} corresponds to the alkyne groups [146-147]. The peak at 1720 cm^{-1} and 1530 cm^{-1} attributed to the presence of dibutyl phthalate, and 4–ethyl–2–methoxyphenol, respectively [158,159]. The peak at 1710 cm^{-1} and 1680 cm^{-1} represents phthalic acid [160]. C–H stretching between 1380 cm^{-1} and 1500 cm^{-1} confirmed the presence of alkane groups in the bio-oil [147]. The peak at 1330 cm^{-1} represents the stretching vibration of C–H groups, thus indicating the presence of methyl groups [155]. The peaks in the range 2000 cm^{-1} to 1650 cm^{-1} correspond to the C–H bending of the aromatic compounds [155]. Also, the peaks between 900 cm^{-1} to 650 cm^{-1} represent the aromatics [152].

TH-3101_166107009

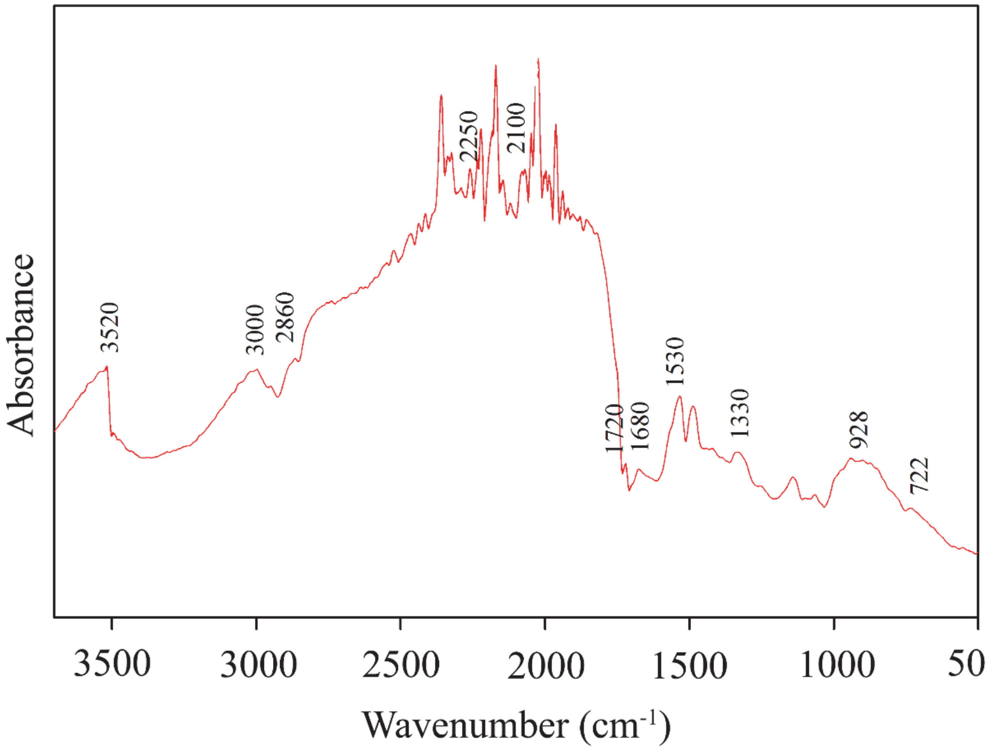

Figure 3.7. FT–IR spectra of bio-oil obtained at optimized condition.

Table 3.4. Comparison of different parameters between upgraded bio-oil and ASTM burner fuel standards.

Property	**Test method**	**Typical range***	**Upgraded bio-oil**
Calorific value (MJ/kg)	D240	14–19	14.56±0.75
Water content (wt%)	E203	20–30	25.83±1.23
pH	E70	2–3	2.3
Kinematic viscosity at 40 °C (mm^2/s)	D445	15–40	16.5
Density at 15 °C (kg/dm^3)	D4052	1.11–1.30	1.1
Pour point	D97	-9 °C	-12 °C
Ash content (%)	D482	0.25	0.28

*Typical range given by ASTM standards [161]

Table 3.5. GC–MS based identification of bio-oil constituents.

Acids	**Area (%)**
Acetic acid	0.65
Pthalic acid	10.01
Cis -10- heptadecenoic acid	6.85
Ketones	
Heptacosane	3.49
1-Heptacosanol	1.06
Phenols	
Phenol,4-Ethyl-2-Methoxy	2.16
Ethanone,1-(2-Hydroxy-5-Methylphenyl)	0.82
Phenol,2,6,Dimethoxy	0.98
Phenol,2-Methoxy-4-(1-Propenyl)	0.23
Benzene,1-Ethyl-3-(phenylmethyl)	0.76
Aromatics	
Benzene,1,2,3-trimethoxy-5-methyl	1.16
Beta-sitosterol acetate	1.80
1,2,3-trimethoxybenzene	2.75
Esters	
Dibutyl pthalate	7.93
1,2-benzenedicarboxylic acid,butyloctyl ester	0.93
Octadecanoicacid,butyl ester	0.68
1,2-benzene dicarboxylic acid, mono(2-ethylphenyl) ester	1.22
Others	3.08

3.7 Non-condensable gas composition at optimized condition

Non-condensable gas samples yield was calculated based on the material balance of all three products (Equation 2.5). The non-condensable gas yield was found to be 15.3 wt%, which is reported based on the difference in the bio-oil and bio-char yield value with respect to the feed. The gas sample was collected in the tedlar bag for GC analysis. The amount of N_2 present in the non-condensable gases could not be identified, as N_2 was used as a carrier gas in GC analysis. The obtained gas composition (volume %) is shown in Table 3.6. It was observed that at optimized pyrolysis conditions, carbon monoxide content (CO) was found to be 76.8% [162] because the temperature (427 °C) condition was not sufficient for the complete combustion of the biomass. Mainly, CO was formed by the decomposition of hemicellulose and cellulose; also, the cracking of carbonyl and carboxyl groups present in the biomass contributes to the formation of CO [163]. It also constitutes 13.6% of CO_2 and 9.5% methane, which can be used as fuel. Also, studies reported on RH suggest a similar pattern wherein the CO volume% was higher than CO_2 and CH_4 [162].

Table 3.6. GC based identification of non-condensable gases.

Gas	Volume (%)
CO	76.8
CO_2	13.6
CH_4	9.5

3.8 Summary

Slow pyrolysis has been presented to achieve significant bio-oil yield from RH, which includes process optimization using the RSM technique. Initial enrichment of the bio-mass was realized by an acid-treatment technique which considerably improved the quality of biomass by concentrating the volatiles and leaching out the inorganics. The acid-treated biomass was converted into value-added products such as bio-oil, bio-char, and other valuables by employing a slow pyrolysis method. The yield of bio-oil primarily depends on the system temperature, followed by holding time and N_2 flow rate. RSM technique was carried out to determine the optimum process condition to achieve a maximum bio-oil yield of 35.5 wt%. The extensive analytical characterization of the upgraded bio-oil revealed a higher calorific value with lower water content comprising a mixture of complex compounds consisting of acids, ketones, esters, and phenolics, among other substances. Furthermore, the non-condensable gas composition at the optimum condition contains a high CO amount, followed by CO_2 and CH_4. Further modifications of the bio-oil to increase calorific value and reduce water content may be performed wherein these liquid fuels could be successfully altered to gasoline, kerosene, or chemicals like aromatics. However, these techniques are still in very nascent stages and are considered under the future scope of this work.

Indian Institute of Technology Guwahati

CHAPTER IV

Catalytic upgradation of bio-oil using slow pyrolysis process under reactive environment

Effect of process variables on bio-oil production

Optimization of slow pyrolysis process using RSM with CCD design

Catalytic upgradation of bio-oil

Physico-chemical characterization of upgraded bio-oil

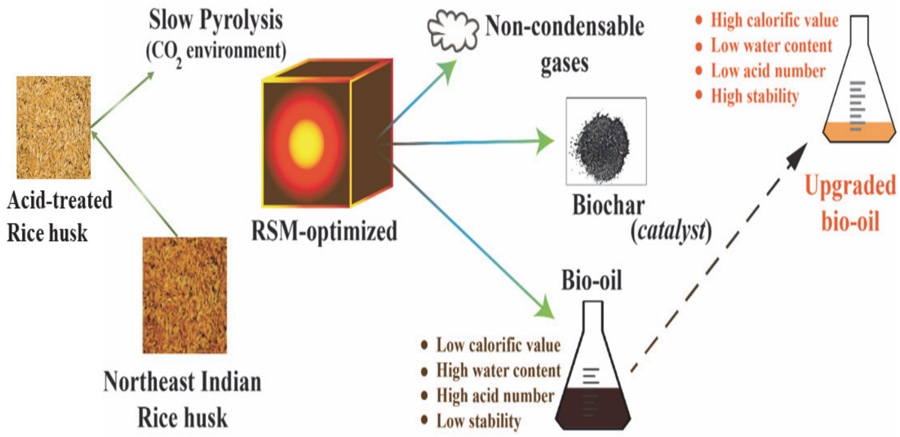

Chapter IV

Catalytic upgradation of bio-oil using slow pyrolysis process under reactive environment

Rice husks (RH) are the major by-product of the paddy industry and a major cause of air pollution in the northern part of India. In this work, experiments have been performed to utilize this waste sustainably to produce bio-oil and other valuables such as bio-char and non-condensable gases via a slow-pyrolysis method in the presence of a reactive environment. Major variables affecting the pyrolysis process, i.e., pyrolysis temperature, gas flowrate, and holding time, were optimized using the Response surface methodology (RSM) technique. The quadratic equation was developed to correlate the variables with the bio-oil yield. Among all the process variables, temperature significantly affected the pyrolysis process. Holding time and gas flowrate were found to have a negligible effect on the process. The highest bio-oil yield (31.7 wt%) reported was at 551 °C, 1.1 L/min, and 53 min. The initial characterization of the bio-oil prompted its further upgradation by utilizing the produced bio-char as a catalyst to improve the bio-oil's physical characteristics to be later used as a burner fuel. Extensive characterization of the upgraded bio-oil showed that they were in accordance with ASTM standards.

4.1 Characterization of biomass

The detailed physico-chemical characteristics of untreated and acid-treated RH have been discussed in the previous chapter (Chapter 3). Before slow pyrolysis, TGA analysis was performed to fundamentally understand the thermolytic profiles under both N_2 and CO_2 environments. The TGA and DTG profiles are drawn as a function of temperature and shown in Figure 4.1. The plot indicates that biomass degradation is more under CO_2 environment compared to N_2. The final residual mass at 800 °C was around 28% (under CO_2 environment) and 38% (under N_2 environment). It may be noted that the RH sample was characterized as per the protocol by NREL and found that the biomass contained 32% cellulose, 15% hemicellulose, and 24% lignin. TGA profile indicated an initial weight loss in the biomass from ambient temperature up to 115 °C resulting from water expulsion and low molecular weight volatiles [137,164]. The change in TGA and DTG profiles beyond 200 °C and up to 400 °C corresponds to the defragmentation of hemicellulose, cellulose (up to 350 °C) and lignin (up to 400 °C). DTG peak shift at 305 °C resulted from the removal of volatiles. Beyond 415 °C, a gradual change in the mass loss was observed under both environments, which may correspond to the carbonization process resulting in the formation of bio-char. While the mass loss continued to decrease under the N_2 environment, a sharp decrease was observed at ~680 °C under the CO_2 environment. This may have resulted from the Boudouard reaction ($C + CO_2 \leftrightarrow 2CO$), which involves the interaction of CO_2 with the solid carbon content in the biomass. Thermodynamically, this heterogeneous reaction starts at temperatures greater than 680 °C and leads to a higher amount of CO in the non-condensable gases [165]. Thus based on the onset temperature of degradation i.e. ~340 °C appropriate pyrolysis temperature range was selected.

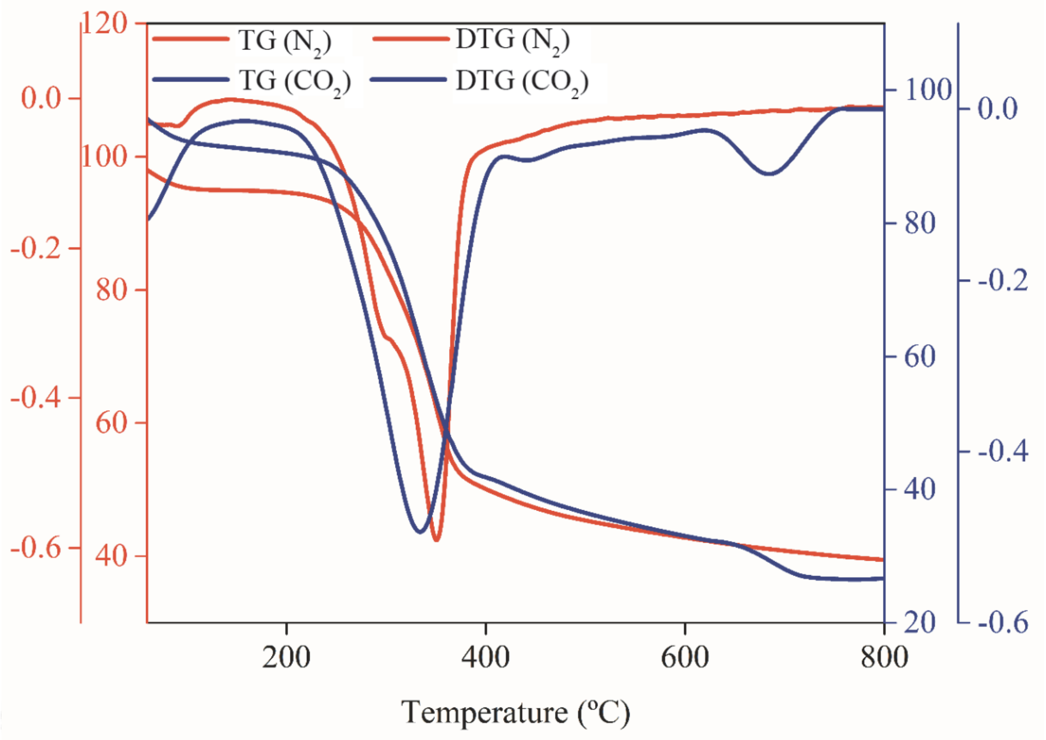

Figure 4.1. Thermogravimetry and derivative thermogravimetry profile of acid-treated RH at 10 °C/min under N_2 and CO_2 environment to generate the conversion profiles.

4.2 Identification of process variables operating range

The pyrolysis of lignocellulosic biomass depends on temperature, gas holding time, pressure, inert gas flow rate, condensate temperature, and heating rate. Among the different variables, few significantly affect the pyrolysis process compared to others. A prior-art [141,147,156] concerning slow pyrolysis of biomass revealed that temperature, holding time, heating rate, and CO_2 flow rate played a significant role compared to other variables. As mentioned earlier, the present study utilizes a constant heating rate of 10 °C/min for the slow-pyrolysis process. As a result, temperature, holding time, and CO_2 flowrate had been considered as independent variables.

Indian Institute of Technology Guwahati

Therefore, detailed preliminary experiments were carried out to determine the operating ranges of variables. From the TG analysis of acid-treated RH, the onset temperature (temperature around which volatiles generation occur) was observed to be ~345 °C at 27 min for the CO_2 environment. It was also observed that the Bourdouard reaction was not significant beyond 700 °C at 60 min (CO_2); however, the reaction continued till the temperature reached 800 °C. Therefore, the temperature and holding time were varied within the range ~300–700 °C and 20–60 min, respectively. As per the reported literature [148,166,167] CO_2 flowrate range was determined to be 0.7–1.5, respectively.

4.3 Preliminary Experimental Data

4.3.1 Effect of temperature

In order to analyze the effect of temperature on the bio-oil yield, preliminary experiments were carried out at a fixed CO_2 flowrate of 0.7 L/min with a holding time of 60 min, respectively. The corresponding bio-oil and bio-char yield was found to be 15 wt% and 60 wt% at 300 °C (Figure 4.2 (a)). As the temperature increased to 400 °C, the bio-oil yield increased to 20 wt%, whereas the bio-char yield decreased to 55 wt%. Thereafter at 500 °C, the bio-oil yield increased to 28 wt% with subsequent reduction in the bio-char yield to 48 wt%. Further, with the increase in temperature to 600 °C, both the bio-oil and bio-char yield decreased to 25 wt% and 41 wt%, respectively. As the decrease in bio-oil yield was not that significant at 600 °C, the temperature was raised further to 700 °C, wherein a significant drop in bio-oil (22.7 wt%) was observed, confirming the conversion of all the volatiles. The results obtained in the present study were consistent with that reported by Pilon [168]. The enhancement in bio-oil yield up to 500 °C was attributed to the generation of the maximum volatiles; however, further increased in the temperature resulted in the initiation of secondary cracking reactions, which decreased the bio-oil yield and subsequently improved the non-condensable gas yield to 34 wt% at 600 °C. Also, the highest bio-char yield at 300 °C was because of the incomplete degradation of the pretreated biomass as its onset temperature was found to be 342 °C (Figure 4.1). The reduction in bio-char yield to 41 wt% at 600 °C was because of secondary cracking reactions. Hence, for further pyrolysis experiments, 500 °C was set as the fixed operating temperature.

4.3.2 Effect of holding time

The effect of holding time on the bio-oil yield was investigated at 500 °C and a constant CO_2 flowrate of 0.7 L/min. The minimum bio-oil yield of 24 wt% with a respective bio-char yield of 49.1 wt% was obtained at 20 min holding time (Figure 4.2 (b)). Further increase in the holding time to 40 min resulted in 26 wt% of bio-oil yield and 47 wt% of bio-char yield. Thereafter, the bio-oil yield marginally increased to 27 wt%, and bio-char yield reduced to 41.9 wt% at 60 min, whereas the gas yield increased by 4 wt%. This could be because of the initiation of repolymerization, which increased the gas yield. Moreover, most of the volatiles would have already converted to bio-oil within 40 min. Beyond that period, there was just a 1% increase in the bio-oil yield and subsequent reduction in the bio-char yield due to the secondary cracking reactions [168].

4.3.3 Effect of CO_2 flowrate

The effect of CO_2 flowrate on the bio-oil yield was monitored by performing a pyrolysis experiment at 500 °C and at a fixed holding time of 40 min. The variation in the bio-oil yield with respect to CO_2 flowrate is depicted in Figure 4.2 (c). The maximum output of bio-oil was found to be 26.3 wt% at 1 L/min, whereas at 0.7 and 1.5 L/min, no significant difference was noticed in the bio-oil yield. The slight reduction in the bio-oil yield and subsequent increment in the gas yield with increasing CO_2 flowrate could be due to the insufficient quenching of the volatiles. The maximum bio-char yield of 48.3 wt% was observed at 0.5 L/min and further increased in the CO_2 flowrate to 1.5 L/min decreased the bio-char yield (46.7 wt%).

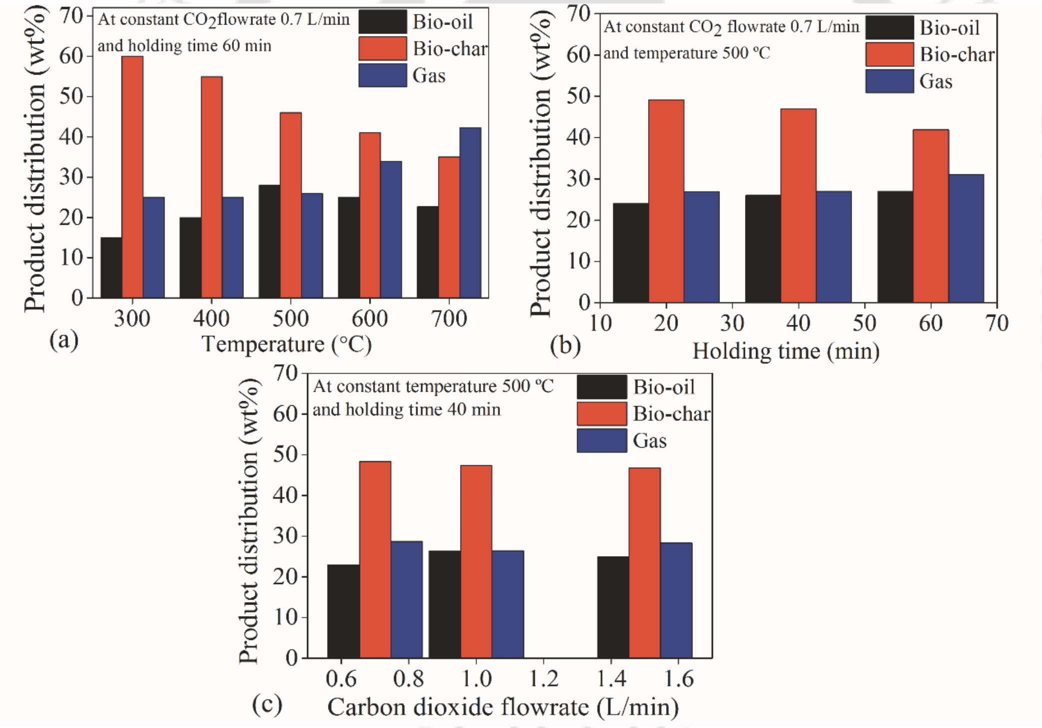

Figure 4.2. Individual effect of process variables (a) temperature, (b) holding time and (c) carbon-dioxide flowrate, on the bio-oil output as observed upon the completion of the slow pyrolysis of acid-treated rice husk.

4.4 Optimization of process variables using RSM

4.4.1 ANOVA analysis and model fitting

The RSM design matrix consisting of model predicted and experimentally obtained values are shown in Table 4.1. The effect of individual variables as well as their interactive effect on the bio-oil yield during slow pyrolysis under CO_2 environment can be evaluated from the F-test of ANOVA (Table 4.2). The experimentally obtained and model predicted values were found to be in good agreement (Figure 4.3). CCD model designed 20 sets of experiments and the bio-oil yield varied in the range 10–32.5 wt%. Furthermore, the experimentally obtained bio-oil yield data was used to develop the model. p-value and F-value tests were carried out to gauge the significance of the model. The larger the F value's magnitude and smaller the 'p>F' value, the more significant is the corresponding coefficient [169,170]. From the table 4.2, it was observed that the quadratic model possessed an F-value and p-value of 94.32 and <0.0001, respectively. This confirms the model to be significant. Comparative analysis of different process variables revealed that temperature to be the most significant variable (F-value of 93.2 and p-value <0.0001) followed by holding time (F-value of 62.46 p-value <0.0001). Flowrate was found to have least effect on the system which was confirmed by the very low F value of 1.83 and high p- value of 0.2063. Moreover, the squared term of temperature (A^2) and holding time (B^2) were also found to be relatively significant. Out of the interaction terms, AC was found to be relatively significant compared to AB and BC terms. To determine the dependability of the model, a test of lack of fit was performed. The results obtained indicated that the lack of fit was not significant as it had an F–value of 0.33 and p-value>0.05, implying an overall good model fitting. Also, the suitability of the model was measured by calculating the regression coefficient (R^2) value, which was found to be 0.98, suggesting model to be significant. Predicted R^2 was also found to be 0.98, confirming that the model can be used to predict response for a given set of independent variables within the range of respective process variables. Low coefficient of variation (C.V.) value of 3.73% indicated the correctness and dependability of the performed experiments. Further, RSM developed model, based on the sequential square model sum was a quadratic equation to estimate the bio-oil yield output in terms of the coded variables (Equation 4.1). The result showed a close agreement between the model estimated data and experimental analysis, as presented in Figure 4.3.

$$\begin{aligned} Bio-oil\ yield\ (Coded) &= +30.79+(2.37\times A)+(0.33\times B)+(1.94\times C)+(0.05\times A\times B) \\ &+(1.1\times A\times C)-(0.23\times \mathrm{B}\times \mathrm{C})-(6\times A^2)-(1.95\times B^2)-(1.63\times C^2) \end{aligned} \quad 4.1$$

In Equation 4.1, *A* (temperature (°C)), *B* (flowrate (L/min)), and *C* (holding time (min)) were the variables in coded terms.

Indian Institute of Technology Guwahati

Table 4.1. Central Composite design matrix with the corresponding experimental and predicted response.

Sl. No.	**Actual value**			**Bio-oil yield (%)**	
	Temperature (°C)	**Flowrate (L/min)**	**Holding time (min)**	**Experimental**	**RSM predicted**
1	300	0.7	20	17.30	17.51
2	700	0.7	20	20.20	19.94
3	300	1.5	20	18.30	18.52
4	700	1.5	20	21.10	21.15
5	300	0.7	60	20.00	19.63
6	700	0.7	60	27.00	26.46
7	300	1.5	60	19.80	19.74
8	700	1.5	60	27.30	26.77
9	163.64	1.1	40	10	9.85
10	836.34	1.1	40	17.20	17.81
11	500	0.43	40	24.30	24.72
12	500	1.77	40	25.80	25.83
13	500	1.1	6.36	23.20	22.92
14	500	1.1	73.63	28.70	29.44
15	500	1.1	40	29.50	30.79
16	500	1.1	40	30.70	30.79
17	500	1.1	40	31.70	30.79
18	500	1.1	40	32.50	30.79
19	500	1.1	40	30.10	30.79
20	500	1.1	40	30.30	30.79

Table 4.2. Analysis of variance (ANOVA) for the response surface quadratic model to obtain maximum bio-oil yield.

Source	**Sum of squares**	**Df**	**Mean square**	**F–value**	**p-value Prob> F**
Model	696.19	9	77.35	94.32	< 0.0001
A–Temperature	76.44	1	76.44	93.20	< 0.0001
B–CO_2 flowrate	1.5	1	1.5	1.83	0.2063
C–Holding time	51.23	1	51.23	62.46	< 0.0001
AB	0.02	1	0.02	0.02	0.8790
AC	9.68	1	9.68	11.80	0.0064
BC	0.40	1	0.40	0.49	0.4983
A^2	518.10	1	518.10	631.75	< 0.0001
B^2	54.67	1	54.67	66.66	< 0.0001
C^2	38.27	1	38.27	46.66	<0.0001
Residual	8.20	10	0.82	–	–
Lack of fit	2.06	5	0.41	0.33	0.8720
Pure error	6.14	5	1.23	–	–
Cor total	704.39	19	–	–	–
R^2	–	–	–	–	0.9884

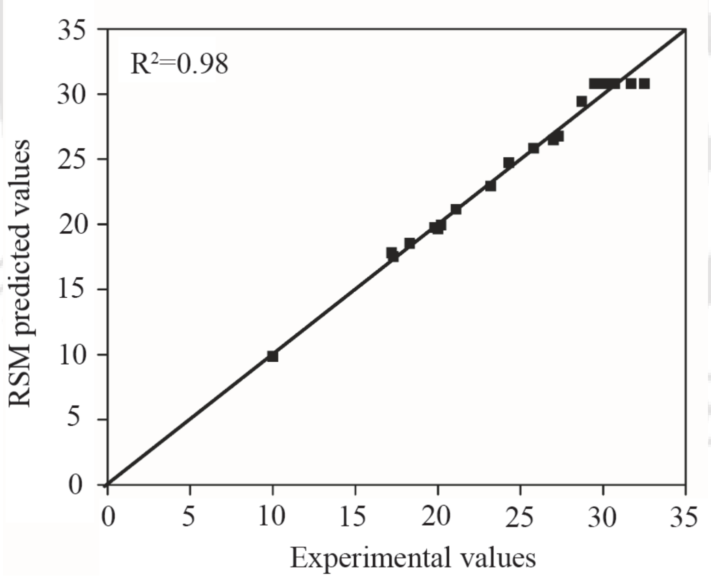

Figure 4.3. Comparison plot between actual and model predicted values for bio-oil yield.

The association between the different process variables as well as response function is shown in Figure 4.4 (a–c). As mentioned earlier, temperature had a highest effect on bio-oil yield followed by reaction time, while CO_2 flowrate had least or marginal effect. Moreover, the 3D response surface, contour plots representing the cumulative effect of pyrolysis temperature (300−700 °C) and holding time (20−60 min) at a constant CO_2 flowrate of 1.1 L/min, is shown in Figure 4.4 (a). The bio-oil yield improved from 22 wt% at 300 °C to 32.5 wt% at 550 °C and decreased thereafter. The highest bio-oil yield obtained was 32.5 wt%, with the respective solid (bio-char) yield of 46 wt%. The increment in bio-oil yield upto 550 °C was mainly because of the conversion of volatiles. However, as the temperature increased to 600 °C, the secondary cracking reactions were initiated which are responsible for the reduction in bio-oil yield. Pilon et al., [162] reported a similar observation, wherein they studied pyrolysis of switchgrass under a CO_2 environment in which the reaction temperature was varied from 300−500 °C and reported the highest bio-oil yield of 38 wt% at 500 °C. The bio-oil yield did not change significantly with the change in CO_2 flowrate, as presented in Figures 4.4 (a) and 4.4 (b). The bio-oil yield varied with the rise in holding time. It increased to a maximum of 31.7 wt% at around 53 min and after showed a decreasing trend, which could be due to the completion of pyrolysis reaction [147].

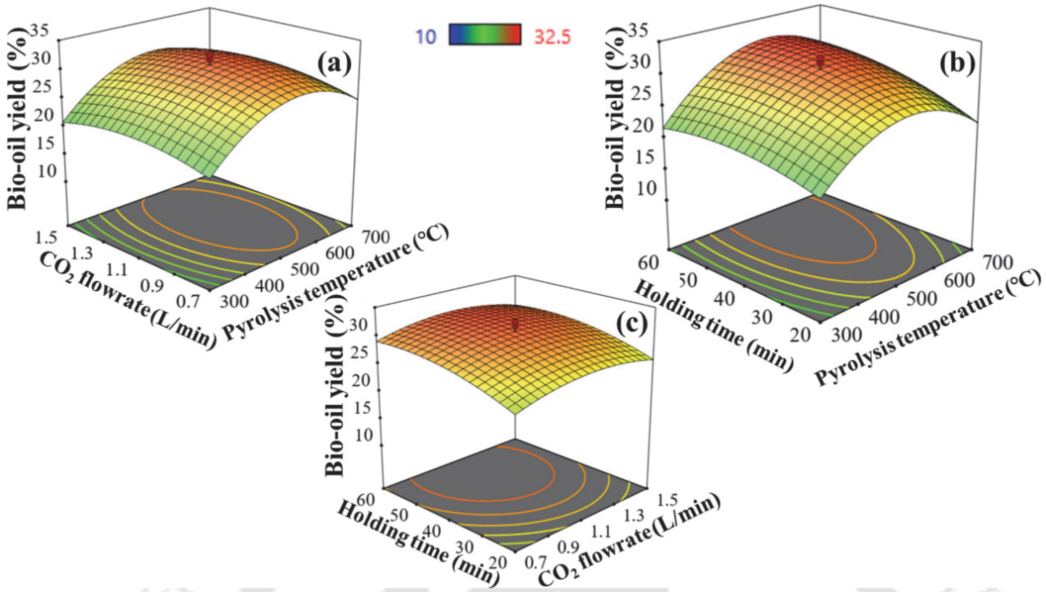

Figure 4.4. 3D response surface plot of (a): temperature (°C) and holding time (min) (b): temperature (°C) and flowrate (L/min) on bio–oil yield (c): holding time (min) and flowrate (L/min).

4.5 Optimization of process variables

The desirability function tool in the design expert software was applied to identify the optimal set of process variables operating within the selected range. The maximum estimated bio-oil output was 31.7 wt% at 551 °C, 1.1 L/min, and 53 min at the highest desirability of 0.97. Experiments completed at the model-estimated condition indicated a 30.2 wt% bio-oil yield with a 1.5% deviation from the estimated yield (RSM). This suggested that the developed model reasonably estimated the bio-oil yield within the selected process variables operational range. Also, at this optimized condition, the bio-char and non-condensable gas output was observed to be 48.3 wt% and 20 wt%, respectively.

4.6 Characterization of catalyst (bio-char)

The obtained bio-char at optimal condition was extensively characterized and its characteristics have been presented in Table 4.3. The bio-char was observed to have lower volatile matter (18.5 wt%) and higher ash content (37 wt%) as most of the volatiles were converted to bio-oil during the pyrolysis. The higher ash content suggests that the bio-char consists of inorganics (for example K and Fe) that have catalytic properties and thus will take part in cracking during pyrolysis [171]. The mineral composition of the bio-char was examined using atomic absorption spectroscopy (AAS) and the details have been shown in Table 4.3. Also, the carbon content in bio-char was found to be 38.7 wt%; higher carbon content provides a more reactive carbon surface during refinement of pyrolysis vapors.

Further, the BET surface area of bio-char was found to be 86.1 m^2/g with a porosity of 0.073 cm^3/g. At higher temperatures, the aliphatic side chains start splitting from the aromatic rings, releasing volatile organic compounds (VOC). CO_2 being reactive, it reacts with VOCs and induces its removal from the surface of bio-char, thereby making it porous and provides a higher surface area. The FESEM images (Figure 4.5) of the bio-char also confirmed the presence of porous structure on its surface. Therefore, it can be concluded that the bio-char obtained from the slow pyrolysis of rice husk could be utilized as a potential bio-based adsorbent.

Table 4.3. Physico-chemical characterization of catalyst (bio-char).

Proximate analysis	**Bio-char (catalyst)**
Volatile Matter (%)	18.5±0.90
Ash (%)	36.3±1.70
Fixed Carbon (%)	45.2
Ultimate Analysis	
C (%)	38.70
H (%)	1.30
O (%)	23.47
N (%)	0.23
BET Surface area (m^2/g)	86.1
Total pore volume (cm^3/g)	0.073
pH	9.2
Calorific value (MJ/kg)	19.9
Metal Composition	**ppm**
Fe	41.2
K	32
Zn	26
Pb	12.8
Cd	55.3

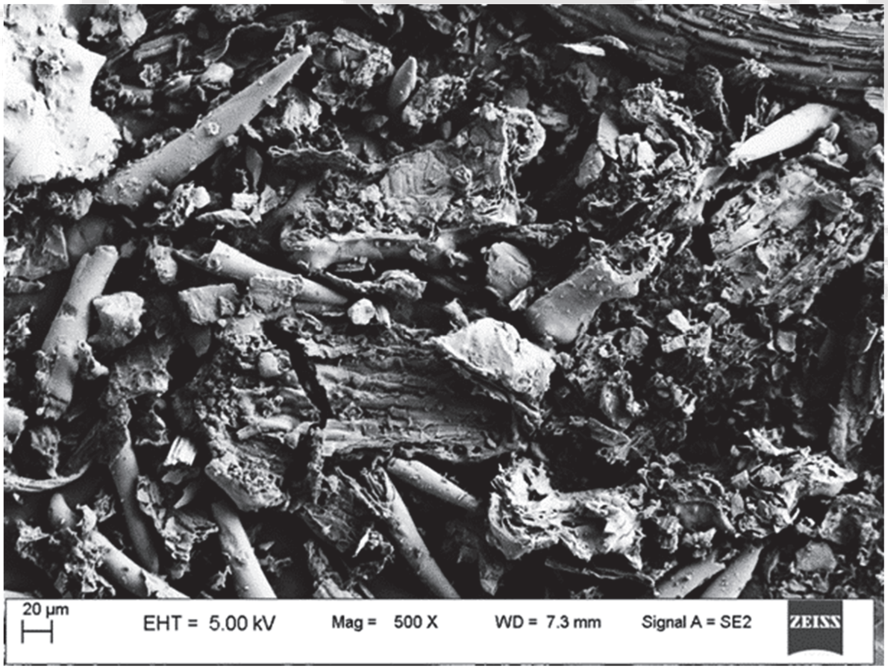

Figure 4.5. FESEM profile of bio-char obtained at optimal condition. The image has been taken at 500 X magnification.

4.7 Upgradation of bio-oil

Initial characterization of the bio-oil, i.e. water content (21.4 ±1.3%), its composition and calorific value (9.5±0.5 MJ/kg) suggested that the obtained bio-oil was of poor quality [156]. Therefore, to improve its properties, so that it could be utilized as a boiler fuel supplement, an in-situ catalytic pyrolysis process was carried out. The bio-char produced at the optimized condition was used as a catalyst in three different proportions. Table 4.4 shows the bio-oil, bio-char, and non-condensable gases obtained during catalytic pyrolysis. The study results revealed that as the bio-char (catalyst) proportion in the feed increases, the bio-oil yield decreases. This could be because the volatile matter present in the bio-char is less as compared to RH, so, increasing the bio-char proportion reduces the overall volatile content in the feed. The bio-char yield increases proportionally with the addition of the catalyst. The addition of catalyst promotes the secondary cracking reactions, promoting bio-char formation. The non-condensable gas yield was found to be lowest (13 wt%) in the case of C_3 and similar (~15 wt%) for C_1 and C_2.

Table 4.4. The percentage yield of bio-oil, bio-char, and non-condensable gases.

Yield percentage	**Bio-oil (wt%)**	**Bio-char (wt%)**	**Non-condensable gases (wt%)**
Optimized bio-oil (OBO)	31.5	45	23.5
C_1 (25 wt%)	30	55	15
C_2 (33 wt%)	20	65	15
C_3 (50 wt%)	15	72	13

4.8 Characterization of upgraded bio-oil

To further understand the bio-oil quality, its calorific value, water content, viscosity, density, and ash content were determined. Table 4.5 represents the properties of optimized bio-oil and the upgraded bio-oil estimated using ASTM standards. The water content in the raw bio-oil was found to be 21.4 wt%. This increased to 24.3 wt%, 25.1 wt%, and 28.3 wt% upon addition of 25 wt%, 33 wt% and 50 wt% catalysts, respectively. The catalytic pyrolysis removes oxygen in the form of water and CO_2 via dehydration and decarboxylation reactions, which was responsible for increased water content in the upgraded bio-oil. The upgraded bio-oil was found to have an enhanced calorific value of 16.7 MJ/kg (C_1), 17.3 MJ/kg (C_2), and 18.8 MJ/kg (C_3), respectively. It was observed, that the acid content decreased with the addition of catalyst, as a result, the pH of the upgraded bio-oil increased from 2.3 (OBO) to 2.4, 2.7 and 3.4 for C_1, C_2 and C_3 respectively. This finding has been further discussed in detail in the following section. Along with the above, the acid value of the raw bio-oil was also found to be 89.7 mg KOH/gm which significantly reduced to 26.7, 25.8 and 15.7 mg KOH/gm in case of C_1, C_2 and C_3, respectively [172]. The viscosity of the raw bio-oil was 10.3 mm^2/s and further decreased with catalytic pyrolysis. This may due to the formation of lower molecular weight compounds [65]. Thus, the upgraded bio-oil was found to have improved characteristics compared to raw bio-oil. Other properties, like density and ash content of the upgraded bio-oil were found to comply with the ASTM standard.

Table 4.5. Characteristics of upgraded bio-oil and ASTM burner fuel standard.

	Test method	**Typical range***	**OBO**	**25 wt% (C_1)**	**33 wt% (C_2)**	**50 wt% (C_3)**
Calorific value (MJ/kg)	D240	14–19	9.5	16.7 ±0.8	17.3 ±1.2	18.8 ±1.4
Water content (wt%)	E203	20–30	21.4	24.3 ±1.1	25.1 ±0.83	28.3 ±0.75
pH	E70	2–3	2.3	2.4	2.7	3.4
Kinematic viscosity at 40 °C (mm^2/s)	D445	15–40	10.3	15	15.8	16.2
Density at 15 °C (kg/dm^3)	D4052	1.11–1.30	1.21	1.20	1.11	0.99
Ash content (%)	D482	0.25	0.24	0.21	0.22	0.21

*Typical range given by ASTM standards [161]

4.8.1 Compositional analysis of upgraded bio-oil

GC-MS was employed to carry out the compositional analysis of the bio-oil. The analysis indicated the presence of different compounds such as phenols, ester, acids, ketones and aromatics, as shown in Table 4.6. Performing an in-situ catalytic upgradation with the help of bio-char catalyst, resulted in removal of unwanted oxygen-containing compounds such as furans, acids, esters and aldehydes while simultaneously improving the useful aromatic and phenolic content. Phenolic content in the upgraded bio-oil indicates its relative stability. The presence of these compounds in higher proportions within the GC-MS spectra, pointed towards more stable nature and higher resistance of bio-oil against oxidation under ambient conditions. The catalytic pyrolysis has also been reported to aid in the conversion of acids to ester, thereby reducing the corrosiveness and poisoning of catalysts [164]. These acidic compounds were present in higher percentage in the optimized bio-oil, which reduced its calorific value and stability but increased the pH, water content and acid value. Hence, the in-situ catalytic pyrolysis not only improved the bio-oil characteristics but also affected its composition.

Table 4.6. Compositional analysis of optimized and upgraded bio-oil using GC-MS.

Compound	**RT**	**OBO**	**25 wt% (C_1)**	**33 wt% (C_2)**	**50 wt% (C_3)**
Triethyl silane	8.028	3.50	3.91	5.41	2.05
Hexanoic acid, 2-Ethyl-1-1dimethyl ethyl ester	8.128	1.76	–	–	0.23
Furfural	9.304	2.89	2.33	0.48	1.63
Ethanol, pentamethyl	9.479	0.64	0.50	–	0.31
2,3-Pentadienoic acid, ethyl ester	9.684	1.33	0.12	0.15	0.11
3-Hexadecanone	9.744	0.37	0.12	–	0.12
Propanoic acid, 1-methylethylester	10.564	0.59	0.21	0.17	0.11
2(5H)-Furanone	10.755	1.51	0.46	–	0.59
Phenol	11.925	1.85	2.44	2.81	3.82
Furan 2,5-diethoxytetrahydro	12.455	3.46	0.27	0.16	0.91
Dimethyl olpropanoic acid	12.515	3.39	0.26	0.29	0.77

2-Ethyl-5-propylcyclopentane	12.85	1.91	1.02	0.29	1.59
p-Cresol	13.691	0.53	0.78	0.94	1.88
3,3-Diethoxy-1-propanol, butylether	13.746	0.78	0.48	0.14	0.15
Phenol, 2-methoxy	14.081	3.40	3.79	4.08	4.35
Levoglucosenone	14.6	0.51	10.49	8.19	7.65
1-Pentene, 4-4 dimethyl	14.261	1.82	0.12	0.2	0.57
Hexane,1,1-Diethoxy	15.181	0.59	0.27	0.17	0.43
Phenol, 4-ethyl	15.536	0.48	0.40	0.45	0.59
Cresol	16.177	1.24	1.50	0.71	0.67
2-Propenoic acid, 2-methyl-octylester	16.712	6.85	4.85	3.13	1.02
N-Decanoic acid	22.454	10.32	7.57	5.71	–
Tetrasiloxane, decamethyl	39.076	0.40	0.25	0.2	0.1

As the overall bio-oil yield decreased with the addition of catalyst, we need to strike a balance between the bio-oil yield and its properties. Hence, the catalyst proportion of 33 wt% was considered as the optimal to achieve the desired yield.

4.9 Non-condensable gas composition at optimized condition

The non-condensable gas yield was calculated based on the method discussed in section 3.7. The non-condensable gas yield was found to be highest (22.3 wt%) in CO_2 as compared to N_2 environment (15 wt%). The optimal pyrolysis temperature was found to be 550 °C. At the optimized pyrolysis condition, the non-condensable gases were primarily composed of CO, CO_2 and CH_4. CO component was present in the maximum amount (45.36%) in the non-condensable gases. This may be due to the presence of a reactive environment as well as insufficient temperature to complete biomass degradation [173]. Complete degradation of biomass at very high temperatures leads to generation of CO_2 gas. In this case, owing to the lack of high temperature, incomplete biomass degradation would have led to increase in CO concentration. Moreover, under a reactive CO_2 environment, the cracking of volatile organic compounds [174] as well as different carbonyl and carboxyl group containing compounds in the RH may have contributed toward the generation of CO [175]. The non-condensable gas composition in terms of volume% is shown in Table 4.7. The non-condensable gas sample also contained 17.3% of CO_2 along with 34.63% methane, which could be utilized as an alternate source of fuel. As reported in the literature temperatures beyond ~550 °C, mostly initiate the secondary cracking reactions, which favors the formation of CH_4 and CO [173]. At high temperatures, the structure of bio-char could be destroyed, thus further encouraged the cracking of aliphatic structure within bio-char. These cracking reactions lead to the removal of carbonyl groups, thereby facilitating the formation of CH_4 [176].

Table 4.7. Compositional analysis of non-condensable gases using GC at optimized condition.

Gas	Volume (%)
CO	45.36
CO_2	17.3
CH_4	34.63

4.10 Summary

The present study elaborates a process that is optimized to improve the quality of bio-oil derived from slow pyrolysis of rice husk, via another pyrolysis derivative i.e. bio-char. The initial enrichment of the biomass was carried out using an acid pretreatment step to concentrate the volatiles and leach out the inorganics. Thereafter, a critical analysis of the slow pyrolysis process that utilized the biomass revealed that the bio-oil yield was mainly affected by the system temperature and holding time. The overall process was designed and optimized using a RSM technique that primarily determined the operating range for the different process parameters such as temperature, holding time and flowrate to obtain maximum bio-oil yield of 31.7 wt%. Moreover, under the optimum condition, the non-condensable gases contained highest amount of CO (45.36%), followed by CH_4 (34.63%) and CO_2 (17.63%). In order to improve the quality of the potential fuel supplement (bio-oil), the generated bio-char was subsequently used as a catalyst in different proportions before performing slow pyrolysis (in-situ) at the optimal condition. Increasing the bio-char content in the feedstock improved the quality of the produced bio-oil, however it reduced the bio-oil

TH-3101_166107009

yield. Therefore, 33 wt% of catalyst proportion was chosen as the optimal catalyst proportion to obtain upgraded bio-oil as at this ratio, 20 wt% of bio-oil yield was obtained with improved quality. GC-MS analysis of the obtained, upgraded bio-oil confirmed the presence of a complex mixture mostly esters, phenols, alcohols and acids, among other substances. This upgradation of the bio-oil utilizing bio-char as catalyst, resulted in the improvement of its physico-chemical characteristics such as calorific value, water content and acid number.

CHAPTER V

Optimal production of bio-char with maximum carbon content under both inert (N_2) and reactive (CO_2) environment

Effect of process variables on bio-char production

Optimization of slow pyrolysis process for bio-char production using RSM

Bio-char mechanism

Physico-chemical characterization of bio-char obtained at optimized condition

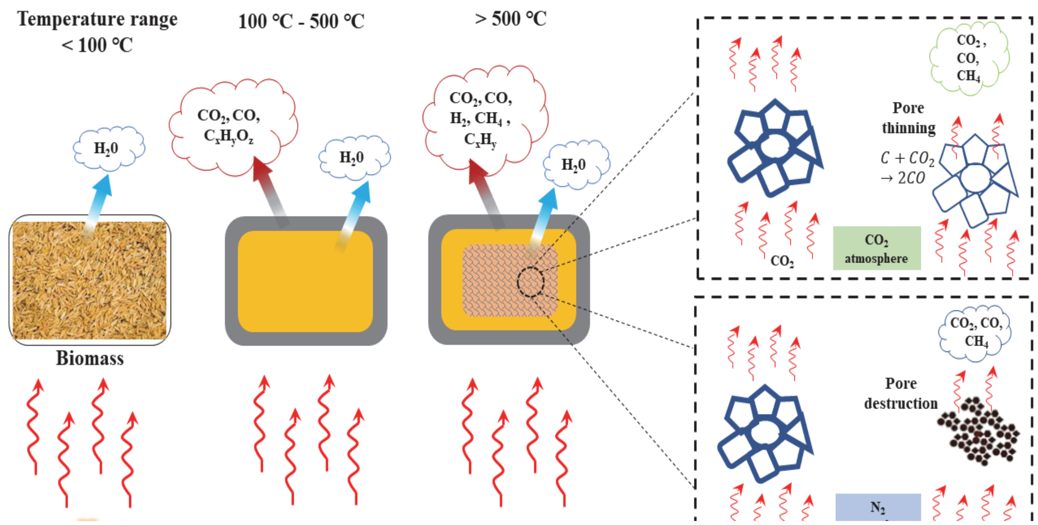

भारतीय प्रौद्योगिकी संस्थान गुवाहाटी • Indian Institute of Technology Guwahati •

Chapter V

Optimal production of bio-char with maximum carbon content under both inert (N_2) and reactive (CO_2) environment

This study employs a design optimization (RSM) tool to analyze the slow pyrolysis of RH under two different environments – inert (N_2) and reactive (CO_2). The process was optimized to get a favorable response in terms of bio-char yield and carbon content. The optimal conditions under the N_2 environment were 521 °C, 48 min, 0.87 L/min, and under the CO_2 environment were 545 °C, 0.87 L/min, and 43 min, respectively. The bio-char obtained under the CO_2 environment was found to have higher porosity, surface area, pH, aromaticity, and hydrophilicity. This indicates that the obtained bio-char can be used as a potential adsorbent. However, the bio-char obtained under the N_2 environment was found to have higher carbon content and thus, could be utilized as soil conditioners or soil enhancers to increase soil fertility.

5.1 Preliminary experimental data

The selection of process variables and their ranges are discussed in sections 3.1 (Chapter 3) and 4.1 (Chapter 4) for N_2 and CO_2 environments. Therefore, based on the previous study in this chapter, the ranges of the variables have been fixed as pyrolysis temperature: 300–600 °C, gas flow rate: 0.87–1.5 L/min, and holding time: 20–60 min.

TH-3101_166107009

5.2 Development of the regression model

The entire design matrix with the obtained responses (experimental values) to predict the optimal bio-char yield and its carbon content under both N_2 and CO_2 environments are shown in Table 5.1. Twenty sets of experiments were performed to statistically optimize the experimental process variables (temperature, flowrate, and holding time) and estimate their effect on carbon content and bio-char yield. Based on the sequential square model sum, the quadratic model was recommended by the Design-Expert® software. The final empirical models in terms of coded factors are shown in Equations 5.1–5.4.

$$\begin{aligned} Bio-char\ yield\,(N_2) &= 48.64-8.33A-1.34B-2.97C+0.0875AB \\ &\quad +0.3375AC+0.9125BC-1.87A^2-0.9135\mathrm{B}^2-1.5\mathrm{C}^2 \end{aligned} \qquad 5.1$$

$$\begin{aligned} Bio-char\ yield\,(CO_2) &= 48.09-7.52A-0.5515B-1.17C-0.675AB \\ &\quad +1.7AC+1.32BC+2.62A^2-0.4996B^2-0.0484C^2 \end{aligned} \qquad 5.2$$

$$Carbon-content(N_2)=39.93+13.88A+3.38C-2.76AC-6.16A^2-4.23C^2 \qquad 5.3$$

$$Carbon-content(CO_2)=35.21+11.51A+2.04C-2.02AC-5.74A^2-1.80C^2 \qquad 5.4$$

where, *A* represents the temperature (°C), *B* (flowrate (L/min)), and *C* (holding time (min)) in coded terms.

The coefficient with one factor represents the influence of that particular factor, while the coefficient with two factors represents the interaction between two factors, and those with second-order terms represent the quadratic effect.

Table 5.1. Central Composite design matrix with corresponding experimental and predicted response.

S. No.	Actual			Bio-char yield (N_2) (%)		Carbon content yield (N_2) (wt%)		Bio-char yield (CO_2) (%)		Carbon content yield (CO_2) (wt%)	
	T (°C)	**FR (L/min)**	**HT (min)**	**EXP**	**RSM**	**EXP**	**RSM**	**EXP**	**RSM**	**EXP**	**RSM**
1	300	0.87	20	58.10	58.34	6.80	9.51	62.30	62.76	9.70	10.94
2	600	0.87	20	40.90	40.82	45.10	42.80	45.50	45.66	39.10	38.56
3	300	1.50	20	53.20	53.66	9.30	9.51	60.30	60.36	10.70	12.15
4	600	1.50	20	36.70	36.49	42.30	42.80	40.20	40.56	37.40	38.67
5	300	0.87	60	49.20	49.90	20.00	21.80	53.80	54.36	20.20	19.73
6	600	0.87	60	33.70	33.73	43.20	44.04	43.20	44.06	39.90	39.25
7	300	1.50	60	48.30	48.87	18.30	21.80	56.50	57.26	18.30	19.63
8	600	1.50	60	32.80	33.05	44.30	44.04	43.80	44.26	38.50	38.06
9	197.73	1.20	40	58.30	57.37	3.20	-0.84	68.80	68.15	2.10	0.37

TH-3101_166107009

10	702.27	1.20	40	29.10	29.34	44.30	45.86	43.50	42.85	38.50	39.10
11	450	0.65	40	48.60	48.31	38.40	39.93	51.20	50.43	31.70	32.33
12	450	1.71	40	44.20	43.80	39.00	39.93	49.10	48.57	34.10	32.34
13	450	1.20	6.36	49.40	49.40	22.10	22.27	50.10	49.43	29.10	27.45
14	450	1.20	73.63	40.10	39.41	36.30	33.65	47.10	45.97	33.80	34.32
15	450	1.20	40	50.20	48.64	38.20	39.93	47.60	48.09	38.70	36.38
16	450	1.20	40	49.20	48.64	40.40	39.93	48.10	48.09	35.10	36.38
17	450	1.20	40	49.80	48.64	39.30	39.93	48.70	48.09	34.90	36.38
18	450	1.20	40	48.60	48.64	43.80	39.93	49.20	48.09	36.90	36.38
19	450	1.2	40	47.70	48.64	41.70	39.93	47.60	48.09	38.70	36.38
20	450	1.2	40	46.20	48.64	40.70	39.93	47.10	48.09	33.80	36.38

TH-3101_166107009

5.3 ANOVA analysis and model fitting

ANOVA was used to determine the statistical significance of quadratic models and their respective model coefficients. The model F values of bio-char yield and carbon content were found to be 95.31 and 125.78 under the N_2 environment. The model F values of bio-char yield and carbon content under the CO_2 environment were found to be 125.78 and 95.58 (Table 5.2 (a–d)). The p-values of all the developed models were <0.0001, suggesting the models to be significant. Further, the lack of fit for each model was not significant (p-value>0.05), implying overall good model fitting. The coefficient of variation (CV%) values denote reproducibility and repeatability, and values less than 30% are considered reproducible models [177]. The CV% of all the developed models was found to be <10%, confirming their reproducibility (Table 5.3).

In the case of bio-char yield, under both the environment, all the three variables, i.e., pyrolysis temperature, N_2/CO_2 flow rate, and holding time, were found to be significant (p-value<0.05) (Table 5.2 (a)–(d)). Out of these, pyrolysis temperature (F-value 688.45 (N_2 environment) and 932.68 (CO_2 environment)) was found to be the most significant variable followed by holding time (F-value 87.36 (N_2 environment) and 22.74 (CO_2 environment)) and flow rate (F-value 17.8 (N_2 environment) and 5.01 (CO_2 environment)). Compared to other variables, flow rate did not significantly affect the bio-char yield. Similar findings were documented by Jamaluddin et al., [178] wherein the flowrate was observed to have a marginal effect. Out of the interactive variables, BC and AC were found to be significant variables under N_2 and CO_2 environments, respectively. In the case of carbon content, under both the environment, the pyrolysis temperature and the holding time were significant. As the p-values of both the N_2 and

CO_2 flowrate were greater than 0.05, i.e., insignificant, thus excluded from the equation and their respective interactive effects [179]. The temperature (F-value 457.78 (N_2) and 574.75 (CO_2)) was found to be the most significant process variable followed by holding time (F-value 27.15 (N_2) and 18.11 (CO_2)).

Table 5.2(a). Analysis of variance (ANOVA) for the suggested quadratic mode of experimental design to obtain bio-char yield by the suggested quadratic model.

	Bio-char yield (%) (N_2 environment)				
Source	Sum of squares	Df	Mean square	F–value	p–value Prob> F
Model	1181.69	9	131.30	95.31	< 0.0001
A–Temperature	948.41	1	948.41	688.45	< 0.0001
B–N_2 Flowrate	24.52	1	24.52	17.80	0.0018
C–Holding time	120.35	1	120.35	87.36	< 0.0001
AB	0.0612	1	0.0612	0.0445	0.8372
AC	0.9112	1	0.9112	0.6615	0.4350
BC	6.66	1	6.66	4.84	0.0525
A^2	50.29	1	50.29	36.51	0.0001
B^2	12.03	1	12.03	8.73	0.0144
C^2	32.29	1	32.29	23.44	0.0007
Residual	13.78	10	1.38	–	–
Lack of fit	2.85	5	0.5695	0.2606	0.9169
Pure error	10.93	5	2.19	–	–
Core total	1195.47	19	–	–	–

Table 5.2(b). ANOVA for the experimental design to obtain bio-char yield as proposed by the quadratic model.

Bio-char yield (%) (CO_2 environment)					
Source	Sum of squares	Df	Mean square	F–value	p–value Prob> F
Model	938.30	9	104.26	125.78	< 0.0001
A–Temperature	773.05	1	773.05	932.68	< 0.0001
B–CO_2 flowrate	4.15	1	4.15	5.01	0.0491
C–Holding time	18.85	1	18.85	22.74	0.0008
AB	3.65	1	3.65	4.40	0.0624
AC	23.12	1	23.12	27.89	0.0004
BC	14.04	1	14.04	16.95	0.0021
A^2	99.00	1	99.00	119.44	<0.0001
B^2	3.60	1	3.60	4.34	0.0638
C^2	0.034	1	0.034	0.041	0.8442
Residual	8.29	10	0.83	–	–
Lack of fit	5.23	5	1.05	1.71	0.2845
Pure error	3.06	5	0.61	–	–
Core total	946.59	19	–	–	–

Table 5.2(c). ANOVA for the experimental design to obtain carbon content as proposed by the quadratic model.

Carbon content (%) (N_2 environment)					
Source	Sum of squares	Df	Mean square	F-value	p-value Prob> F
Model	3600.49	5	720.10	125.78	< 0.0001
A–Temperature	2632.85	1	2632.85	457.78	< 0.0001
C–Holding time	156.17	1	156.17	27.15	0.0001
AC	61.05	1	61.05	10.62	0.0057
A^2	552.14	1	552.14	96.00	< 0.0001
C^2	260.71	1	260.71	45.33	< 0.0001
Residual	80.52	14	5.75	–	–
Lack of fit	61.61	9	6.85	1.81	0.266
Pure error	18.91	5	3.78	–	–
Core total	3681.01	19	–	–	–

Table 5.2(d). ANOVA for the experimental design to obtain carbon content as proposed by the quadratic model.

Carbon content (%) (CO_2 environment)					
Source	Sum of squares	Df	Mean square	F-value	p-value Prob> F
Model	2403.90	5	480.78	95.58	< 0.0001
A–Temperature	1809.88	1	1809.88	359.80	< 0.0001
C–Holding time	57.02	1	57.02	11.33	0.0046
AC	32.80	1	32.80	6.52	0.0230
A^2	480.07	1	480.07	95.44	< 0.0001
C^2	47.21	1	47.21	9.39	0.0084
Residual	70.42	14	5.03	–	–
Lack of fit	48.91	9	5.43	1.26	0.4186
Pure error	21.52	5	4.30	–	–
Core total	2474.33	19	–	–	–

The accuracy of the developed model was judged on the basis of standard deviation, CV%, adjusted and predicted R^2 value (Table 5.3). The standard deviation belonging to the different responses was small, suggesting a good fit. The CV values of each of the models was found to be less than 10% which confirmed their reproducibility. The high R^2 values confirmed that the developed model could predict the data well. The adjusted and predicted R^2 values were in reasonable agreement for each developed model as the difference between them was less than 0.2 [179].

Table 5.3. Developed model summary statistics indicating goodness of fit.

Statistical parameter	Bio-char yield (%)(N_2)	Bio-char yield (%) (CO_2)	Carbon content (%)(N_2)	Carbon content (%)(CO_2)
Standard deviation	1.17	0.91	2.4	2.24
Mean (%)	45.72	50.19	32.84	30.06
Coefficient of variation (%)	2.57	1.81	7.30	7.46
R^2 value	0.9885	0.9912	0.9781	0.9715
Adjusted R^2 value	0.9781	0.9834	0.9703	0.9614
Predicted R^2 value	0.9687	0.9533	0.9319	0.9347
Adequate precision	34.94	42.86	35.55	32.22

5.4 Diagnostics and adequacy checking

The suitability of the developed models was analyzed using the externally studentized residual plots along with the predicted vs actual plots. For a model to be properly fit, the residuals should be randomly and normally distributed. Figure 5.1 (a–d), shows the points on the normal probability of the internally studentized residuals of both the bio-char and carbon content under N_2 and CO_2 environment, respectively. Each of these plots confirms a straight line, thereby confirming the normal distribution of data. Figure 5.2 (a–d), represents the actual vs predicted plots. The plots show minimal divergence from the straight line, confirming high R^2 values.

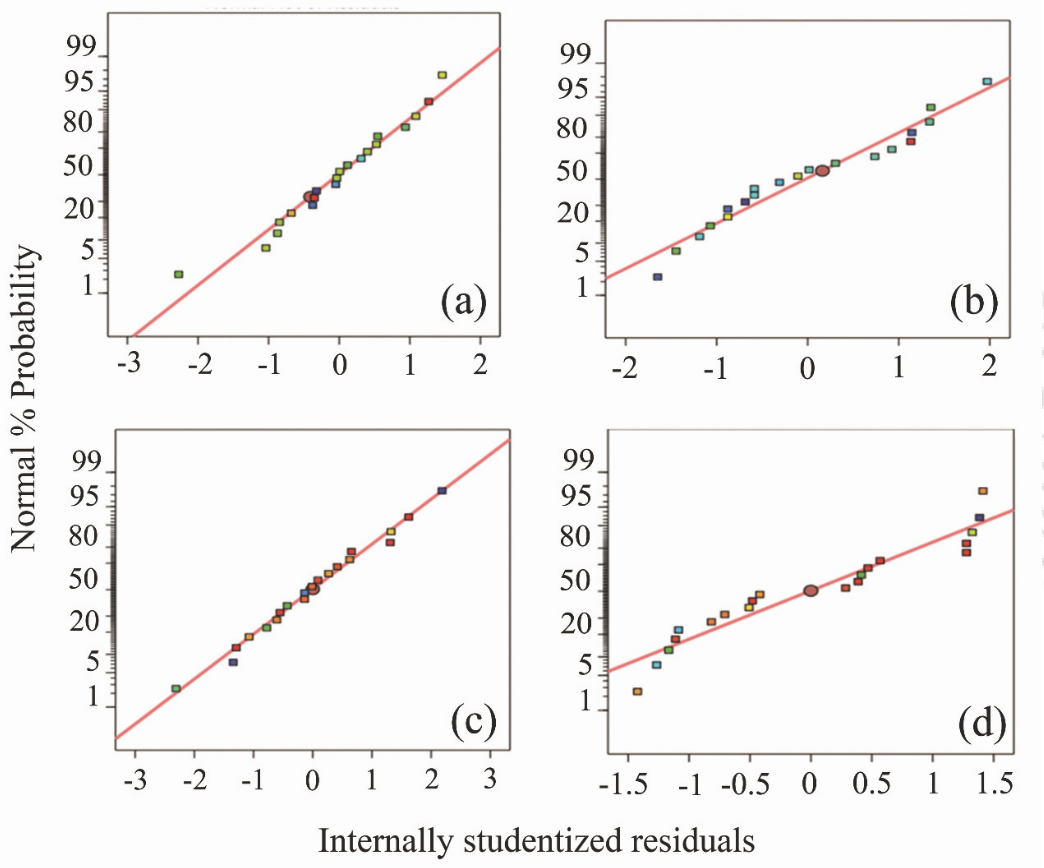

Figure 5.1. Normal probability plot of residue for a) bio-char yield under N_2 environment, b) bio-char yield under CO_2 environment, c) carbon content under N_2 environment, d) carbon content under CO_2 environment.

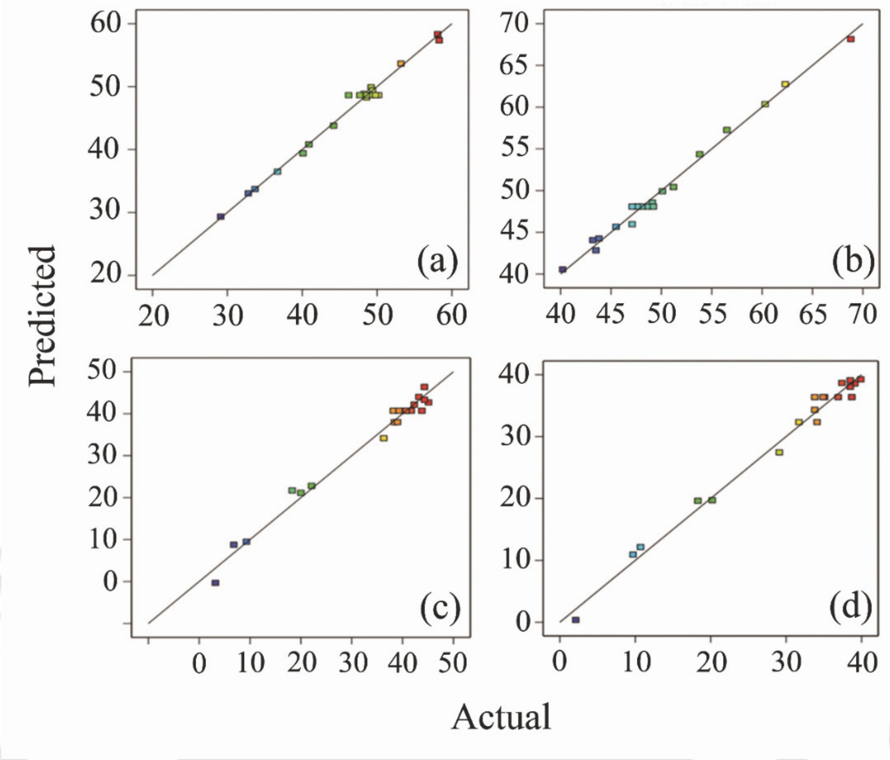

Figure 5.2. Predicted vs actual values for a) bio-char yield under N_2 environment, b) bio-char yield under CO_2 environment, c) carbon content under N_2 environment, d) carbon content under CO_2 environment.

5.5 Analysis of responses

The interactive effects between the variables are shown in the form of three-dimensional plots (Figure 5.3 (a–c)). These plots help to understand the correlations between pyrolysis temperature, N_2/CO_2 flowrate, and holding time in their respective ranges. Figure 5.4 (a), shows how the pyrolysis temperature and N_2 flow rate affect the bio-char yield at constant holding time. As the pyrolysis temperature increases from 300 to 600 °C, the bio-char yield decreases. The decrease in the bio-char yield is due to the removal of volatiles along with secondary decomposition of bio-char [180,181], which increases the formation of liquid and gas products. Although, at a lower temperature, higher bio-char yield is observed, which suggests partial pyrolysis of the biomass, and hence the respective carbon content of the obtained product is very low. At the peak temperature of 600 °C, as the N_2 flow rate increases from 0.87 to 1.2, there is not much bio-char yield change. Figure 5.3 (b), depicts the effect of pyrolysis temperature and holding time on bio-char yield at a constant N_2 flow rate of 1.1 L/min. The bio-char yield initially increased as the holding time increased from 20 to 50 min but further increased in time, leading to a decrease in bio-char yield. The decrease could be due to the completion of the pyrolysis process. Figure 5.3 (c) clearly indicates that N_2 flowrate does not affect the bio-char yield as it almost remains constant when the flow rate increases from 0.87 to 1.5 L/min. Similar results were reported by Menya et al., wherein temperature had the most influence on bio-char yield followed by holding time [179].

Indian Institute of Technology Guwahati

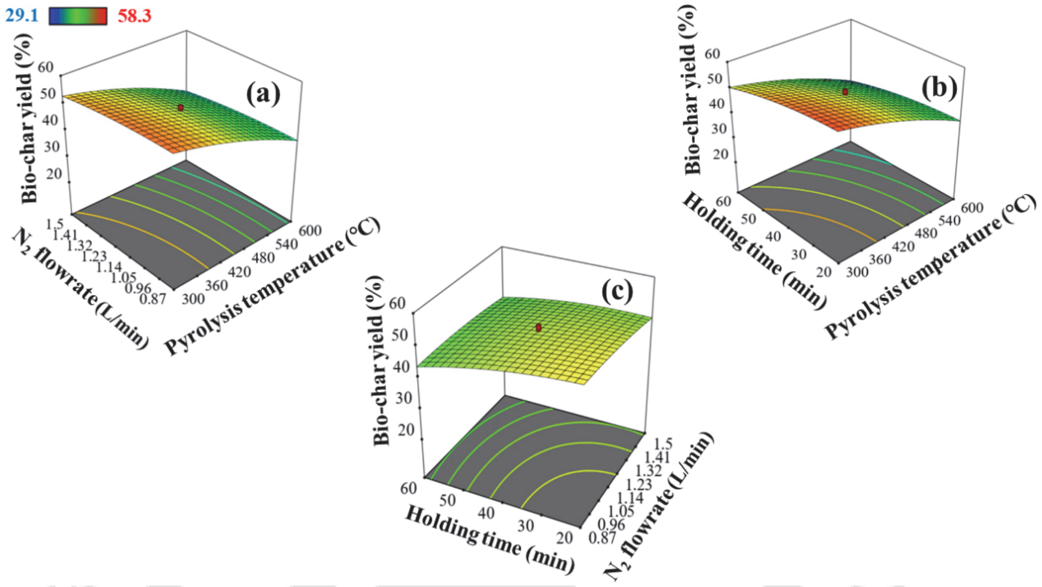

Figure 5.3. 3D response surface plots of bio-char yield under N_2 environment a) Effect of temperature and N_2 flowrate at a fixed holding time of 38 min b) Effect of temperature and holding time at a fixed N_2 flowrate of 1.13 L/min c) Effect of N_2 flowrate and holding time at a fixed temperature of 429 °C.

Figure 5.4 (a–c) represents the effect of pyrolysis temperature, holding time, and CO_2 flow rate on the bio-char yield. Similar profiles are observed in the case of pyrolysis under CO_2 flow rate, wherein the temperature was found to have the highest effect followed by holding time. The CO_2 flow rate had no significant effect (in comparison with other variables) on the bio-char yield. This could be confirmed from Figure 5.4 (a) and (c), wherein, with the increase in CO_2 flowrate, there is not much significant increase in the bio-char yield. A similar study has been reported by Lee et al., in which they pyrolyzed oil palm wastes to obtain bio-char [182]. They reported that the flow rate had minimal effect on the bio-char yield; a very high flow rate would purge out the volatiles too fast, thereby inhibiting the secondary reactions that favor the bio-char

TH-3101_166107009

yield. However, another study by Mohammed et al., on pyrolysis of napier grass to obtain bio-char reported flow rate to be a significant variable [183]. Therefore, from the above discussion, it is inferred that each pyrolysis variable also depends on the biomass characteristics.

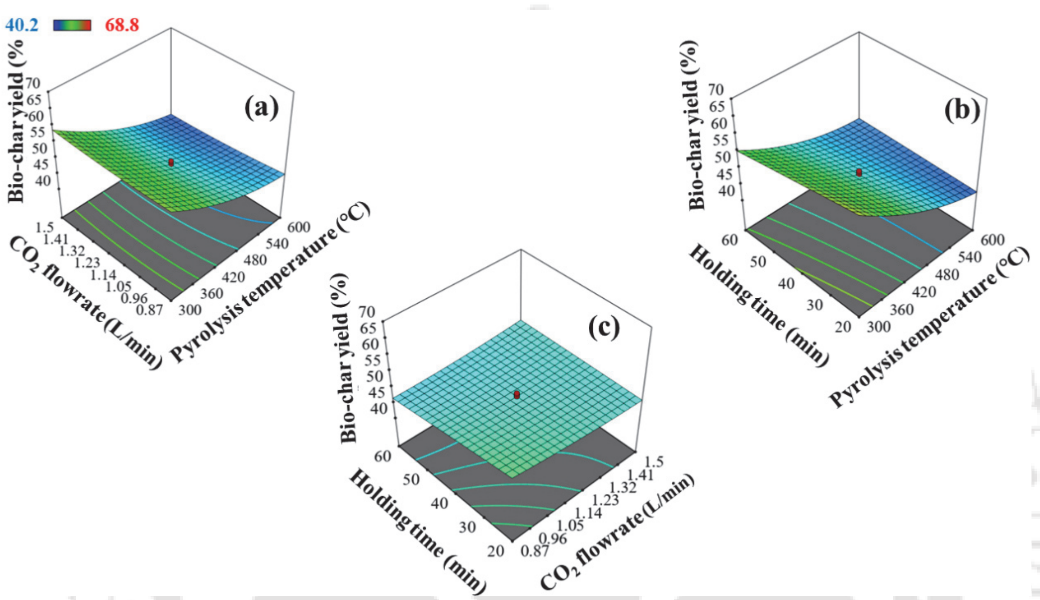

Figure 5.4. 3D response surface plots of bio-char yield under CO_2 environment a) Effect of temperature and CO_2 flowrate at a fixed holding time of 40 min b) Effect of temperature and holding time at a fixed CO_2 flowrate of 1.18 L/min c) Effect of CO_2 flowrate and holding time at a fixed temperature of 429 °C.

Figure 5.5 (a) and (b) represents the effect of pyrolysis temperature and holding time on the carbon content under N_2 and CO_2 environment, respectively. Holding time and pyrolysis temperature both have an encouraging influence on the carbon content. This could be because the low temperature is not sufficient enough for the initiation of carbonization. With the increase in holding time, secondary reactions occur, increasing the carbon content. Similar trends were reported by Yabari et al., wherein they studied the effect of temperature and holding time on the characteristics of bio-char produced from RH. They also reported a positive effect of both temperature and holding time to improve the property in terms of total carbon content (TOC), pH, and cation exchange capacity (CEC) [184].

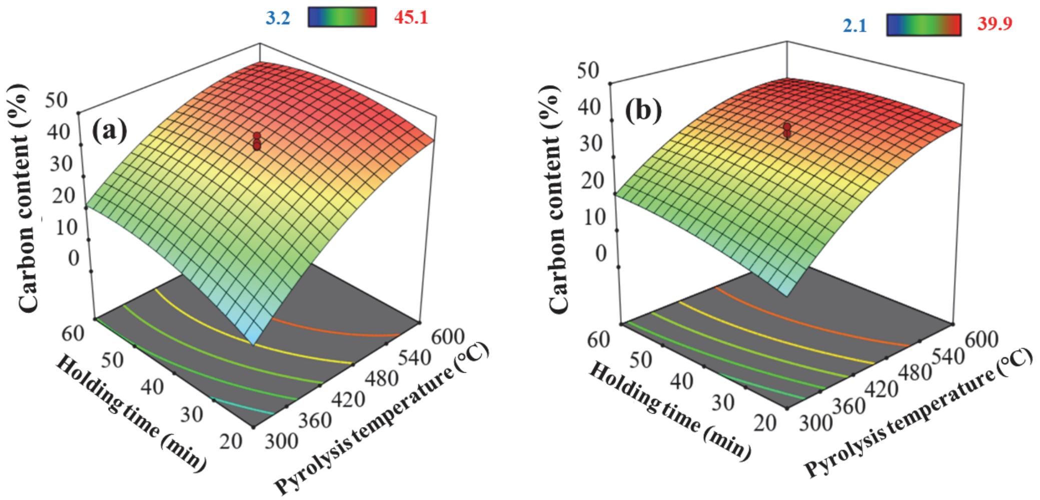

Figure 5.5. 3D response surface plots of carbon content a) Effect of temperature and holding time at a fixed N_2 flowrate of 1.18 L/min. b) Effect of temperature and holding time at a fixed CO_2 flowrate of 1.18 L/min.

5.6 Optimization of the process variable

The main aim of the present study is to have an optimum bio-char yield with maximum carbon content. Hence, the numerical optimization tool present in the Design software was employed to predict the optimum conditions. The optimum bio-char yield of 43% with a maximum carbon content of 45.3% was predicted at pyrolysis temperature of 521 °C, holding time of 48 min, and N_2 flowrate of 0.87 L/min with the maximum desirability of 1. The bio-oil yield at this optimized condition was 30.2 wt%. The actual experiment was conducted under these conditions, resulting in 44.1%±2.1 bio-char yield with 44.8% carbon content. The same technique was employed for the optimization under the CO_2 environment. The predicted optimum bio-char yield of 45.6% with a carbon content of 40% at pyrolysis temperature of 545 °C, holding time of 43 min, and CO_2 flow rate of 0.87 L/min with the maximum desirability of 1. The bio-oil yield at this optimized condition was 20.5 wt%. The actual experimental result was found to be 42.8%±1.7 bio-char yield with 43.1% carbon content. The difference between the actual and estimated values was 2.8 significantly small, i.e., within 3%, suggesting a reasonable agreement between the experimental and calculated values.

5.7 Non-condensable gas analysis

The non-condensable gas amount was calculated based on the material balance equation of the system. The gas composition (wt%) under both environments has been presented in Table 5.4. It was observed that for pyrolysis under the N_2 environment, the CO composition in the outlet gas at optimized conditions was relatively high (79.8%) compared to under the CO_2 environment. The enhancement in the CO composition under an inert environment could be due to extensive hemicellulose degradation. Furthermore, lignin degradation also gets initiated beyond 500 °C, which contributes to CO content [56]. Also, in the literature, it has been reported that CO production is positively affected by the cracking of carbonyl and carboxyl groups within the precursor [163]. The gas composition follows a similar trend as reported elsewhere, wherein CO content was higher than CH_4 and CO_2 [162]. Under a reactive CO_2 environment, the char-gasification reaction starts around 600 °C, which promotes CO gas formation [185]. However, in the present study, the optimum conditions are below 600 °C, which could be a plausible reason for the formation of less CO. The CH_4 gas is mainly produced by cracking of methoxyl–O–CH_3 present in hemicellulose, cellulose, and lignin at temperatures below 600 °C [56]. The higher amount of CH_4 in the CO_2 environment could be due to the higher degradation of lignin, as lignin contributes most to methane formation.

Table 5.4. Non-condensable gas composition under N_2 and CO_2 environment.

N_2 environment			**CO_2 environment**		
CO (%)	CO_2 (%)	CH_4 (%)	CO (%)	CO_2 (%)	CH_4 (%)
79.88	7.09	13.02	45.36	17.3	34.63

5.8 Optimized bio-char characterization under both N_2 and CO_2 environment

5.8.1 Physico-chemical characterization

The bio-char obtained under optimized conditions was further characterized to understand the effect of respective environments on the characteristics of bio-char. The proximate, ultimate analysis, followed by pH, surface area, and calorific value, was determined and presented in Table 5.5.

Table 5.5. Optimized bio-char characteristics obtained under N_2 and CO_2 environment.

Proximate analysis	**Bio-char (N_2)**	**Bio-char (CO_2)**
Volatile matter (%)	18.5±1.08	20.5±1.40
Ash (%)	36.8±1.10	35.4±1.20
Fixed carbon (%)	44.7	44.1
Ultimate analysis		
C (%)	44.1	38.1
H (%)	0.71	1.6
O (%)	18.01	24.6
N (%)	0.38	0.30
BET surface area (m^2/gm)	39	167
Total pore volume (cm^3/g)	0.001	0.068
pH	9	9.2
Calorific value (MJ/kg)	18.2	19.5

The volatile matter and fixed carbon mainly constitute the labile and stable compounds present in bio-char. The volatile matter in the bio-char decreased with the increment in pyrolysis temperature. This could be due to the cracking of volatiles into low molecular weight compound gases instead of bio-char [186]. However, the volatile matter is higher in the case of bio-char obtained under CO_2 environment. The CO_2 environment was found to have higher hydrogen (H) and oxygen (O) content compared to N_2. This suggests that the CO_2 inhibits the removal of H and O containing groups from the bio-char [187]. The ash content improves with increased pyrolysis temperature as the organic components get progressively removed, concentrating the inorganics [188]. The H/C (0.042) and O/C (1.57) ratio of bio-char under CO_2 environment is higher, which suggests it has higher aromaticity, and hydrophilic and polar compared to bio-char under N_2. However, the carbon content was higher under the N_2 environment, which could be because N_2 does not react with the bio-char. The specific surface area was higher in the case of bio-char obtained under the CO_2 environment. This could be because, at higher temperatures, thermal cracking takes place, which removes the pore-blocking elements, thereby increasing the externally accessible surface area [186]. As the CO_2 is reactive, it reacts with the bio-char causing pore thinning, which enhances the porosity and leads to material loss. In the case of the N_2 environment, as it is inert, it fills into the pores, and eventually, when it saturates the pores, it gets destructed. Hence the porosity of the bio-char under CO_2 environment was higher than N_2 environment. A schematic diagram has been presented in Figure 5.6 to emphasize the formation of bio-char and its porous texture morphology. Thus as indicated in the previous finding, the development of porosity of the bio-char was utilized for developing high-surface-area adsorbents as reported in other literature [31]. The pH of the bio-char is directly related to the temperature; as the temperature increases, the pH increases. The separation of alkali salts from the organics begins at temperatures above 300 °C, and complete separation occurs around 600 °C [189]. As the temperature increases, the separation also progresses, thereby increasing the pH of the bio-char. Hence, bio-char under CO_2 has a higher pH than N_2 environment.

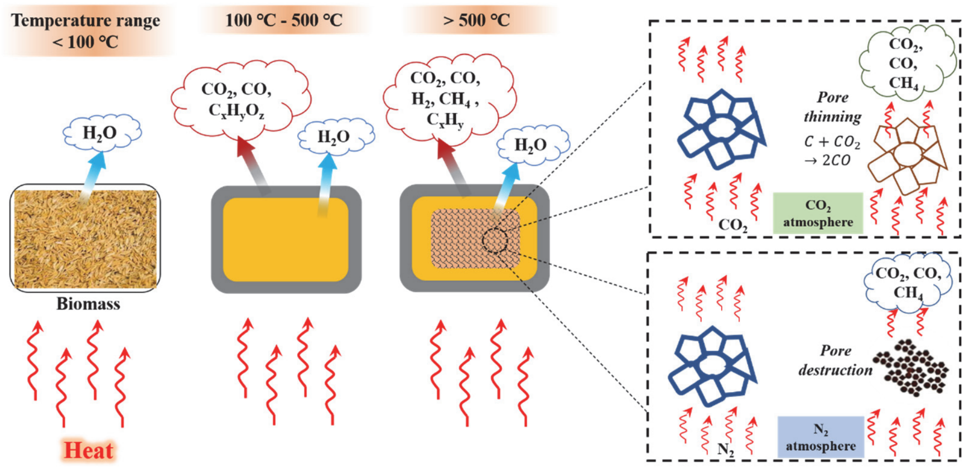

Figure 5.6. Formation of bio-char mechanism under N2 and CO2 environment.

A simple scheme has been presented to depict the structural change variation within the pyrolyzed biomass sample. The biomass initially starts to lose moisture as it is heated to ~100 °C. Once the temperature increases, the non-condensable gases like CO_2, CO, and CxHyOz are released. Further increasing the temperature beyond 500 °C results in changing the properties of bio-char formed. In the case of CO_2 environment, as CO_2 fills inside the pores, it reacts with the bio-char, i.e., carbon, and forms carbon-monoxide, causing pore thinning. This phenomenon increases the surface area of the bio-char formed under CO_2. Also, the separation of carbon atoms from the active sites leads to the formation of new pores, which allows the permeation of oxygen molecules and further leads to the removal of carbon compounds. Hence, the carbon content is less in the case of bio-char obtained under the CO_2 environment. However, in the case of N_2 environment, as it fills inside the pores, it doesn't react with bio-char due to its inertness and results in pore destruction, thereby reducing the surface area. Also, as more and more bio-oil is formed with a temperature beyond 500 °C, the pores start to clog, thereby inhibiting the permeation of oxygen molecules and prohibiting the removal of carbon compounds. This may be the reason behind the increased carbon amount in the N_2 environment.

5.8.2 FT-IR analysis

FT-IR spectroscopy is the tool to identify the shifts in chemical composition. The composition of both the bio-char obtained under N_2 and CO_2 environments were notably similar as presented (Figure 5.7). At higher temperature, the aliphatic chains break down which is confirmed by the absence of representative peak of C–H stretching at 2950–2850 cm^{-1} for both the bio-char. However, the presence of typical aromatic carbon peaks were confirmed by the C–H stretching at 800 cm^{-1}, C–C and C–O stretching at 1623 cm^{-1} [190]. Lee et al., also reported a similar behavior wherein the charring temperature significantly reduced the aliphatic carbon but increased aromatic carbon [191]. Also, the presence of hydroxyl group (O–H stretching) was confirmed by the peak at 3481 cm^{-1}. The peak at 1075 cm^{-1} corresponds to the silica which were present in the pretreated RH, thereby confirming the silicon-carbon framework [190]. The typical peak of C–O stretching bonds at 1090 cm^{-1} [155] present in the original RH [17], started to disappear in the bio-char's (N_2 and CO_2). This advocates the degradation and depolymerization of hemicellulose, cellulose and lignin [192]. However, the peak area of C–O stretching bonds were higher in case of bio-char under N_2 environment, thereby confirming presence of more amount of CO containing compounds.

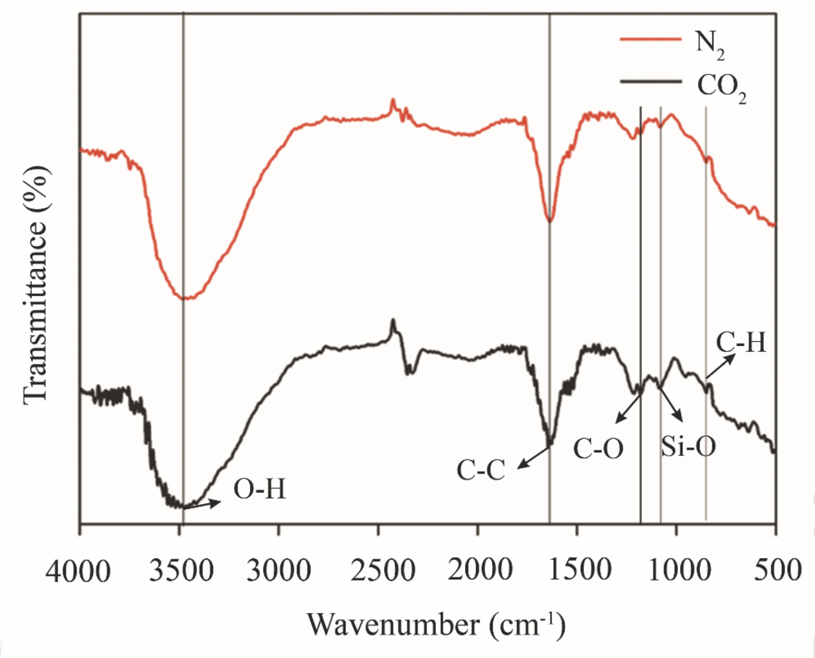

Figure 5.7. FT-IR spectra of bio-char under N_2 and CO_2 environment.

5.8.3 TG analysis

TG analysis revealed that the prepared bio-char is thermal more stable i.e., only 10% degradation was observed at a very high temperature of 800 °C (Figure 5.8). In case of bio-char under N_2 environment, the DTG curve shows two peaks with very low intensity around 340 °C (cellulose) and 400 °C (lignin), which are related to the degradation of cellulose and lignin, respectively. In case of bio-char under CO_2 environment, the high intensity peak at 340 °C compared to N_2, also confirms the presence of high volatile matter in the respective bio-char. It can also be hypothesized that the major volatile matter was derived from the lignin content and hence to obtain a bio-char with high fixed carbon ratio and less volatiles, the pyrolysis process should be operated above 300 °C. Also, in case of CO_2 bio-char, the peak at 750 °C could be due to the decomposition of lignin content. Overall, the bio-char obtained under N_2 and CO_2 environments were found to be highly (thermally) stable.

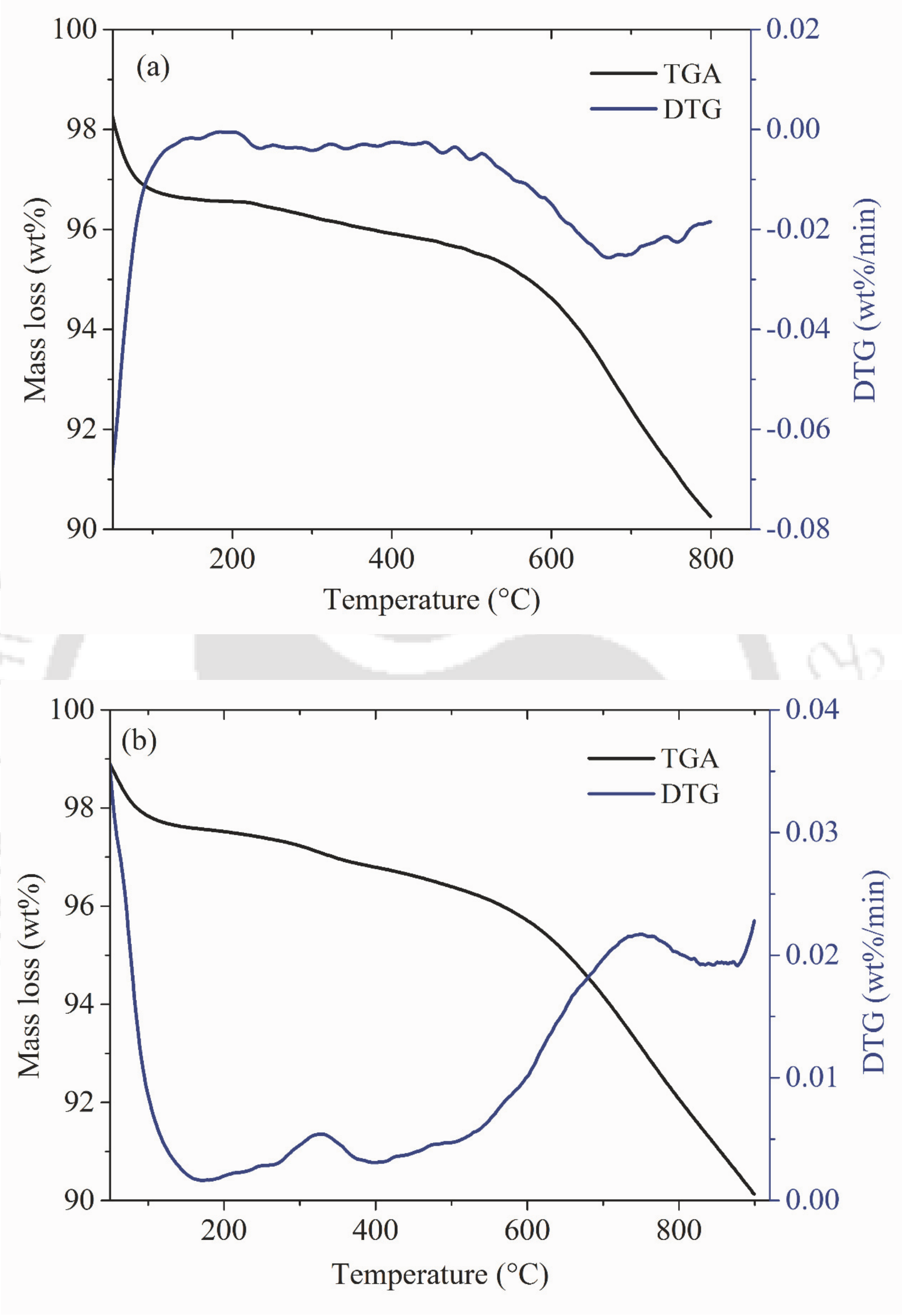

Figure 5.8. TG and DTG analysis of bio-char under (a) N_2 and (b) CO_2 environment.

5.8.4 Morphology analysis

FESEM analysis of the bio-char was performed to analyze the effect of pyrolysis environment on the structure of bio-char (Figure 5.9). It was observed from the images that there was a significant difference in the dimensions and texture of bio-char obtained under N_2 and CO_2 environments, respectively. Under an inert N_2 environment, degradation of lignocellulosic components under higher temperatures does modify the structure of bio-char, leading to existence of uneven/non-uniform morphology. However, presence of a reactive CO_2 environment alters the physico-chemical characteristics of the bio-char. Along with modifying the internal composition of bio-char, the in-situ reactions also lead to the destruction of bio-char stability and render an overall porous texture. The highlighted portions of the FESEM image (right) provide evidence of destruction.

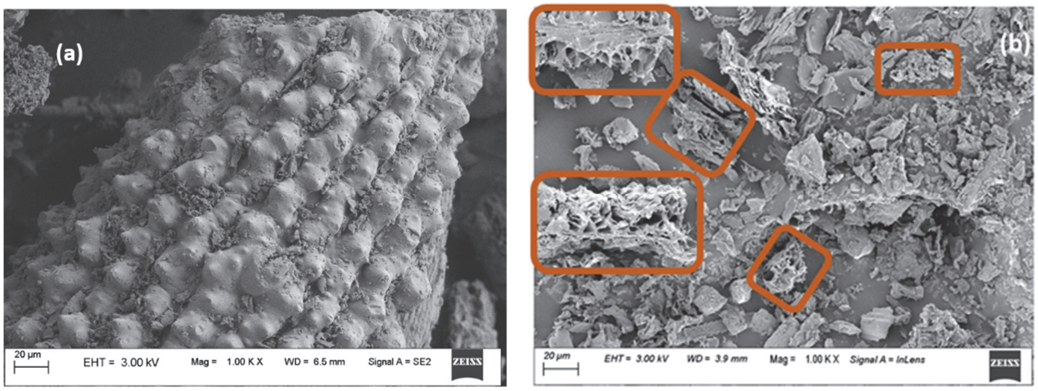

Figure 5.9. FESEM images of bio-char under (a) N_2, (b) CO_2. Highlighted regions in the right image present the porous texture of the bio-char. All the images have been taken at 1000 X magnification.

5.9 Summary

The slow pyrolysis process for generating bio-char from RH under two different environments—N2 and CO_2—has been studied. The main variables affecting the pyrolysis process were temperature, holding time, and flow rate. RSM optimization technique was utilized to obtain the optimal bio-char yield with maximum carbon content. The bio-char yield was observed to be higher under the CO_2 environment, although the carbon content was higher in the case of N_2 environment. The optimum condition obtained for bio-char yield and carbon content were 521 °C, 48 min and 0.87 L/min for N_2 environment and 545 °C, 43 min and 0.87 L/min for CO_2 environment. The physico-chemical characterization revealed that bio-char under CO_2 had higher aromaticity, surface area and was relatively more hydrophilic and polar. This study could conclude that bio-char with appropriate physico-chemical characteristics could be developed based on the targeted application. The bio-char prepared under a CO_2 environment can be used as an adsorbent as it has high porosity and surface area, which is confirmed by the morphological analysis, whereas for soil conditioners, bio-char under N_2 environment is preferable.

भारतीय प्रौद्योगिकी संस्थान गुवाहाटी • Indian Institute of Technology Guwahati •

CHAPTER VI

Utilization of bio-char produced under reactive environment for the separation of ranitidine from synthetic wastewater

---

Alkali activation (KOH) of bio-char

Physico-chemical characterization of activated bio-char

Adsorption kinetics and isotherms

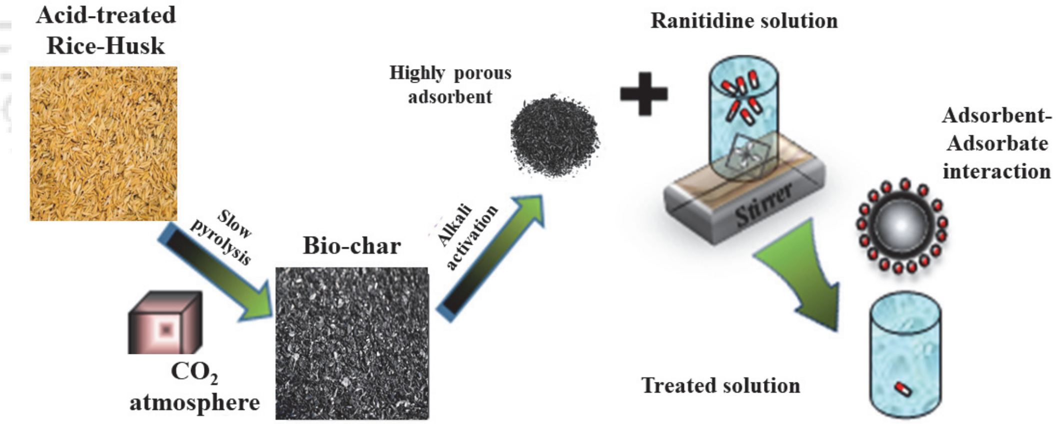

Chapter VI

Utilization of bio-char produced under reactive environment for the separation of ranitidine from synthetic wastewater

Employing sustainable techniques that utilize waste resources to generate valuable products is pivotal towards establishing economically-sound technologies. Moreover, directing these techniques towards creating entities that aid in alleviating environmental pollution concerns is highly desirable. Rice husks (RH) are abundantly available biomass that are usually convert to organic matter via inefficient means such as dumping and incineration. Their utilization in thermochemical processes such as pyrolysis yields fruitful, high-utility products like bio-char and bio-oil. Bio-char presents ideal platforms for developing highly-porous organic adsorbents. This work utilizes a slow pyrolysis method for converting RH to bio-char under various temperatures in a CO_2 *environment. The utilization of* CO_2 *influences the textural and chemical nature of the developed bio-char, and its deployment also lends an environmentally-conscious facet to this work, as it helps lower the overall carbon footprint. As-prepared bio-char was activated in the presence of an alkali that enhanced its overall surface area to 440* m^2/g*. Activated bio-char was utilized as an adsorbent for the removal of commonly-found pharmaceutical pollutant, Ranitidine. Different parametric studies, such as variation in pH, adsorbent dosage, and pyrolysis temperature, were performed to understand their effect on the adsorption capacity of prepared adsorbents. Adsorption of 50 ppm ranitidine on the activated bio-char at pH*

9 resulted in the removal of 88.3% reactant at 100 mg adsorbent dosage. Under those conditions, activated bio-char displayed a maximum adsorption capacity of 65.8 mg/g. Adsorption kinetics followed a pseudo-second-order pathway, while the Langmuir model could describe the adsorption isotherm.

6.1 Characterization of bio-char and activated bio-char

6.1.1 Textural properties

N_2 adsorption isotherm of both samples represented in black and blue curve respectively showed type II isotherm pattern (Figure. 6.1 (a)) [193]. However, the corresponding desorption isotherm showed hysteresis nature as observed from black, red, and green plots, respectively, for samples $ARHB_{300}$, $ARHB_{500}$, and $ARHB_{700}$. Hysteresis is usually due to different behavior during the adsorption and desorption process. The hysteresis nature was similar to type H3. This hysteresis is usually found on solids consisting of aggregates or agglomerates of particles forming slit-shaped pores/ plates or edged particles (like cubes), or non-uniform size and/or shape. Similarly, the pore size distribution of the sample was compared and shown in Table 6.1. The average pore size of $ARHB_{500}$ was 13.61 nm with a total pore volume of 0.237 cm^3/g, and that of $ARHB_{700}$ was 13.96 nm with a total pore volume of 0.181 cm^3/g (Figure. 6.1 (b)). The result agrees well with the BET surface area. BET surface area of $ARHB_{500}$ (440.88 m^2/g) was slightly higher than $ARHB_{700}$ (429.84 m^2/g), and the least was for $ARHB_{300}$ (245.20 m^2/g) (Table 6.2). The pore size distribution confirmed the presence of micropores (0-2 nm) and mesopores (2-20 nm), as the volume of N_2 adsorbed lie in the range of pore width between 0-30 nm. $ARHB_{700}$ had the highest micropore followed by $ARHB_{500}$ and $ARHB_{300}$, whereas $ARHB_{500}$ had the highest mesopores followed by $ARHB_{700}$ and $ARHB_{300}$, which is also coherent with the higher BET surface area and pore volume of $ARHB_{500}$. Hence, activation of the bio-char substantially increased both the adsorption capacity and ranitidine removal as reaction with alkali cleared the partly blocked pores of the bio-char [131].

Table 6.1. Pore size distribution table of activated bio-char.

Sample	**V micro (cm^3/g)**	**V meso (cm^3/g)**
$ARHB_{300}$	0.022	0.007
$ARHB_{500}$	0.034	0.102
$ARHB_{700}$	0.111	0.071

Note. Macro pores was absent in the activated bio-char.

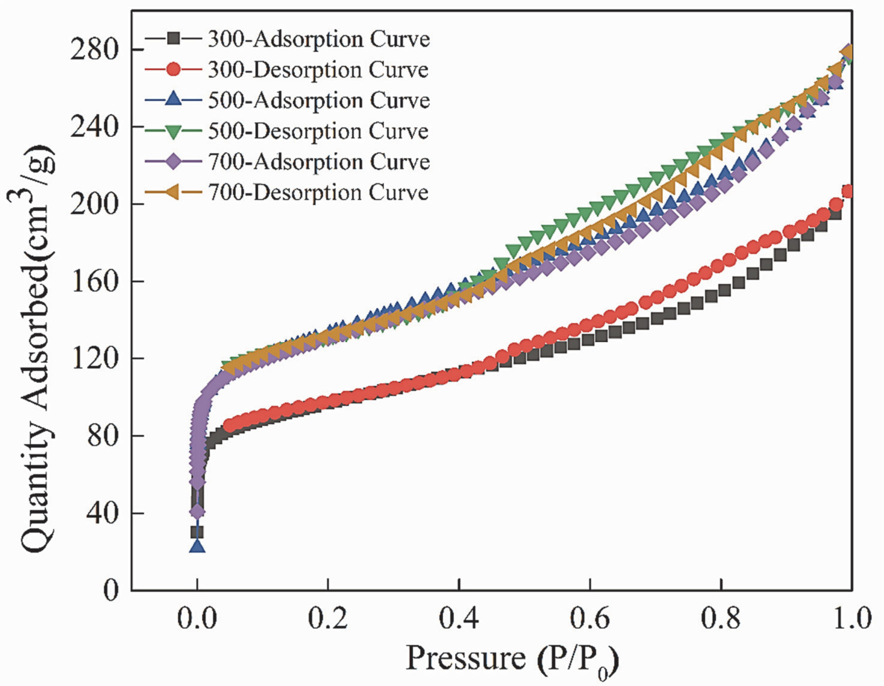

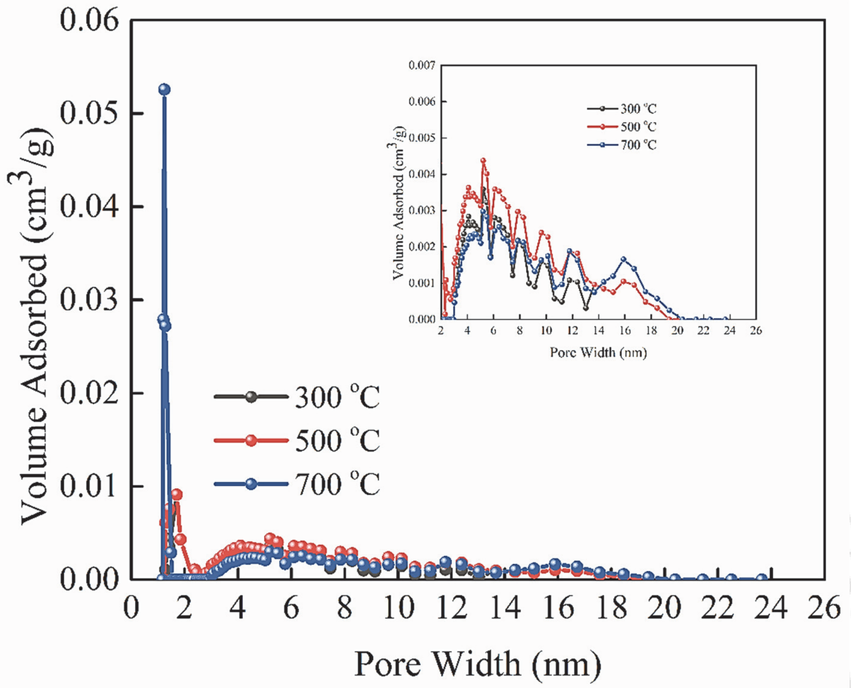

Figure 6.1. (a) Nitrogen adsorption/desorption isotherm for activated bio-char and (b) Pore size distribution.

6.1.2. Physico-chemical analysis

The results of the physicochemical analysis of bio-char and activated bio-char are shown in Table 6.2. The bio-char characteristics changes with the increased pyrolysis temperature. The volatile content in the RH_{300} bio-char was higher than RH_{500} and RH_{700}. The reason behind this is mainly the incomplete or partial degradation of biomass. The volatile content decreases post-activation as the chemical activators change the structure of bio-char. These may also cause degradation of organic compounds, thereby decreasing the overall volatile matter [194]. The KOH activation, an alkali treatment, mainly leaches out the silica from the bio-char, thereby reducing the ash content of the activated bio-char [195,196]. The BET surface area increased

Indian Institute of Technology Guwahati

post-activation, as the chemical activators helped to develop porosity in the bio-char by degrading the bio-char structure.

Table 6.2. Physico-chemical analysis of bio-char and activated bio-char.

	RH_{300}	**$ARHB_{300}$**	**RH_{500}**	**$ARHB_{500}$**	**RH_{700}**	**$ARHB_{700}$**
Moisture (%)	4.8	4.5	3.9	3.6	3.3	3.1
Ash (%)	25.3	7.1	36.1	16.9	37.3	18.2
Volatile matter (%)	46.2	25.4	28.3	19.7	16.5	10.1
FC (%)	23.7	63	31.7	59.8	42.9	68.6
BET surface area (m^2/g)	0.725	245.2	52.4	440.9	93.1	429.8

6.1.3 FT-IR analysis

FTIR analysis of the bio-char and activated bio-char showed similar peaks, but the peak's intensity varied, which confirmed that the functional groups remained intact during the activation process (Figure. 6.2). However, as the pyrolysis temperature increases, the intensity of the individual peaks decreases for both the bio-char and activated bio-char samples. The possible reason for this could be that as the temperature increased, the different characteristic groups present in the samples, such as hydroxyl, carbonyl, carboxyl, and methoxy, gradually underwent thermal cracking reaction and converted to liquid gaseous products. The presence of a peak in the range 3600 cm^{-1} to 3200 cm^{-1} indicates the O–H stretching vibrations as well as the presence of phenolics. The peak at 2378 cm^{-1} corresponds to the C–H stretching vibration from the aliphatic $-CH_2$ and alkanes $-CH_3$ groups. The absorbance peak at 1649 cm^{-1} is ascribed to the stretching vibration of C=O from carbonyl and carboxyl groups. The C–O stretching vibration was indicated by the peak obtained at 1311 cm^{-1}. The peaks at 1168 cm^{-1} and

716 cm^{-1} correspond to the silica's Si-O-Si asymmetric and symmetric stretching vibration, respectively [197].

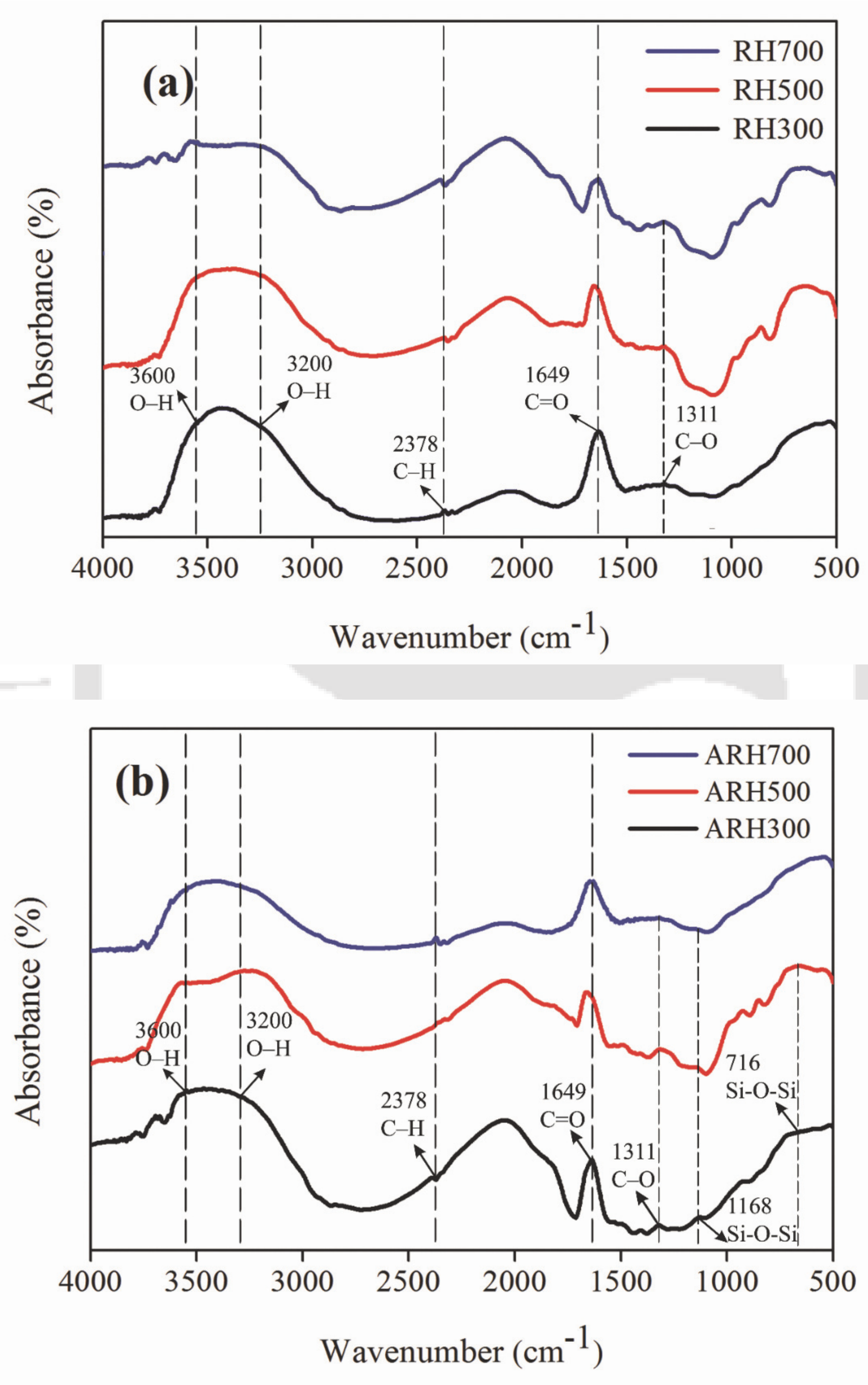

Figure 6.2. FT-IR spectra of (a) bio-char, (b) activated bio-char.

6.1.4 FESEM analysis

FESEM micrographs of bio-char and activated bio-char are shown in Figure. 6.3 to illustrate the potential physical changes caused by the activation process. The FESEM image of bio-char shows a smooth and non-porous surface. However, the activated bio-char appeared to have a rough, broken, and porous surface. During pyrolysis, the biomass lignin fraction might degrade with increased temperature to form the compounds such as phenolics, synringols, and guaiacols [198]. The modified lignin is possibly cross-linked with the organic acids formed during the degradation of biomass carbohydrate fraction. The presence of these compounds might have partially blocked the pores, and therefore, the surface appeared to be non-porous. During the activation process, the hydroxyl ion from the KOH reacted with the lignin and cleaved the ether linkages in the lignin to form soluble phenolics that eventually made the surface more porous and rough [131].

Indian Institute of Technology Guwahati

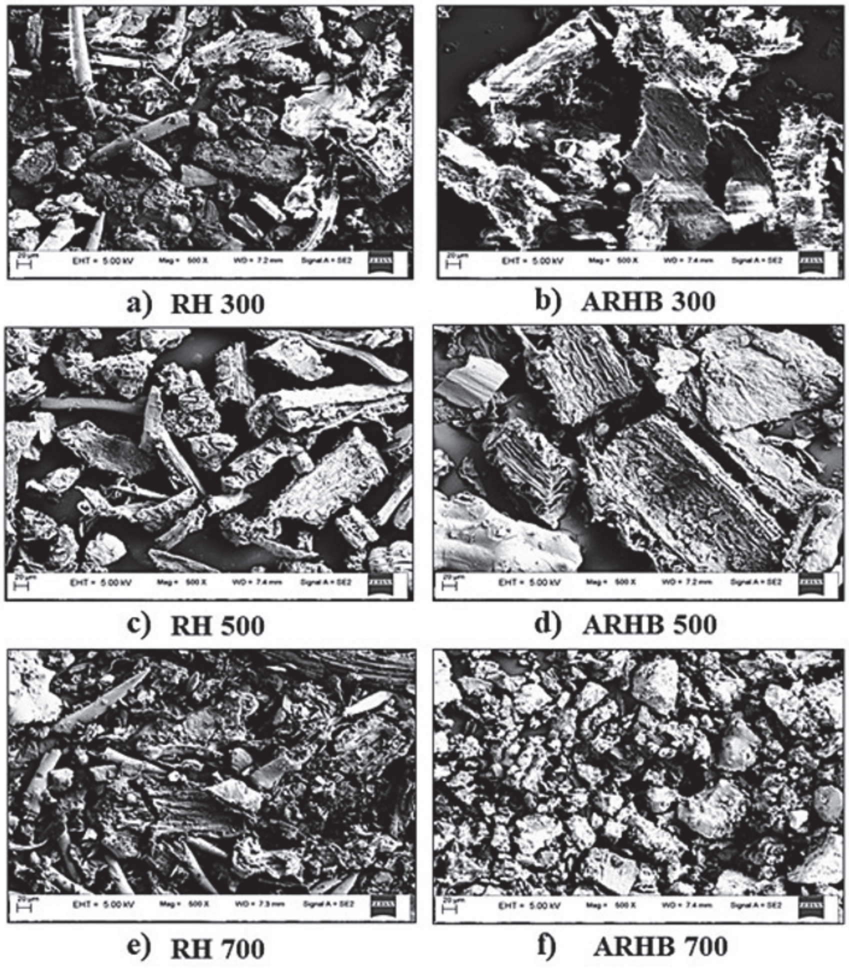

Figure 6.3. FESEM micrographs of the obtained and activated rice husk at 300, 500, and 700 °C. All images have been taken at 500 X magnification.

6.2 Adsorption kinetics

The four models, i.e., pseudo-first-order, pseudo-second-order, Elovich, and intraparticle diffusion models, were tested for their applicability to adsorption of ranitidine on $ARHB_{500}$. The equations employed for each model are shown in Table 2.1 (Chapter 2). In the case of adsorption of ranitidine on $ARHB_{500}$, fast adsorption kinetics was observed, allowing equilibrium to reach in 140 min. A similar observation was

Indian Institute of Technology Guwahati

reported by Bojic et al., during their study on ranitidine adsorption using Lagneria vulgaris shell [132], where the equilibrium was attained in about ~60 min. In another study by Mondal et al., ranitidine adsorption using moong bean husk as adsorbent was also observed to reach equilibrium in about ~90 min [199].

From Table 6.3, it can be seen that the pH greatly influences the adsorbent's adsorption capacity on the adsorbate. Therefore, in order to optimize the pH of the solution, the experiments were performed keeping other variables, such as initial drug concentration (50 mg/L), equilibrium time (140 min), adsorbent dosage (100 mg) at a fixed value. The pseudo-second-order gave the best correlation out of the four models tested. This model implies sharing of electrons between the adsorbate and the adsorbent surface. During the study, it was further observed that at pH 9, the adsorption capacity was around 44.44 mg/g, which was very close to the experimental value of 44.14 mg/g. Therefore, to verify the influence of mass transfer resistance on the adsorption of ranitidine, the intra particle model was used to fit the data, which gave the maximum correlation coefficient of 0.96 (i.e. $R^2 = 0.96$). The plot of the average particle loading, q_e (mg/g) vs $t^{0.5}$ (the square root of time) will yield a straight line passing through the origin if the adsorption process obeys the intraparticle diffusion model. The slope of the line gives the intraparticle diffusion rate constant. In case for the given data set, when q_e (mg/g) is plotted against $t^{0.5}$, a straight line (passing through origin) is obtained which indicates that the intraparticle diffusion model is the rate-controlling step and the boundary layer diffusion is not playing any significant role in determining the adsorption kinetics [132]. However, from Figure. 6.4, it can be seen that the plot did not pass through the origin, which indicates a significant mass transfer resistance by the boundary layer and the multi-step resistance to the adsorption within the particle [199].

The adsorbate adsorption had been postulated to take place in three stages. The first stage involved the movement of the adsorbate species through the bulk of the solution via the boundary layer on the adsorbent surface. The second stage involved the intra particle diffusion stage, which took a relatively long time, as the foreign molecules travel through the surface into the bulk of the adsorbent material via large-sized pores. The third stage involved diffusion through smaller pores which correspond to reduced adsorption rates since the concentration gradient of the adsorbate species reduced significantly. This eventually led to establishing the equilibrium between the two sets of materials [200]. Interestingly, from Table 6.3, it can be observed that with an increase in pH, the correlation coefficient increased and confirmed that the controlling step was the diffusion of ranitidine into the pores of $ARHB_{500}$. Therefore, the kinetics was influenced by the adsorbate's speed penetrated through the porous adsorbent. From Figure. 6.4 it appears that the initial rapid increase in the adsorption corresponds to the boundary layer diffusion-controlled process. After that, the decrease in adsorption rate could be correlated to the intra-particle movement through the adsorbent species. The decrease in slope value for the adsorption capacity of the adsorbent corresponds to increased resistance to mass transfer within the mesopores as the process was controlled by pore diffusion.

Table 6.3. Comparison for kinetic parameters for adsorption of ranitidine on to activated bio-char.

Model	**Constant**	**pH 3**	**pH 5**	**pH 7**	**pH 9**	**pH 11**
Pseudo-first order	q_e (mg/g)	4.64	10.63	4.32	11.98	8.32
	k_1 (g/mg min)	0.03	0.016	0.022	0.013	0.03
	R^2	0.82	0.90	0.81	0.94	0.92
Pseudo-second order	q_e (mg/g)	30.21	38.16	38.31	44.44	32.36
	k_2 (g/mg min)	0.05	0.01	0.02	0.005	0.012
	R^2	0.99	0.99	0.99	0.99	0.99
Elovich	α (mg/g min)	2.11×10^8	5.19×10^4	3.64×10^9	5.92×10^4	8.7×10^3
	β (g/mg)	0.59	0.39	0.69	0.35	0.40
	R^2	0.85	0.97	0.94	0.84	0.96
Intra-particle diffusion	k_{id} (g/mg min)	0.58	0.95	0.52	1.18	0.89
	R^2	0.69	0.90	0.81	0.96	0.84

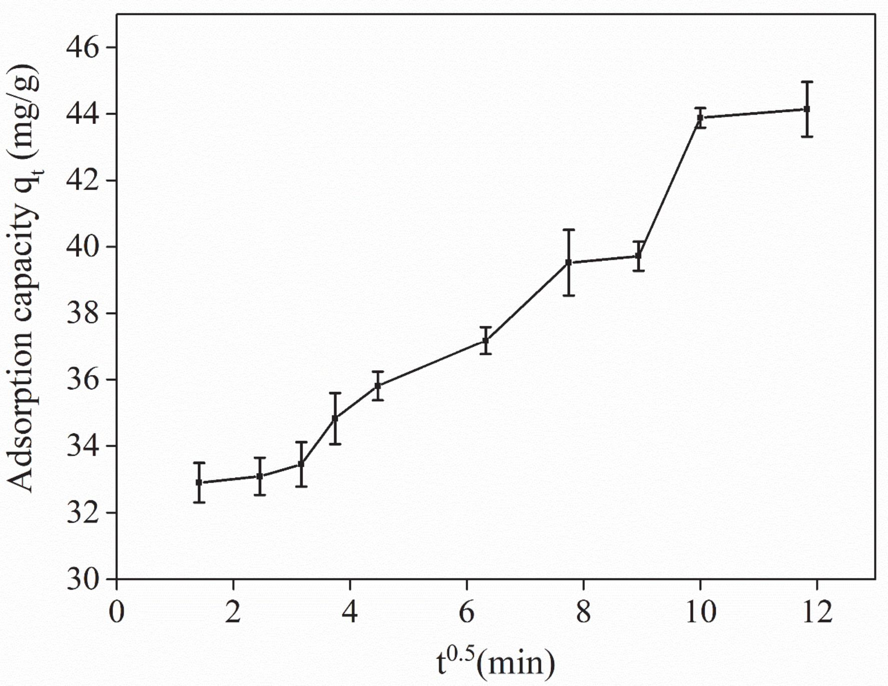

Figure 6.4. Kinetics of ranitidine adsorption according to the intra particle diffusion model (experimental conditions: initial drug concentration: 50 mg/L, equilibrium time: 100 min, adsorbent dosage: 100 mg, pH 9).

6.2.1 Influence of pH

From figure. 6.5, it can be observed that the adsorption capacity quickly increased in the first fifteen minutes of contact time and then gradually attained equilibrium. This depicted a high affinity of the adsorbent to bind to the substrates in the solution. The effect of pH on ranitidine removal was studied across a wide range of pH, i.e. 3–11. The pH was adjusted using 1 M HCl/NaOH. The activated bio-char ($ARHB_{500}$) with the highest surface area was used for all the experiments. The pH analysis results revealed the highest ranitidine removal capacity (88.3%) was obtained at pH 9. In order to analyze the adsorption process, parameters such as pH_{pzc} of the adsorbent (bio-char) and pK_a of the drug, were explored. pH_{pzc} value is the pH at which all the surface charges on the adsorbent have been neutralized. pKa value of the drug informs about the tendency of the drug to undergo protonation/deprotonation under different conditions. The pH_{pzc} of adsorbent ($ARHB_{500}$) was found to be 7.3, which was similar to the value as reported by Shen et. al., [195] and the pK_a value of the drug was found to be 8.2 [199]. It may be noted that, below pH_{pzc}, a positive charge developed on the surface of the adsorbent due to protonation in the presence of high H^+ ions in the solution. Therefore, there was electrostatic repulsion between the adsorbate and adsorbent at lower pH, leading to lower adsorption. Since the pK_a value of the drug was higher, at lower pH the drug underwent protonation and acquired a positive surface charge. A similar phenomenon might have occurred beyond a particular pH, as both the surfaces of the adsorbent and the drug would have developed a negative charge, which would have resulted in lower adsorption due to electrostatic repulsion [201]. In the current study, lower drug uptake was noticed at pH 3, 5, 7, and 11 (Figure. 6.5). However, maximum drug adsorption was observed at pH 9. This may have occurred as at this condition, pH of the solution was higher than pH_{pzc}, hence, the adsorbent surface remained negatively charged. Similarly, the ranitidine molecules may have gradually deprotonated at this pH as the pK_a value of the drug was lower than the solution pH. Thus, at this transition region, the adsorption was highest due to electrostatic forces because of the occurrence of opposite charges on both surfaces. Therefore, pH 9 was considered as the optimal pH and used for further experiments. It may also be noted that the experiments performed under various pH conditions displayed a trend in adsorption capacity that was akin to the one observed during adsorption kinetics analysis. The adsorption capacity rapidly increased up to 20 min, which indicates higher interaction with the clean pores of the adsorbent on account of a strong drug-concentration gradient directed towards the adsorbent surface. With time, the rate of adsorption capacity decreased, as shown in Figure 6.5. It may be due to the limited pores interacting with the drug molecules. Meanwhile, there might be a gradual development of a diffusion layer around the adsorbent, suppressing the initial, high drug-concentration gradient. Eventually, as the pores get saturated, it leads to the generation of a constant rate of adsorption capacity. These observations could be correlated with the intraparticle diffusion model analysis described in section 6.2.

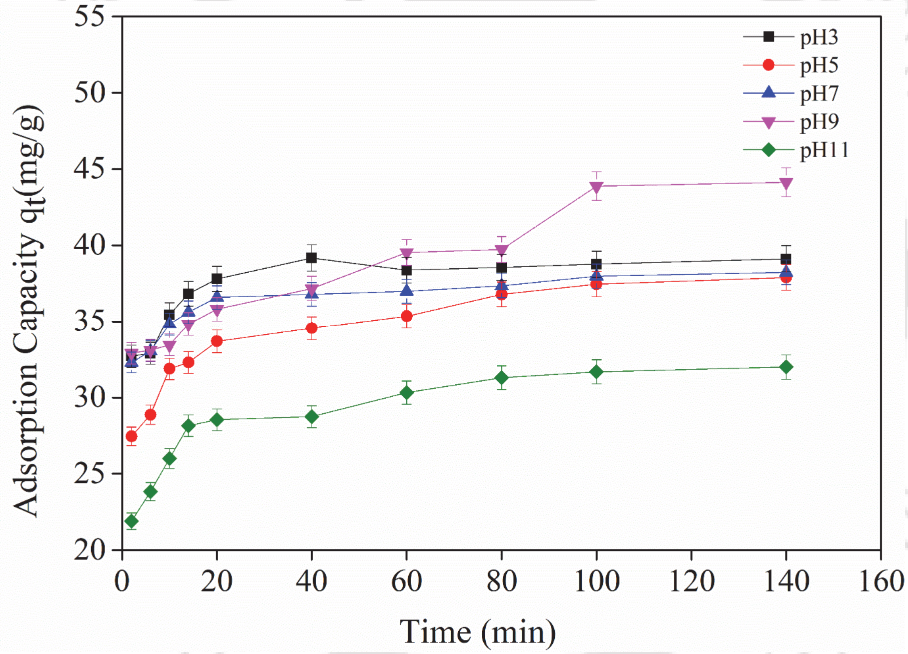

Figure 6.5. Effect of pH on the adsorption capacity of ARHB$_{500}$ (experimental conditions: initial drug concentration: 50 mg/L, equilibrium time: 140 min, adsorbent dosage: 100 mg).

ute of Technology

6.2.2 Influence of adsorbent dosage

The sorption capacity is an important parameter in the adsorption process, and hence the adsorbent dosage was varied from 50–150 mg/L. With an increase in the adsorbent dosage (from 50 to 100 mg/L), there was a progressive increase in the adsorption capacity. The maximum adsorption capacity of 44.14 mg/g was attained at 100 mg/L. This may be due to the sufficient number of available active sites on the adsorbent surface (Figure. 6.6). Further, an increase in the adsorbent dosage to 150 mg/L, slightly decreased the adsorption capacity to 42.29 mg/g. The saturation of all the active sites by ranitidine molecules could have predominantly been the reason for reducing the adsorption capacity [199]. Hence, in all the subsequent experiments, the adsorbent dosage was kept at 100 mg/L.

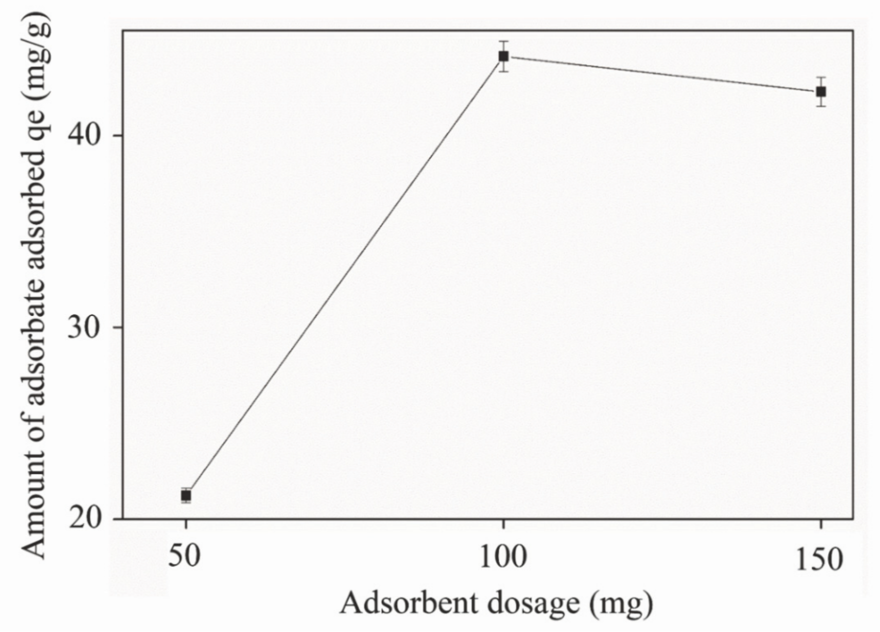

Figure 6.6. Effect of adsorbent dosage on the adsorption capacity of ARHB500 (experimental conditions: initial drug concentration: 50 mg/L, equilibrium time: 140 min, pH 9).

6.2.3 Influence of activated bio-char

The three bio-chars ($ARHB_{300}$, $ARHB_{500}$, and $ARHB_{700}$) were subjected to adsorption at the optimal pH and adsorbent dosage. Figure. 6.7 shows that the maximum adsorption capacity of ranitidine was observed in ARHB500. This could be due to its high surface area, as shown in Table 6.2. However, the difference between $ARHB_{500}$ and $ARHB_{700}$ was not very significant, but the correlation coefficient value obtained for $ARHB_{700}$ was less (Table 6.4). A plausible explanation for this could be as follows. Compared to other derived bio-chars i.e. moong bean or other plant species, the ash and silica content of RH bio-char was relatively high. At higher temperatures (~ 700 °C), relatively higher ash content may have blocked the pores of the adsorbent, thereby leading to generation of a bio-char with lower adsorption capacity. Hence, adsorbent $ARHB_{500}$ was chosen for further experiments.

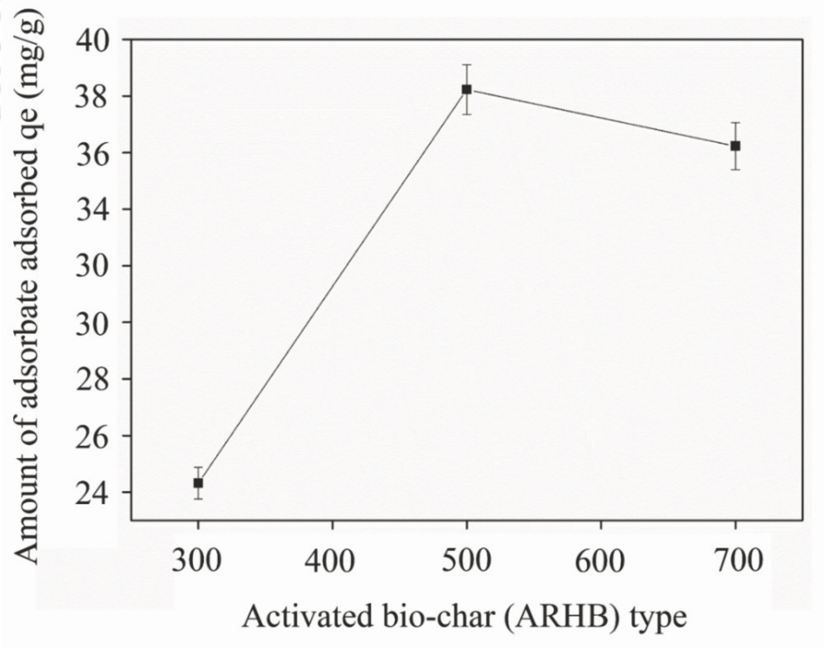

Figure 6.7. Influence of activated bio-char at the experimental conditions: initial drug concentration: 50 mg/L, equilibrium time: 140 min, pH 9.

Table 6.4. Comparison for kinetics parameters for adsorption of ranitidine at optimal conditions on to different activated rice husk chars (ARH).

Model		**ARH_{300}**	**ARH_{500}**	**ARH_{700}**
Pseudo-first order	q_e (mg/g)	14.55	11.98	15.11
	k_1 (g/mg min)	0.023	0.013	0.024
	R^2	0.74	0.94	0.74
Pseudo-second order	q_e (mg/g)	26.52	44.44	38.31
	k_2 (g/mg min)	0.002	0.005	0.003
	R^2	0.95	0.99	0.98
Elovich	α (mg/g min)	8.00	5.92×10^4	46.38
	β (g/mg)	0.25	0.35	0.20
	R^2	0.82	0.84	0.89
Intra particle diffusion	k_{id} (g/mg min)	1.66	1.18	2.00
	R^2	0.94	0.96	0.95

6.2.4 Adsorption isotherm

The adsorption isotherm is the most commonly used method to represent the equilibrium states of an adsorption system. The adsorption isotherm describes the relationship between the adsorbate concentration in the bulk solution to the amount adsorbed at the solid/solution interface. The equilibrium data were used to fit into various linearized isotherm models, as shown in Table 2.2 (Chapter 2). The experimental conditions for the equilibrium studies were: initial drug concentration

50 mg/L, equilibrium time 140 min, pH 9, adsorbent dosage 100 mg, and bio-char ARHB$_{500}$. The Langmuir model is mainly valid for the monolayer adsorption on the adsorbent surface. The constant b (L/mg) is the equilibrium adsorption coefficient, and Q_m (mg/g) is the maximum adsorption capacity calculated from the plot of C_e/q_e vs C_e [133,134]. The efficiency of the process is ascertained by the R_L (dimensionless equilibrium parameter) value.

$$R_L = \frac{1}{1+bC_o} \qquad 6.1$$

Where, C_o is the initial drug concentration (mg/L). The adsorption is considered as favourable when $0<R_L<1$, unfavourable when $R_L >1$, linear when $R_L =1$ and irreversible when $R_L =0$ [202].

Table 6.5 represents the values of Q_m, b, R_L, and R^2. The value of R_L was found to be 0.11, which confirmed the adsorption was favorable towards ranitidine. The value of Q_m was found to be 69.93 (mg/g), which was quite close to the experimental value of 65.8 (mg/g). The correlation coefficient value was found to be close to 1, which suggested that the Langmuir model could well characterize the adsorption isotherms. Freundlich model depicts adsorption on multiple surfaces. The terms k_f (mg/g) and n represent adsorption capacity and intensity. The present study calculates k_f and n from log q_e vs log C_e plot. The values of k_f, n, and correlation coefficient R^2 are presented in Table 6.5. The n value of 3.46 signified that the adsorption was satisfactory [203]. The correlation coefficient value for Freundlich isotherm was found to be 0.97. Thus, the Temkin model was used to understand the relationship between the adsorbent and adsorbate. The k_t (L/mg) represents the binding energy, and B=RT/b gives the heat of adsorption, where R= 8.314×10^{-3} (kJ/mol), T is the absolute temperature (K), and b (kJ/mol) is the isotherm constant. The values of B and k_t were obtained by plotting q_e vs ln C_e. The positive value of B (Table 6.5) indicates that the adsorption was exothermic, suggesting monolayer adsorption [204]. Sips isotherm is mainly a combination of the Freundlich and Langmuir isotherm model. The K_s (/mg) and Q_{max} (mg/g) represented the Sip's equilibrium constant and maximum adsorption capacity. This isotherm is characterized by the heterogeneity factor n, which is between 0 and 1. When n=1, it reduces to the Langmuir model, suggesting homogeneous adsorption [135]. When n is considered as 0.2, the correlation coefficient was found to be 0.94; however, at n=0.9 (close to unity), the correlation coefficient changed to 0.98, confirming the adsorption to be monolayer.

Table 6.5. Isotherm parameter for ranitidine removal by $ARHB_{500}$. Experimental conditions: initial drug concentration 50 mg/L, equilibrium time 140 min, pH 9, adsorbent dosage 100 mg.

Constant	Value
Langmuir isotherm	
b (L/mg)	0.34
Q_m(mg/g)	69.9
R_L	0.11
R^2	0.99
Freundlich isotherm	
k_f ((mg/g)(1/mg)$^{1/n}$)	24.25
N	3.46
R^2	0.98
Temkin isotherm	
B	0.085
k_t (L/mg)	7.04×10^{-11}
R^2	0.99
Sip's Isotherm	
R^2 (n=0.2)	0.94
R^2 (n=0.9)	0.98

6.3 Summary

The present study aims to develop a low-cost-adsorbent from an agricultural by-product RH to adsorb ranitidine drug. The RH was pyrolyzed at different temperatures and activated using alkali treatment (KOH) to enhance its properties. The adsorbent was thoroughly characterized for maximum ranitidine removal by varying process parameters such as solution pH, dug dosage, bio-char type. The kinetics study showed that the adsorption followed the pseudo-second-order model. The Langmuir adsorption isotherm model best represented the experimental data. A good correlation was observed between experimental adsorption capacity of 65.8 mg/g and theoretical adsorption capacity of 69.9 mg/g. This implied chemical adsorption onto the active sites of the adsorbent. pH played an important role, and the adsorption was favorable in basic solution wherein the adsorbent and the drug were oppositely charged. Thus, this technique utilized a waste by-product to synthesize an efficient economic adsorbent and laid down the groundwork for developing a potentially sustainable adsorbent for drug removal.

TH-3101_166107009

CHAPTER VII

Optimal synthesis of silica nanoparticle from bio-char produced during the pyrolysis process under reactive environment and its application towards preparation of superhydrophobic coatings

---

Bio-char as feedstock for generation of silica nanoparticles

Physico-chemical characterization of silica nanoparticles

Functionalization of silica nanoparticles

Application of functionalized silica nanoparticles

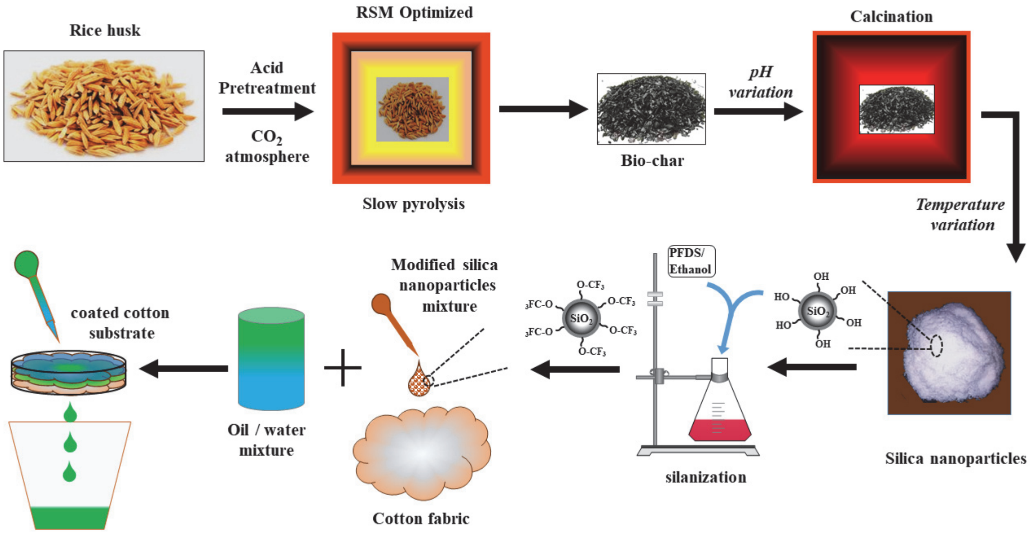

Chapter VII

Optimal synthesis of silica nanoparticle from bio-char produced during the pyrolysis process under reactive environment and its application towards the preparation of superhydrophobic coatings

The wide-scale prevalence of functional silica nanoparticles across different applications such as imaging, catalysis, and drug delivery has been documented in the literature, highlighting its potential. These silica nanoparticles can be tailored and functionalized accordingly to the requirement. However, the generation of silica nanoparticles at a large scale usually entails huge consumption of harsh chemicals, energy, and capital cost. Along with this, the process involved generate wastes that negatively impact the environment. This work utilizes agro-waste such as rice husk (RH) to produce silica nanoparticles, thereby providing a more facile alternative to conventional methodologies. The RH is pyrolyzed under a CO_2 *environment to obtain bio-char. Furthermore, the produced bio-char is also treated at different pH before being utilized to synthesize nanoparticles. The treated bio-char is then calcined to generate silica nanoparticles. The nanoparticles were then modified using silanes to make them superhydrophobic. Different characterization techniques are employed to investigate its physico-chemical properties. This chapter demonstrates a proof-of-concept highlighting the application of superhydrophobic and oleophilic silica nanoparticles towards oil-water separation.*

TH-3101_166107009

7.1 Compositional analysis

The elemental composition of rice husk and bio-char determined through the XRF is shown in Table 7.1. The results showed the relative silica content in the rice husk improved from 84.8 wt% to 96.5 wt%, as the inorganics were leached out during the pretreatment process. Variation in the silica concentration (%) was observed through the change in the pyrolysis temperature, and the highest was at 500 °C (98.7 wt%). The reason behind the increased concentration of silica with the pyrolysis temperature was due to dehydration reactions or decomposition of oxygenated compounds, which releases low molecular weight byproducts containing H and O [205]. Table 7.1 also shows similar results, wherein the oxygen-containing compounds decreased at higher temperatures. Beyond 500 °C, the decrease in the silica content could be due to clogging of pores inside the bio-char, as more liquid products are condensed and devolatilized. The clogging prevents the oxygen molecules from penetrating into the pores. As a result, the carbon compounds were not removed completely, thus decreasing the silica content [206]. Therefore, bio-char obtained at 500 °C was considered for further experiments.

Table 7.1. Compositional analysis (wt %) of raw RH, pretreated RH and derived bio-chars.

Compound	Raw RH	Pretreated RH	Bio-char (300 °C)	Bio-char (500 °C)	Bio-char (700 °C)
SiO_2	84.8	96.5	97.5	98.7	97.4
Na_2O	0.6	0.19	0.15	0.13	0.09
MgO	0.9	0.15	0.09	0.06	0.08
Al_2O_3	1.16	0.6	0.27	0.31	0.23
P_2O_5	2.7	0.17	0.04	0.03	0.03
SO_3	2.5	1.6	0.53	0.35	0.33
Cl	0.7	0.1	0.06	0.09	0.08
K_2O	3.8	0.1	0.06	0.08	0.06
CaO	0.9	0.08	0.04	0.03	0.02
TiO_2	0.08	0.07	0.03	0.04	0.04
Fe_2O_3	1.7	0.2	1.09	0.09	1.54

7.2 Characterization of silica nanoparticles at different pH

Considering that the maximum amount of silica was obtained in the pyrolytic residue at 500 °C, the subsequent experiments were carried out at 500 °C. Experiments were also performed to evaluate the effect of pH (i.e., pH 3–9) on the size of silica nanoparticles; similarly, different characterization techniques were used to analyze the physico-chemical characteristics of silica nanoparticles.

Table 7.2. Silica nanoparticles characterization at different pH.

Temperature (°C)	pH	Average particle size (nm)	Surface charge (mV)	BET Surface area (m^2/g)
500	3	25.04	-9.5	187.31
	5	18.19	-18.7	270.18
	7	36.28	-14.7	221.34
	9	38.47	-15.5	195.26

7.2.1 Surface charge and FESEM analysis

A zeta potential analyzer measured the surface charge of produced silica nanoparticles at different pH levels. The result showed that the average potential value of silica nanoparticles was less than ± 20mV. This indicates that the particles exist in the agglomerated state as they did not have sufficient electrostatic charges to overcome the intermolecular forces [207]. The highest value of zeta potential was obtained at pH 5, indicating the presence of finer silica nanoparticles as the surface charge allowed the particles to prevent coalescence for a relatively long time. At higher alkaline conditions (~pH 9), the zeta potential value drops due to further attachment of the hydroxyl groups onto the surface of silica nanoparticles. This might lead to the attraction of counter ions from the solution, reducing the surface charge. Furthermore, particle size also increases at these conditions with an increase in the degree of agglomeration. Similar observations regarding silica nanoparticles configuration have been observed using FESEM images [207].

As mentioned earlier, the obtained silica nanoparticles particle size was analyzed through the SEM technique, and the lowest particle size (relatively higher surface area) was observed at 500 °C for pH 5. The SEM images (Figure 7.1)of the particles indicated the presence of small particle aggregates, which could be due to a lower surface charge [205]. The zeta potential analysis of the obtained silica nanoparticles found that its surface charge was beyond the stable range of ± 30 mV to ± 50 mV [208]. Since particles having a surface charge outside this range are considered to be not stable, this is probably the reason behind the formation of such aggregates as observed under different pH conditions.

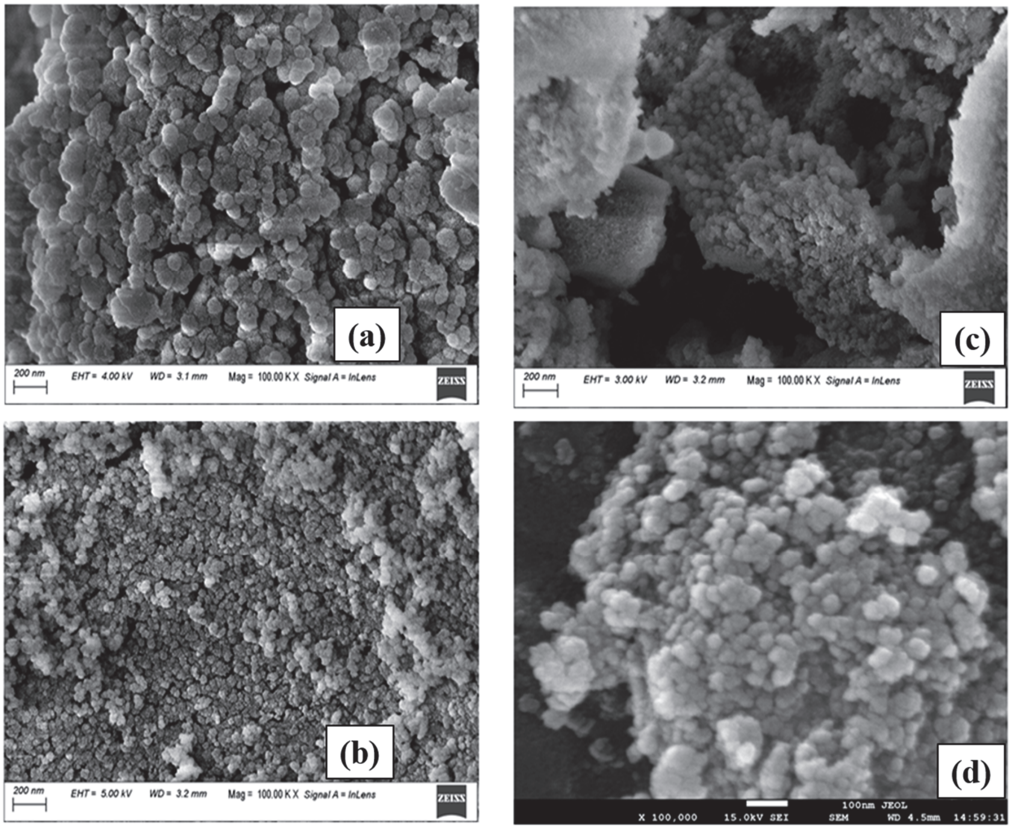

Figure 7.1. SEM images of silica nanoparticles at different pH conditions: (a) pH 3, (b) pH 5, (c) pH 7 and (d) pH 9. Silica nanoparticles were derived from bio-char generated at 500 °C. All the images have been taken at 100 kX magnification.

7.2.2 XRD analysis

The XRD analysis depicts the structure and chemical compositions of silica nanoparticles. The XRD spectral analysis of samples at different pH showed various peaks that confirm the formation of different phases of silica i.e., quartz (Q), cristobalite (C), and mullite (M), as depicted in Figure 7.2 [209]. The phase formation could result from the pH adjustment of bio-char, which finally affects the size of the nanoparticle. The literature reports that the unit cell volume of phase C is higher than phase Q, which could be a probable reason for the smallest size of silica nanoparticles produced at pH 5 (500 °C). A single higher intensity peak was observed at pH 5 (500 °C), indicating the presence of Q phase silica with the smallest average particle size of 18 nm and the highest surface area of 270.18 m^2/g. Hence, this particular pH condition was further employed to produce silica nanoparticles for creating superhydrophobic and oleophilic silica nanoparticles surfaces. The relative conversion of the quartz phase and associated decrement in the 2θ value may be due to the presence of thermally induced phase transition.

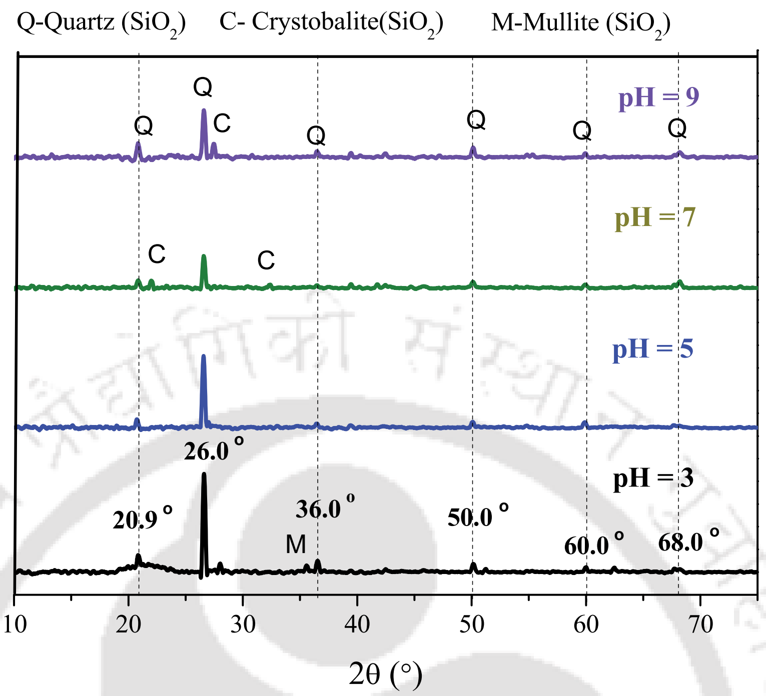

Figure 7.2. XRD patterns of silica nanoparticles (derived from bio-char generated at 500 °C) at different pH.

7.3 Functionalized silica nanoparticles

Four different types of silanes (DCMS, PFDS, TCDS, and ODTMS) and stearic acid were tested for functionalizing silica nanoparticles to make them hydrophobic. Each modified silica nanoparticles was sprayed over clean glass slides and then dried at 80 °C for an hour. The water contact angle obtained on each glass slide is presented in Figure 7.3. The water contact angle for DCMS, TCDS, ODTMS, and SA were found to be in the hydrophobic range, i.e., $90° < \theta < 150°$. Interestingly, PFDS modified silica nanoparticles contact angle was observed to be in the superhydrophobic range, i.e., $\theta > 150°$, as shown in Figure 7.3 [210]. That is mainly attributed to the least surface energy of PFDS among all the silanes as it has F atoms with low atomic radius, high electronegativity, and low polarizability. Moreover, the bond length of C–F was just 1.35 Å, which is very small. As a result, different groups such as OH cannot replace it, rendering the surface with low surface energy and correspondingly high-water contact angle [211]. Hence, water faces difficulty in wetting the surface, indicating a high hydrophobicity of the surface.

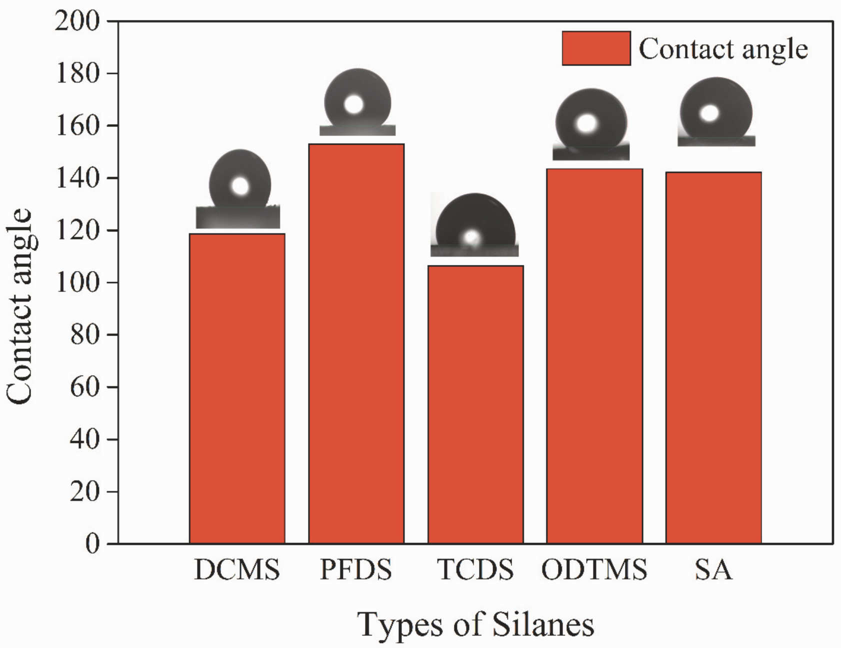

Figure 7.3. The contact angle of different silane-coated silica nanoparticles surfaces.

7.3.1 Optimization of coating agent concentration

Since the highest hydrophobicity was obtained using PFDS, the effect of its concentration was further investigated and shown in Figure 7.4. Four different proportions of PFDS, i.e., 50 µL, 100 µL, 200 µL, and 300 µL was added to the mixture of 40 mg silica nanoparticles and 10 mL ethanol. The results showed that the hydrophobicity of silica nanoparticles increased by increasing the concentration. This could be due to the extremely low surface energy of PFDS, which eventually lowers the silica nanoparticles surface energy. Therefore, the liquid was unable to wet the coated surface.

Further, increasing the concentration to 300 µL led to decreased the hydrophobicity to 145°. The possible reason for this could be more functionalized silica nanoparticles were available, and their attachment to the surface might have resulted in the formation of a multi-layer structure. This might have reduced the overall roughness and increased solid-liquid interfacial area, reducing the water contact angle. Thus, 200 µL PFDS was fixed as the optimal concentration.

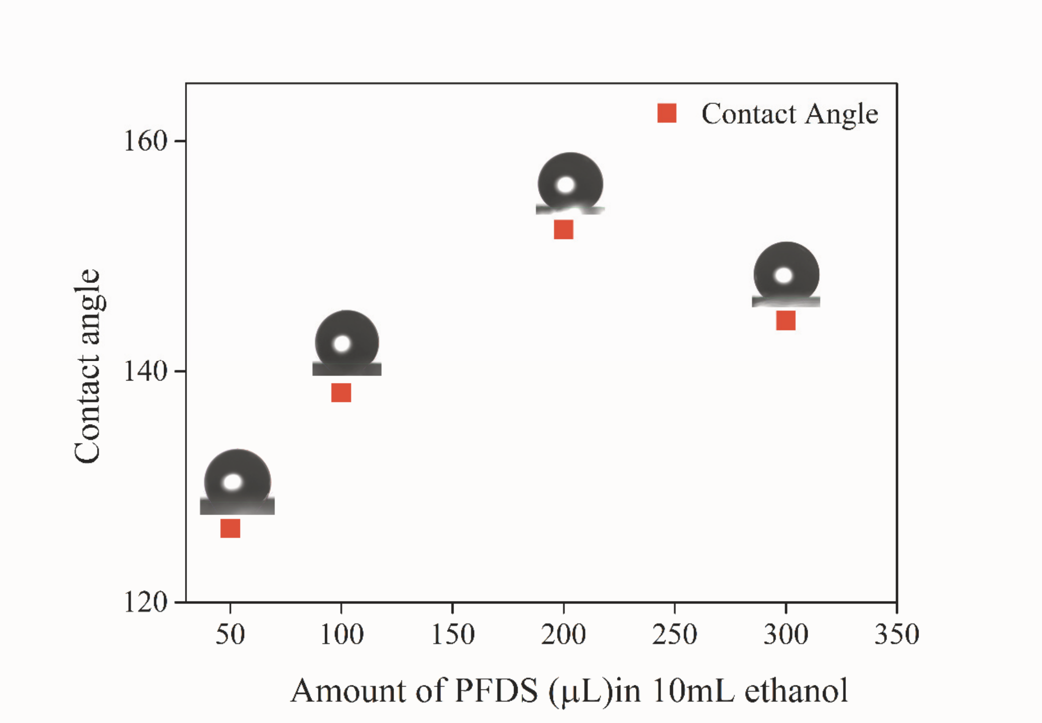

Figure 7.4. Contact angle variation of different silane functional group coated silica nanoparticles surface.

7.3.2 FT-IR analysis of pristine and modified silica nanoparticles

The FT-IR spectral analysis of modified silica nanoparticles was carried out to determine various functional groups in the test sample. Figure 7.5 shows the FT-IR spectra of pristine and the modified silica nanoparticles. The peak at 1063 cm^{-1} corresponds to the Si–O stretching within the SiO_4 tetrahedra structure of silica nanoparticles. A shift in the peak to 1100 cm^{-1} after modification confirms the formation of Si–O–Si bond and represents the asymmetrical stretching of Si–O–Si. Moreover, peaks around 1085 cm^{-1} indicated the presence of –OH groups on the coated silica nanoparticles that aided in forming covalent bonds with PFDS groups [210]. The peak obtained at 1201 cm^{-1} represents $-CF_2$ stretching vibrations from the surface-functionalized groups. The peaks at 1372 and 1444 cm^{-1} corresponds to the deformation of $-CF_3$ and $-CF_2$ groups, whereas the peaks at 2910 cm^{-1} correspond to the –CH stretching vibrations [212].

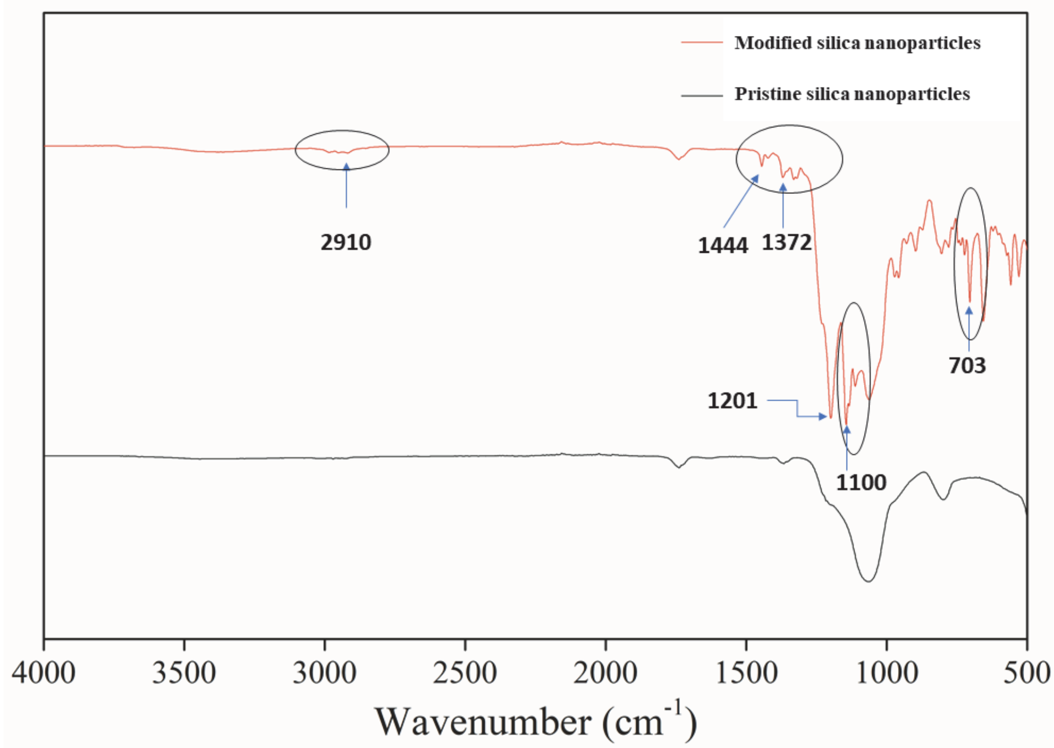

Figure 7.5. FT-IR spectra of pristine and modified silica nanoparticles.

7.3.3 EDX analysis of pristine and modified silica nanoparticles

The mineralogical composition of coated and uncoated silica nanoparticles estimated using EDX analysis is depicted in Figures 7.6 (a) and (b). The analysis result revealed the presence of C, O, and Si on the surface of uncoated particles, and no other element was significantly present on the surface. As a part of elemental spectra of PFDS coated nanoparticles, the presence of F group was apparent onto the surface with a major peak. Thus, surface coated with PFDS had low surface energy and gave the highest water contact angle because of the different attributes related to the presence of CF_3 group.

Indian Institute of Technology Guwahati

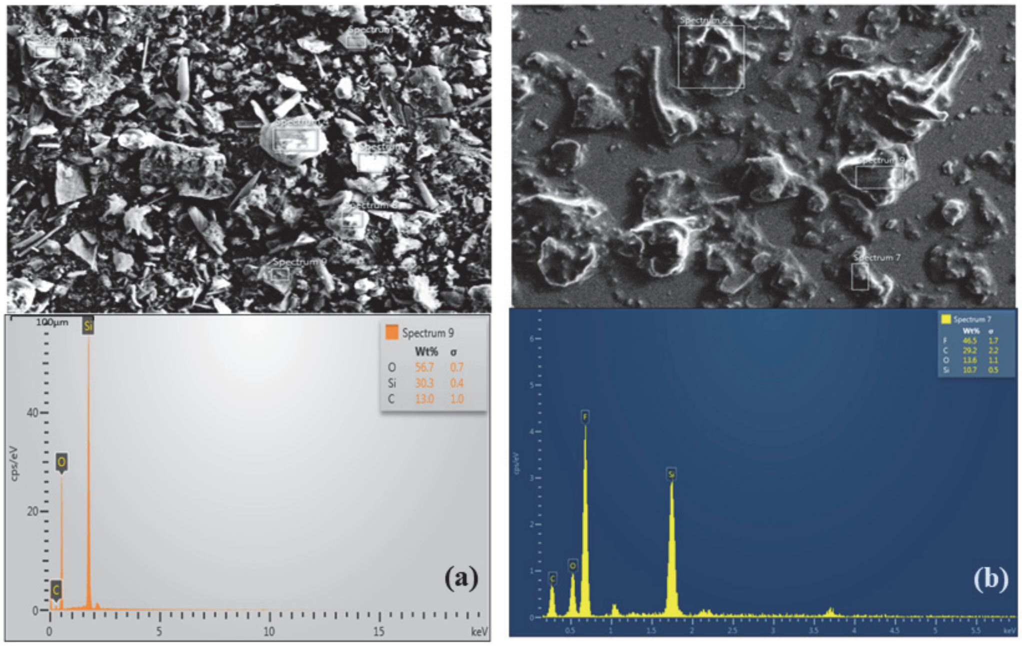

Figure 7.6. EDX spectra of pristine and modified silica nanoparticles.

7.3.4 AFM Analysis of modified silica nanoparticles

Figure 7.7 demonstrates the roughness of PFDS coated silica nanoparticles. The coated particles were deposited on a glass substrate and analyzed using AFM. For a patch of 20 µm by 20 µm, the average roughness of the surface was observed to be ~10 nm. This indicates the presence of nanoscale-induced features on the surface of the substrate. Upon depositing a water droplet on the modified substrate, the droplet assumed a configuration whose wetting characteristics could be defined using a Cassie-Baxter analysis. As the modified glass substrate had a heterogeneous surface texture, the roughness factor of the substrate facilitated a higher volume of trapped air beneath the deposited water droplet and thus increased the apparent water contact angle. The roughness factor may be defined as the fraction of the actual solid-liquid contact area to the projected total solid-liquid contact area [213]. Hence, the disordered structure generated due to the silica nanoparticles aided in increasing the water contact angle.

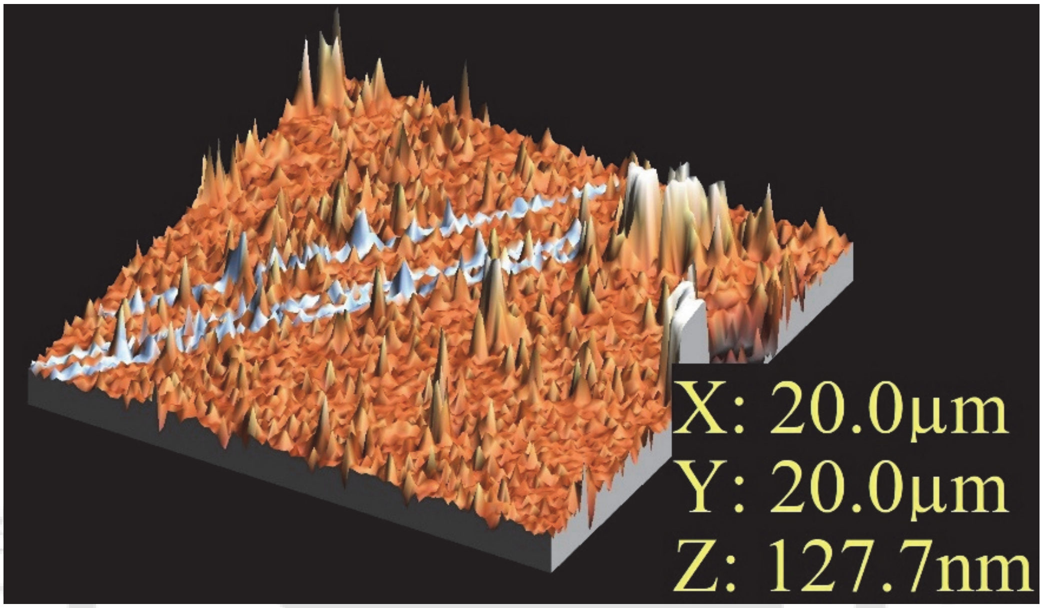

Figure 7.7. The surface profile of modified silica nanoparticles. The average roughness was ~10 nm.

7.4 Application of superhydrophobic silica nanoparticles

The versatile characteristics of silica nanoparticles allow them to be tailored differently according to the final application. In this work, we have utilized the water-repellent characteristics of the modified silica nanoparticles for coating cotton fabric, which was partially hydrophilic. The prepared cotton fabric was later employed to separate fluid-fluid mixtures such as oil-water. Interestingly, the water contact angle on the functionalized silica nanoparticles coated cotton substrate was found to be 161°, which was in the superhydrophobic range. In addition to hydrophobicity, the fabric was

TH-3101_166107009

endowed with a high affinity to oil with a contact angle below 10°. The PFDS silane coated silica NP are attracted towards the hydroxyl groups present on the cotton fabric [214]. Hence, the coated cotton substrate can be applied to separate oil-water mixtures while also providing an environmental-friendly alternative for dealing with oil-spill-related issues.

The SEM analysis of the uncoated and coated cotton was carried out to understand its morphology. Figure 7.8 shows that the uncoated cotton strands are bare and mostly undulated. However, the modified surface has PFDS coated silica nanoparticles attached in a random and close-packed nature. Along with the micron-scale roughness of the cotton fabric surface, nanoscale roughness was introduced by the silica nanoparticles. This hierarchical roughness on the cotton fabric surface was vital for rendering the surface superhydrophobicity. These distinct coated particles will contribute to the formation of porous structures on the surface, enhancing the entrapment of air and decreasing the solid-liquid interfacial area. The magnified images confirmed that the silica nanoparticles were aggregated and likely present at few spaces between the strands of fiber, that is, the inter-fiber region.

TH-3101_166107009

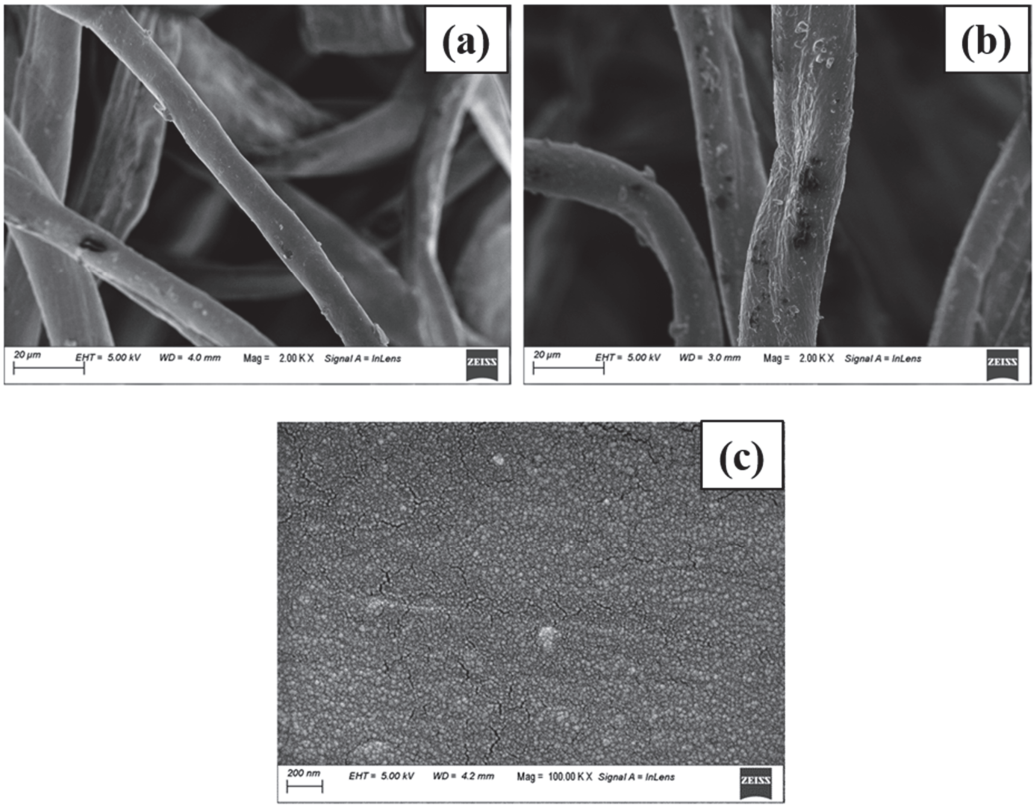

Figure 7.8. FESEM images of pristine (a) and (b) coated cotton fabric. (c) Magnified view of the coated cotton fabric depicting the large-scale coverage of the cotton surface with silica nanoparticles. Top two images have been taken at 2000 X and bottom image has been taken at 100000 X.

7.4.1 Experimental setup for separation of oil from oil-water mixture

A lab-scale experiment was performed to verify the utility of the prepared cotton fibers for the separation of oil-water mixture, wherein 50% oil (dyed with Sudan IV dye) and 50% water (dyed with methylene blue) was mixed in a tube, and both the uncoated, coated cotton substrates were immersed into the mixture for about a minute (Figure 7.9 (a)). As shown in Figure 7.9 (b), the coated cotton substrate displays both

Indian Institute of Technology Guwahati

TH-3101_166107009

superhydrophobic and oleophilic properties and selectively absorbs only oil from the mixture, subsequently turning red in the process. On the other hand, the uncoated cotton in Figure 7.9 (c) displayed both oleophilic and hydrophilic properties. It absorbed both the water and oil fractions and hence had a red and blue color. The presence of hydroxyl and other aliphatic groups on cellulose-fibers allowed the interaction, which facilitated the absorption of both oil and water. Hence, the coated cotton could selectively absorb oil from the oil-water mixture.

In another set of experiments, the oil-water mixture was continuously dropped over the modified cotton fabric. The silica nanoparticles coated substrate was able to retain the water fraction due to its superhydrophobicity while allowing the oil fraction to pass through on account of its oleophilic nature. The schematic and different stages of the process have been shown in Figures 7.10 (a) and (b). The falling water droplets also displayed some hysteresis on the substrate later due to the setup's geometry and the fact that they were now resting upon the oil-drenched cotton fabric.

In order to highlight the water-repellent property of the substrate, a water droplet was deposited on a coated substrate, and a high-resolution camera was used to measure the contact angle as part of the goniometer setup (Figure 7.10 (c). The presence of the corrugated surface due to the inherent roughness of the cotton fabric and that imparted due to the modified silica coating allowed the water droplet to remain in a Cassie-Baxter state of wetting. The trapped air pockets limited the solid-liquid interfacial contact and did not allow the water to wet the surface.

TH-3101_166107009

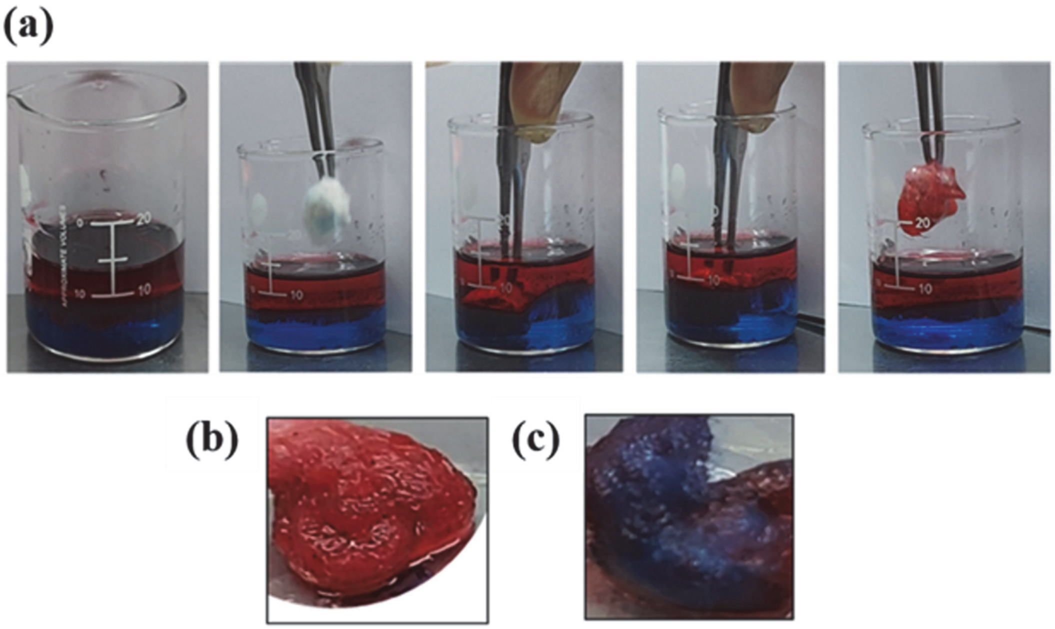

Coated cotton Un-coated cotton

Indian Institute of Technology Guwahati

Figure 7.9. (a) Experiments performed to display the oleophilic and superhydrophobic characteristics of the coated substrate. Uncoated and coated substrates were immersed in a bath. The coated cotton fabric particularly adsorbed oil, while the uncoated adsorbed both oil and water. (b) and (c) Show the results of coated and uncoated cotton fabric.

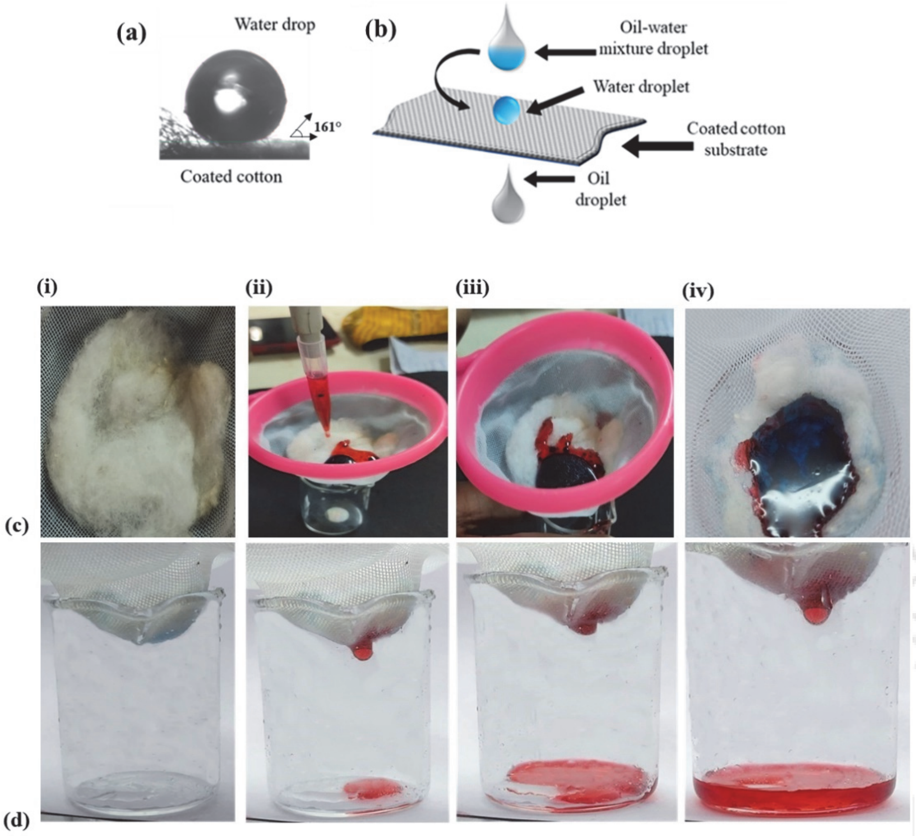

Figure 7.10. (a) Optical micrograph of the superhydrophobic silica nanoparticles coated cotton fabric. (b) Schematic of the oil-water separation process in presence of coated cotton substrate. (c) Snapshots of the process wherein mixture droplets of oil and water were continuously poured over the coated substrate.

The separation efficiency after 1st cycle was observed to be 98.6%, depicted in Figure 7.11. Further, to understand the reusability of the coated fabrics, the contaminated cotton was washed with alcohol and water to remove the absorbed oil. After that, it was dried at 80 °C for 30 min and then reused for the second cycle and observed that the same fabric could be reused for 40 cycles. The coated fabrics could retain their property even after the 40th cycle, as the separation efficiency at the 40th cycle was 97.3%.

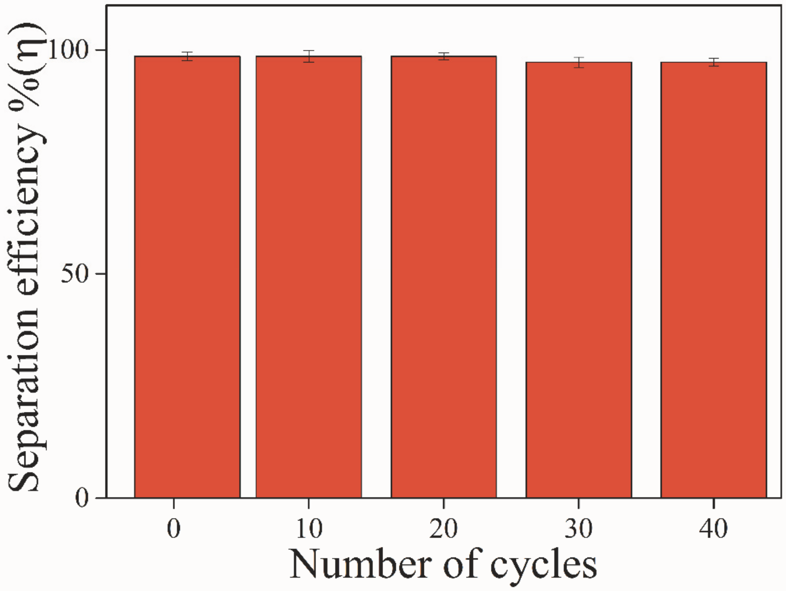

Figure 7.11. The separation efficiency of coated cotton fabrics.

Additional experiments were performed to understand whether the presence of harsh conditions would adversely affect the properties of the coating. The functionalized silica nanoparticles coated cotton substrate was immersed for 24 h in different solutions such as 1 M HCl, 1 M NaOH, and 1 M NaCl. After that, the substrate was allowed to dry at room temperature and further measured for its contact angle by employing a goniometer. The results obtained are depicted in Figure 7.12. The substrate's superhydrophobicity did not alter much, even after exposing the coated cotton surfaces to different environments. In the case of 1M HCl solution, the contact angle was found to be ~160° . While, for other systems, the angle was slightly less (contact angle ~150°) due to the presence of excess salt ions, which might have hindered any electrostatic interactions between the substrate and coating or the hydroxyl groups in the solution, which may interact with the uncovered sites of cotton fabric.

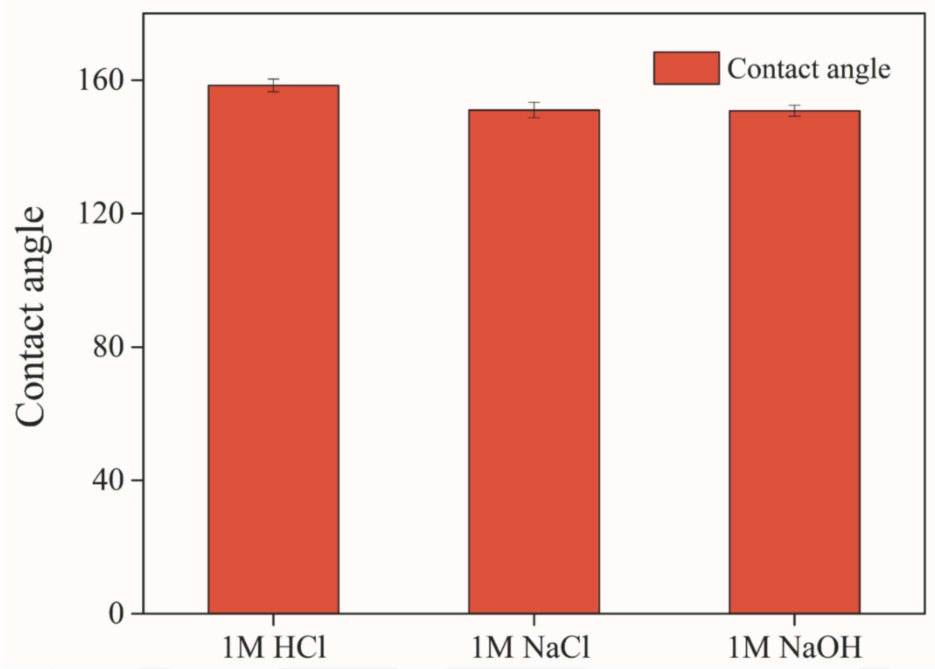

Figure 7.12. Effect of various solutions on the hydrophobicity of the coated substrate.

7.5 Summary

In this work, the bio-char obtained from the slow pyrolysis of RH under CO_2 environment has been utilized to produce silica nanoparticles. RH was pyrolyzed at three different temperatures (300, 500, and 700 °C). The obtained bio-char was subjected to different pH conditions (pH 3, 5, 7 and 9), and the respective bio-char samples were calcined at 610 °C to obtain silica nanoparticles. Bio-char obtained at 500 °C and treated to pH 5 resulted in the lowest average particle size generation.

The silica nanoparticles were modified with different silanes to impart hydrophobicity. The fluro-alkane groups belonging to PFDS reacted with silica nanoparticles and made them superhydrophobic, as indicated by the water contact angle of 158°. The superhydrophobic silica nanoparticles were coated on cotton fabric. A different set of experiments were performed wherein the silica nanoparticles coated substrate were either immersed in or exposed to drops of the oil-water mixture. The unmodified cotton fabric absorbed both oil and water due to hydroxyl and other aliphatic groups on its surface. However, the coated cotton fabric demonstrated water repellant properties while absorbing oil and passing through it. Hence, this work established a proof-of-concept for targeting oil-water separation applications.

Indian Institute of Technology Guwahati

TH-3101_166107009

CHAPTER VIII

Conclusions and scope for future work

The overall conclusion of the thesis

Scope for future work

TH-3101_166107009

भारतीय प्रौद्योगिकी संस्थान गुवाहाटी • Indian Institute of Technology Guwahati •

Chapter VIII

Conclusions and future scope

This chapter sums up the entire work of this thesis based on the initial characterization of the biomass, the conversion processes, and a detailed investigation of the obtained products. This chapter also highlights the avenues for future research in this area.

8.1 Overall conclusions

This thesis proposes an alternative route for utilization of an agricultural residue, RH, and discusses the methodology of slow pyrolysis, under two different environments, for effective conversion of biomass to value-added products. The entire thermochemical process has been optimized with the help of RSM. The main process variables identified, i.e. pyrolysis temperature, holding time, and gas flowrate, are tuned to obtain maximum amounts of bio-oil and bio-char. Bio-oil is a potential energy supplement as indicated by the various physico-chemical characteristics, which also reveals that it confirms the ASTM standards of burner fuel. Further upgradation of the bio-oil utilizing bio-char as an in-situ catalyst or additives improves its overall thermochemical profile. Bio-char is a versatile material that can be tailored accordingly to suit different applications. Its utility as a catalyst for bio-oil upgradation, an adsorbent for pollutant removal, and a feedstock for the generation of silica nanoparticles have been documented in this thesis. Experimental investigations regarding its formation under two different environments and at various temperatures aid in understanding its formation mechanism. It was pretreated with different pH solutions and thereafter

TH-3101_166107009

subjected to high temperatures under limited/no oxygen supply, which led to the generation of silica nanoparticles. The silica nanoparticles obtained were of different dimensions. They were functionalized and subsequently utilized in a membrane for demonstrating a proof-of-concept methodology for an oil-water separation application.

In a nutshell, this thesis delves into the various aspects of RH pyrolytic products: synthesis, characterization, up-gradation and application, and highlights the effectiveness of slow pyrolysis technique for effective thermochemical conversion of the biomass. The different objectives of the thesis have been briefly summarized below.

The initial characterization of RH revealed that it has negligible sulfur content, lower moisture content, higher calorific value, and higher lignocellulosic content (~60%) as compared to other biomasses (Table 1.1). Also, the inherent higher silica content of RH makes it a viable source for the production of pure silica. Therefore, RH was considered an ideal raw material for the production of bio-oil, bio-char and silica NP. In order to utilize the RH for bio-oil production, the slow pyrolysis process under an inert environment (N_2) was optimized using a CCD design-based RSM technique. The optimum conditions for the three major process variables were 427 °C, 0.8 L/min and 45 min to achieve a maximum bio-oil yield of 35.5%. The characterization of bio-oil yield revealed that it had higher water content and lower calorific value. Therefore, solvent extraction was undertaken using hexane, ethyl acetate, and acetone. The extracted or upgraded bio-oil was thoroughly characterized, and the obtained results showed improved properties compared to initial bio-oil. The compositional analysis of upgraded bio-oil revealed a mixture of acids, esters, phenols, and aromatics.

TH-3101_166107009

The characterization of biomass under the CO_2 environment revealed that compared to N_2, higher degradation was observed in the CO_2 environment. The optimization tool used for this study was RSM with CCD model. This tool aided in identifying the optimum operating conditions for slow pyrolysis and they were found to be 551 °C, 1.1 L/min, and 53 min in order to produce the maximum bio-oil yield of 31.7%. The bio-oil obtained was further upgraded via catalytic pyrolysis using the produced bio-char as a catalyst. To improve the characteristics of the obtained bio-oil, catalytic upgradation was employed using bio-adsorbent at three different proportions (25, 33 and 50 wt%). The compositional analysis of upgraded bio-oil revealed that the addition of catalysts decreased the formation of furans and esters and increased the percentage of phenols and aromatics. The upgraded bio-oil was further systematically characterized, which revealed improved pH, water content, and other parameters. Thus, it was observed that the bio-char generated could be used as an effective catalyst for bio-oil up-gradation.

Bio-char was also produced during pyrolysis, and extensive experimental analysis of its formation under two different reaction environments was carried out along with the generation of bio-oil. The results revealed that the bio-char yield obtained under CO_2 (45.6%) environment was higher than the N_2 (43%), but the carbon content% was higher in the case of N_2 environment (45.3%). The physico-chemical characterization revealed that bio-char under CO_2 environment had higher BET surface area and porosity as the CO_2 gets filled into the pores and reacts to form carbon monoxide. This implied that the bio-char obtained under CO_2 environment could be used as an adsorbent and the one under N_2 environment could be used as a soil conditioner. Hence, pyrolysis could be performed under different environments based on the targeted application.

In order to highlight the effectiveness of the bio-char as an adsorbent, a study was performed to remove ranitidine from its aqueous solution. The bio-char's initial characterization revealed that the highest BET surface area was obtained when the pyrolysis temperature was 500 °C (52.4 m^2/g). Further, the bio-char was activated in an alkaline medium (KOH) which enhanced the BET surface area to 440 m^2/g. The adsorption kinetics revealed that the adsorption process followed a pseudo-second-order model. The Langmuir adsorption isotherm model best represented the experimental data. pH played an important role in the adsorption, and basic pH favored the adsorption process, wherein the adsorbent and the drug were oppositely charged. Adsorption of 50 ppm ranitidine on the activated bio-char ($ARHB_{500}$) at pH 9 resulted in the removal of 88.3% reactant when 100 mg adsorbent dosage was provided. The maximum adsorption capacity was found to be 65.8 mg/g.

The role of bio-char as a feedstock for the generation of functional silica nanoparticles has also been discussed. The bio-char produced under a reactive environment under different pyrolysis temperatures was subjected to varying pH conditions (3,5,7 and 9) enroute towards generating silica nanoparticles. The silica nanoparticles generated had an average particle size < 50 nm, with varying zeta potential values. To modify their surface properties, the silica nanoparticles of the smallest dimensions were further treated with different silanes. The characterization revealed that the modified silica nanoparticles had both superhydrophobic and oleophilic characteristics. The superhydrophobic silica nanoparticles were coated on a cotton substrate. The fabric was further characterized, and it displayed significant water-repelling characteristics. The coated cotton was then utilized for selectively absorbing oil from an oil-water mixture.

8.2 Future scope of the work

To summarize, the findings of this work provided insights with respect to the characterization of RH, optimization of the slow pyrolysis process for the production of different valuables employing RSM with CCD design. This thesis can be a reference for future research concerning generation of value-added products from RH, however, further investigations concerning various aspects of this thesis can be carried out. Few of them has been highlighted as:

- Other feedstocks can be utilized for generation of value-added products under RSM optimized conditions and difference with RH can be analyzed.
- The application of upgraded bio-oil obtained under both N_2 and CO_2 environment into real field can be studied.
- The application of bio-char obtained under N_2 environment as soil conditioners into real field can be studied.
- Catalytic pyrolysis can be performed similar conditions in an optimized pyrolysis operation, and the economic viability of catalyst and catalyst-free techniques with respect to rice husk utilization can be realized.
- Functional silica nanoparticles based natural sorbents can be utilized for performing oil/water separation application involving different oils and other different ambient environment conditions.

TH-3101_166107009

भारतीय प्रौद्योगिकी संस्थान गुवाहाटी • Indian Institute of Technology Guwahati •

References

भारतीय प्रौद्योगिकी संस्थान गुवाहाटी • Indian Institute of Technology Guwahati •

भारतीय प्रौद्योगिकी संस्थान गुवाहाटी • Indian Institute of Technology Guwahati •

References

[1] Charles Rajesh Kumar J, Majid MA. Renewable energy for sustainable development in India: Current status, future prospects, challenges, employment, and investment opportunities. Energy Sustain Soc 2020;10:1–36. https://doi.org/10.1186/S13705-019-0232-1/TABLES/37.

[2] Sang Y, Karayaka HB, Yan Y, Yilmaz N, Souders D. 1.18 Ocean (Marine) Energy. Compr Energy Syst 2018;1–5:733–69. https://doi.org/10.1016/B978-0-12-809597-3.00120-6.

[3] Devi LP, Palaniappan S. A study on energy use for excavation and transport of soil during building construction. J Clean Prod 2017;164:543–56. https://doi.org/10.1016/J.JCLEPRO.2017.06.208.

[4] Thakur S, Bhattacharjee M, Dasmahapatra AK, Bandyopadhyay D. Acoustic Wave Catalyzed Urea Detection Utilizing a Pulsatile Microdroplet Sensor. ACS Sustain Chem Eng 2019;7:12069–82. https://doi.org/10.1021/ACSSUSCHEMENG.9B01123/SUPPL_FILE/SC9B01123_SI_005.MPG.

[5] Palencia M, Lerma TA, Garcés V, Mora MA, Martínez JM, Palencia SL. Eco-friendly chemical transformations. Eco-Friendly Funct Polym 2021:155–65. https://doi.org/10.1016/B978-0-12-821842-6.00027-0.

[6] Waldron KW. Bioalcohol Production. Cambridge : Woodhead Publishing Limited; 2010.

[7] Balat M. Potential alternatives to edible oils for biodiesel production – A review of current work. Energy Convers Manag 2011;52:1479–92. https://doi.org/10.1016/J.ENCONMAN.2010.10.011.

[8] Speight JG, editor. The Biofuels Handbook 2011. https://doi.org/10.1039/9781849731027.

[9] Renewables successfully driving down carbon emissions in Europe — European Environment Agency n.d. https://www.eea.europa.eu/highlights/renewables-

successfully-driving-down-carbon (accessed September 7, 2021).

[10] Subject: Scheme to Support Promotion Of Biomass Based Cogeneration In Sugar Mills And Other Industries In The Country (Up To March 2020) 2018.

[11] Chakraborty S, Aggarwal V, Mukherjee D, Andras K. Biomass to biofuel: a review on production technology. Asia-Pacific J Chem Eng 2012;7:S254–62. https://doi.org/10.1002/APJ.1642.

[12] Dickerson T, Soria J. Catalytic Fast Pyrolysis: A Review. Energies 2013, Vol 6, Pages 514-538 2013;6:514–38. https://doi.org/10.3390/EN6010514.

[13] Borugadda VB, Goud V V. Biodiesel production from renewable feedstocks: Status and opportunities. Renew Sustain Energy Rev 2012;16:4763–84. https://doi.org/10.1016/J.RSER.2012.04.010.

[14] Sims REH, Mabee W, Saddler JN, Taylor M. An overview of second generation biofuel technologies. Bioresour Technol 2010;101:1570–80. https://doi.org/10.1016/J.BIORTECH.2009.11.046.

[15] Deshmukh S, Kumar R, Bala K. Microalgae biodiesel: A review on oil extraction, fatty acid composition, properties and effect on engine performance and emissions. Fuel Process Technol 2019;191:232–47. https://doi.org/10.1016/J.FUPROC.2019.03.013.

[16] Branco-Vieira M, Mata TM, Martins AA, Freitas MAV, Caetano NS. Economic analysis of microalgae biodiesel production in a small-scale facility. Energy Reports 2020;6:325–32. https://doi.org/10.1016/J.EGYR.2020.11.156.

[17] Das S, Goud V V. RSM-optimized slow pyrolysis of rice husk for bio-oil production and its upgradation. Energy 2021:120161. https://doi.org/10.1016/j.energy.2021.120161.

[18] Pattiya A. 1 - Fast pyrolysis. Direct Thermochem. Liq. Energy Appl., Elsevier; 2018, p. 3–28. https://doi.org/10.1016/B978-0-08-101029-7.00001-1.

[19] Brassard P, Godbout S, Lévesque V, Palacios JH, Raghavan V, Ahmed A, et al. Biochar for soil amendment. Char Carbon Mater Deriv from Biomass Prod

Charact Appl 2019:109–46. https://doi.org/10.1016/B978-0-12-814893-8.00004-3.

[20] Akintola AT, Akinlabi ET, Masebinu SO. Biochar as an Adsorbent: A Short Overview. Green Energy Technol 2020:399–422. https://doi.org/10.1007/978-3-030-38032-8_19.

[21] Nunes LJR, De Oliveira Matias JC, Da Silva Catalão JP. Applications for Torrefied Biomass. Torrefaction Biomass Energy Appl 2018:203–14. https://doi.org/10.1016/B978-0-12-809462-4.00011-0.

[22] Wimalasiri VK, Weerathunga HU, Kottegoda N, Karunaratne V. Silica Based Superhydrophobic Nanocoatings for Natural Rubber Surfaces. J Nanomater 2017;2017. https://doi.org/10.1155/2017/2102467.

[23] Cao L, Jones AK, Sikka VK, Wu J, Gao D. Anti-Icing superhydrophobic coatings. Langmuir 2009;25:12444–8. https://doi.org/10.1021/LA902882B/SUPPL_FILE/LA902882B_SI_001.PDF.

[24] Mi HY, Jing X, Huang HX, Peng XF, Turng LS. Superhydrophobic Graphene/Cellulose/Silica Aerogel with Hierarchical Structure as Superabsorbers for High Efficiency Selective Oil Absorption and Recovery. Ind Eng Chem Res 2018;57:1745–55. https://doi.org/10.1021/ACS.IECR.7B04388/SUPPL_FILE/IE7B04388_SI_003.MP4.

[25] Anukam A, Berghel J. Biomass Pretreatment and Characterization: A Review. Biotechnol Appl Biomass 2020. https://doi.org/10.5772/INTECHOPEN.93607.

[26] Lim JS, Abdul Manan Z, Wan Alwi SR, Hashim H. A review on utilisation of biomass from rice industry as a source of renewable energy. Renew Sustain Energy Rev 2012;16:3084–94. https://doi.org/10.1016/J.RSER.2012.02.051.

[27] Hu X, Gholizadeh M. Biomass pyrolysis: A review of the process development and challenges from initial researches up to the commercialisation stage. J Energy Chem 2019;39:109–43. https://doi.org/10.1016/J.JECHEM.2019.01.024.

[28] Verma D, Fortunati E, Jain S, Zhang X. Biomass, biopolymer-based materials, and bioenergy: Construction, biomedical, and other industrial applications. Biomass, Biopolym Mater Bioenergy Constr Biomed Other Ind Appl 2019:1–532. https://doi.org/10.1016/C2017-0-00839-X.

[29] Hongzhang Chen, Lan Wang. Biochemical Conversion - an overview. Technol Biochem Convers Biomass 2017;1:1–10.

[30] Wu S, Wang Z, Yang H, Zhang H, Xiao R. The applicability of catalytic esterified biomass-pyrolysis-oil surrogates in diesel engine. Fuel Process Technol 2020;198:106251. https://doi.org/10.1016/J.FUPROC.2019.106251.

[31] Das S, Goud V V. Characterization of a low-cost adsorbent derived from agro-waste for ranitidine removal. Mater Sci Energy Technol 2020;3:879–88. https://doi.org/10.1016/j.mset.2020.10.009.

[32] Mante OD, Agblevor FA, Oyama ST, McClung R. The influence of recycling non-condensable gases in the fractional catalytic pyrolysis of biomass. Bioresour Technol 2012;111:482–90. https://doi.org/10.1016/J.BIORTECH.2012.02.015.

[33] Cardoen D, Joshi P, Diels L, Sarma PM, Pant D. Agriculture biomass in India: Part 1. Estimation and characterization. Resour Conserv Recycl 2015;102:39–48. https://doi.org/10.1016/J.RESCONREC.2015.06.003.

[34] Bakar RA, Yahya R, Gan SN. Production of High Purity Amorphous Silica from Rice Husk. Procedia Chem 2016;19:189–95. https://doi.org/10.1016/J.PROCHE.2016.03.092.

[35] • Top countries based on production of milled rice | Statista n.d. https://www.statista.com/statistics/255945/top-countries-of-destination-for-us-rice-exports-2011/ (accessed November 12, 2021).

[36] Glushankova I, Ketov A, Krasnovskikh M, Rudakova L, Vaisman I. Rice Hulls as a Renewable Complex Material Resource. Resour 2018, Vol 7, Page 31 2018;7:31. https://doi.org/10.3390/RESOURCES7020031.

[37] Tayyab M, Noman A, Islam W, Waheed S, Arafat Y, Ali F, et al. Bioethanol

TH-3101_166107009

production from lignocellulosic biomass by environment-friendly pretreatment methods: A review. Appl Ecol Environ Res 2018;16:225–49. https://doi.org/10.15666/AEER/1601_225249.

[38] Alternative Perspectives | Waste to Energy: Electricity Generation Through Rice Husk n.d. http://www.perspectives.devalt.org/2021/08/01/waste-to-energy-electricity-generation-through-rice-husk/ (accessed August 5, 2022).

[39] Goodman BA. Utilization of waste straw and husks from rice production: A review. J Bioresour Bioprod 2020;5:143–62. https://doi.org/10.1016/J.JOBAB.2020.07.001.

[40] Zoghlami A, Paës G. Lignocellulosic Biomass: Understanding Recalcitrance and Predicting Hydrolysis. Front Chem 2019;7:874. https://doi.org/10.3389/FCHEM.2019.00874/BIBTEX.

[41] Meng X, Pu Y, Yoo CG, Li M, Bali G, Park DY, et al. An In-Depth Understanding of Biomass Recalcitrance Using Natural Poplar Variants as the Feedstock. ChemSusChem 2017;10:139–50. https://doi.org/10.1002/CSSC.201601303.

[42] Baruah J, Nath BK, Sharma R, Kumar S, Deka RC, Baruah DC, et al. Recent trends in the pretreatment of lignocellulosic biomass for value-added products. Front Energy Res 2018;6:141. https://doi.org/10.3389/FENRG.2018.00141/BIBTEX.

[43] Rezaei H, Yazdanpanah F, Lim JC, Lau A, Sokhansanj S. Woody Feedstock Pretreatments to Enhance Pyrolysis Bio-oil Quality and Produce Transportation Fuel. Biomass Bioenergy - Recent Trends Futur Challenges 2018. https://doi.org/10.5772/INTECHOPEN.81818.

[44] Phanthong P, Guan G, Ma Y, Hao X, Abudula A. Effect of ball milling on the production of nanocellulose using mild acid hydrolysis method. J Taiwan Inst Chem Eng 2016;60:617–22. https://doi.org/10.1016/J.JTICE.2015.11.001.

[45] Le Brech Y, Ghislain T, Leclerc S, Bouroukba M, Delmotte L, Brosse N, et al. Effect of Potassium on the Mechanisms of Biomass Pyrolysis Studied using

Complementary Analytical Techniques. ChemSusChem 2016;9:863–72. https://doi.org/10.1002/CSSC.201501560.

[46] Scott DS, Paterson L, Piskorz J, Radlein D. Pretreatment of poplar wood for fast pyrolysis: rate of cation removal. J Anal Appl Pyrolysis 2001;57:169–76. https://doi.org/10.1016/S0165-2370(00)00108-X.

[47] Cai J, Rahman MM, Zhang S, Sarker M, Zhang X, Zhang Y, et al. Review on Aging of Bio-Oil from Biomass Pyrolysis and Strategy to Slowing Aging. Energy & Fuels 2021;35:11665–92. https://doi.org/10.1021/ACS.ENERGYFUELS.1C01214.

[48] Ong HC, Chen WH, Singh Y, Gan YY, Chen CY, Show PL. A state-of-the-art review on thermochemical conversion of biomass for biofuel production: A TG-FTIR approach. Energy Convers Manag 2020;209:112634. https://doi.org/10.1016/J.ENCONMAN.2020.112634.

[49] Yu IKM, Chen H, Abeln F, Auta H, Fan J, Budarin VL, et al. Chemicals from lignocellulosic biomass: A critical comparison between biochemical, microwave and thermochemical conversion methods. Https://DoiOrg/101080/1064338920201753632 2020;51:1479–532. https://doi.org/10.1080/10643389.2020.1753632.

[50] Teter SA, Sutton KB, Emme B. Enzymatic processes and enzyme development in biorefining. Adv Biorefineries Biomass Waste Supply Chain Exploit 2014:199–233. https://doi.org/10.1533/9780857097385.1.199.

[51] Demirbas A. Combustion of Biomass. Http://DxDoiOrg/101080/009083190957694 2007;29:549–61. https://doi.org/10.1080/009083190957694.

[52] Kirubakaran V, Sivaramakrishnan V, Nalini R, Sekar T, Premalatha M, Subramanian P. A review on gasification of biomass. Renew Sustain Energy Rev 2009;13:179–86. https://doi.org/10.1016/J.RSER.2007.07.001.

[53] Girods P, Dufour A, Rogaume Y, Rogaume C, Zoulalian A. Comparison of gasification and pyrolysis of thermal pre-treated wood board waste. J Anal Appl

Pyrolysis 2009;85:171–83. https://doi.org/10.1016/J.JAAP.2008.11.014.

[54] Hu X, Gholizadeh M. Biomass pyrolysis: A review of the process development and challenges from initial researches up to the commercialisation stage. J Energy Chem 2019;39:109–43. https://doi.org/10.1016/J.JECHEM.2019.01.024.

[55] Zaman CZ, Pal K, Yehye WA, SureshSagadevan, Shah ST, Adebisi GA, et al. Pyrolysis: A Sustainable Way to Generate Energy from Waste. Pyrolysis 2017. https://doi.org/10.5772/INTECHOPEN.69036.

[56] Zhang H, Xiao R, Wang D, He G, Shao S, Zhang J, et al. Biomass fast pyrolysis in a fluidized bed reactor under N 2, CO 2, CO, CH 4 and H 2 atmospheres. Bioresour Technol 2011;102:4258–64. https://doi.org/10.1016/j.biortech.2010.12.075.

[57] Kończak M, Oleszczuk P. Co-pyrolysis of sewage sludge and biomass in carbon dioxide as a carrier gas affects the total and leachable metals in biochars. J Hazard Mater 2020;400:123144. https://doi.org/10.1016/J.JHAZMAT.2020.123144.

[58] Balagurumurthy B, Srivastava V, Vinit, Kumar J, Biswas B, Singh R, et al. Value addition to rice straw through pyrolysis in hydrogen and nitrogen environments. Bioresour Technol 2015;188:273–9. https://doi.org/10.1016/J.BIORTECH.2015.01.027.

[59] Fau G, Gascoin N, Gillard P, Steelant J. Methane pyrolysis: Literature survey and comparisons of available data for use in numerical simulations. J Anal Appl Pyrolysis 2013;104:1–9. https://doi.org/10.1016/J.JAAP.2013.04.006.

[60] Leng E, He B, Chen J, Liao G, Ma Y, Zhang F, et al. Prediction of three-phase product distribution and bio-oil heating value of biomass fast pyrolysis based on machine learning. Energy 2021;236:121401. https://doi.org/10.1016/J.ENERGY.2021.121401.

[61] Banks SW, Bridgwater A V. Catalytic fast pyrolysis for improved liquid quality. Handb Biofuels Prod Process Technol Second Ed 2016:391–429.

https://doi.org/10.1016/B978-0-08-100455-5.00014-X.

[62] Lyu G, Wu S, Zhang H. Estimation and comparison of bio-oil components from different pyrolysis conditions. Front Energy Res 2015;3:28. https://doi.org/10.3389/FENRG.2015.00028/ABSTRACT.

[63] Benés M, Bilbao R, Santos JM, Alves Melo J, Wisniewski A, Fonts I. Hydrodeoxygenation of Lignocellulosic Fast Pyrolysis Bio-Oil: Characterization of the Products and Effect of the Catalyst Loading Ratio. Energy and Fuels 2019;33:4272–86. https://doi.org/10.1021/ACS.ENERGYFUELS.9B00265/SUPPL_FILE/EF9B00265_SI_001.PDF.

[64] Garba MU, Musa U, Olugbenga AG, Mohammad YS, Yahaya M, Ibrahim AA. Catalytic upgrading of bio-oil from bagasse: Thermogravimetric analysis and fixed bed pyrolysis. Beni-Suef Univ J Basic Appl Sci 2018;7:776–81. https://doi.org/10.1016/J.BJBAS.2018.11.004.

[65] Kabakcı SB, Hacıbektaşoğlu Ş. Catalytic Pyrolysis of Biomass. Pyrolysis, IntechOpen; 2017. https://doi.org/10.5772/67569.

[66] Mohan D, Pittman CU, Steele PH. Pyrolysis of wood/biomass for bio-oil: a critical review. Energy & Fuels 2006;20:848–89.

[67] Do Minh T, Song J, Deb A, Cha L, Srivastava V, Sillanpää M. Biochar based catalysts for the abatement of emerging pollutants: A review. Chem Eng J 2020;394:124856. https://doi.org/10.1016/J.CEJ.2020.124856.

[68] Li A, Liu HL, Wang H, Xu H Bin, Jin LF, Liu JL, et al. Effects of temperature and heating rate on the characteristics of molded Bio-Char. BioResources 2016;11:3259–74. https://doi.org/10.15376/BIORES.11.2.3259-3274.

[69] Manyà JJ. Pyrolysis for Biochar Purposes: A Review to Establish Current Knowledge Gaps and Research Needs. Environ Sci Technol 2012;46:7939–54. https://doi.org/10.1021/es301029g.

[70] Rawat J, Saxena J, Sanwal P. Biochar: A Sustainable Approach for Improving

TH-3101_166107009

Plant Growth and Soil Properties. Biochar - An Imp Amend Soil Environ 2019. https://doi.org/10.5772/INTECHOPEN.82151.

[71] Gholizadeh M, Hu X, Liu Q. Progress of using biochar as a catalyst in thermal conversion of biomass. Rev Chem Eng 2021;37:229–58. https://doi.org/10.1515/REVCE-2018-0070.

[72] Basu P. Biomass gasification, pyrolysis and torrefaction: Practical design and theory. Biomass Gasification, Pyrolysis Torrefaction Pract Des Theory 2018:1–564. https://doi.org/10.1016/C2016-0-04056-1.

[73] Moreira R, Orsini R, Moreira Vaz J, Penteado C, et al. Production of Biochar, Bio-Oil and Synthesis Gas from Cashew Nut Shell by Slow Pyrolysis Waste and Biomass Valorization 2017; 8; 217-224. https://doi.org/10.1007/s12649-016-9569-2.

[74] Uddin MN, Daud WMAW, Abbas HF. Effects of pyrolysis parameters on hydrogen formations from biomass: a review. RSC Adv 2014;4:10467. https://doi.org/10.1039/c3ra43972k.

[75] Strezov V, Evans TJ, Hayman C. Thermal conversion of elephant grass (Pennisetum purpureum Schum) to bio-gas, bio-oil and charcoal. Bioresour Technol 2008;99:8394–9. https://doi.org/10.1016/J.BIORTECH.2008.02.039.

[76] Dasappa S, Paul P, Mukunda H, Rajan N, Sridhar G, Sridhar H. Biomass gasification technology - a route to meet energy needs. Current Science 2004; 87; 908-916. http://www.jstor.org/stable/24109394.

[77] He M, Xiao B, Liu S, Hu Z, Guo X, Luo S, et al. Syngas production from pyrolysis of municipal solid waste (MSW) with dolomite as downstream catalysts. J Anal Appl Pyrolysis 2010;87:181–7. https://doi.org/10.1016/J.JAAP.2009.11.005.

[78] Capodaglio AG, Bolognesi S. Ecofuel feedstocks and their prospects. Adv Eco-Fuels a Sustain Environ 2019:15–51. https://doi.org/10.1016/B978-0-08-102728-8.00002-4.

[79] Wang W, Martin JC, Fan X, Han A, Luo Z, Sun L. Silica Nanoparticles and Frameworks from Rice Husk Biomass. ACS Appl Mater Interfaces 2012;4:977–81. https://doi.org/10.1021/AM201619U.

[80] Lohan SK, Jat HS, Yadav AK, Sidhu HS, Jat ML, Choudhary M, et al. Burning issues of paddy residue management in north-west states of India. Renew Sustain Energy Rev 2018;81:693–706. https://doi.org/10.1016/J.RSER.2017.08.057.

[81] Bodie AR, Micciche AC, Atungulu GG, Rothrock MJ, Ricke SC. Current Trends of Rice Milling Byproducts for Agricultural Applications and Alternative Food Production Systems. Front Sustain Food Syst 2019;3:47. https://doi.org/10.3389/FSUFS.2019.00047/BIBTEX.

[82] National Air Quality Index n.d. https://app.cpcbccr.com/AQI_India/ (accessed November 16, 2021).

[83] Irmak S. Biomass as Raw Material for Production of High-Value Products. Biomass Vol Estim Valorization Energy 2017. https://doi.org/10.5772/65507

[84] Cen K, Zhang J, Ma Z, Chen D, Zhou J, Ma H. Investigation of the relevance between biomass pyrolysis polygeneration and washing pretreatment under different severities: Water, dilute acid solution and aqueous phase bio-oil. Bioresource Technology 2019; 278; 26-33. https://doi.org/10.1016/j.biortech.2019.01.048.

[85] Kumagai S, Matsuno R, Grause G, Kameda T, Yoshioka T. Enhancement of bio-oil production via pyrolysis of wood biomass by pretreatment with H 2 SO 4. Bioresour Technol 2015. https://doi.org/10.1016/j.biortech.2014.09.146.

[86] Zhang L, Yang Z, Li S, Wang X, Lin R. Comparative study on the two-step pyrolysis of different lignocellulosic biomass: Effects of components. J Anal Appl Pyrolysis 2020;152:104966. https://doi.org/10.1016/J.JAAP.2020.104966.

[87] Zhang L, Yang Z, Liu J, Li D, Li S, Wang X, et al. Comparative study on the one-step and two-step pyrolysis of lignocellulosic biomass: Effects of two-step pyrolysis on improving product quality. Int J Energy Res 2021;45:20219–31. https://doi.org/10.1002/ER.7104.

[88] Zhang B, Yang B, Wu S, Guo W, Zhang J, Wu Z, et al. Effect of torrefaction pretreatment on the fast pyrolysis behavior of biomass: Product distribution and kinetic analysis on spruce-pin-fir sawdust. J Anal Appl Pyrolysis 2021;158:105259. https://doi.org/10.1016/J.JAAP.2021.105259.

[89] Biswas B, Pandey N, Bisht Y, Singh R, Kumar J, Bhaskar T. Pyrolysis of agricultural biomass residues: Comparative study of corn cob, wheat straw, rice straw and rice husk. Bioresour Technol 2017;237:57–63. https://doi.org/10.1016/J.BIORTECH.2017.02.046.

[90] Lin J, Cheng S. Catalytic pyrolysis of crofton weed: Comparison of their pyrolysis product and preliminary economic analysis. Environ Prog Sustain Energy 2021:e13742. https://doi.org/10.1002/EP.13742.

[91] Casoni AI, Gutierrez V, García JM, Cabada S, Acevedo A, Volpe MA. Pyrolytic coproduction of bio-char and upgraded bio-oils from abundant agro-industrial wastes. Brazilian J Chem Eng 2021 2021:1–10. https://doi.org/10.1007/S43153-021-00167-6.

[92] Lin J, Zhang Q, Xia H, Cheng S. Effect of pyrolysis temperature on pyrolysis of pine saw dust and application of bio-char. Int J Environ Sci Technol 2021:1–8. https://doi.org/10.1007/S13762-021-03159-8/FIGURES/4.

[93] Kumar M, Rai D, Bhardwaj G, Upadhyay SN, Mishra PK. Pyrolysis of peanut shell: Kinetic analysis and optimization of thermal degradation process. Ind Crops Prod 2021;174:114128. https://doi.org/10.1016/J.INDCROP.2021.114128.

[94] Tripathi M, Bhatnagar A, Mubarak NM, Sahu JN, Ganesan P. RSM optimization of microwave pyrolysis parameters to produce OPS char with high yield and large BET surface area. Fuel 2020;277:118184. https://doi.org/10.1016/J.FUEL.2020.118184.

[95] Boubacar Laougé Z, Çığgın AS, Merdun H. Optimization and characterization of bio-oil from fast pyrolysis of Pearl Millet and Sida cordifolia L. by using response surface methodology. Fuel 2020;274:117842.

https://doi.org/10.1016/J.FUEL.2020.117842.

[96] Pilon G, Lavoie JM. Pyrolysis of switchgrass (Panicum virgatum L.) at low temperatures within N2 and CO2 environments: Product yield study. ACS Sustain Chem Eng 2013;1:198–204. https://doi.org/10.1021/sc300098e.

[97] Mo L, Dai H, Feng L, Liu B, Li X, Chen Y, et al. In-situ catalytic pyrolysis upgradation of microalgae into hydrocarbon rich bio-oil: Effects of nitrogen and carbon dioxide environment. Bioresour Technol 2020;314:123758. https://doi.org/10.1016/j.biortech.2020.123758.

[98] Biswas B, Singh R, Kumar J, Singh R, Gupta P, Krishna BB, et al. Pyrolysis behavior of rice straw under carbon dioxide for production of bio-oil. Renew Energy 2018;129:686–94.

[99] Biswas B, Krishna BB, Singh R, Kumar J, Bhaskar T. Slow pyrolysis of pine wood: Effect of CO 2 and N 2 atmosphere. Journal of Energy and Environemntal Sustainability. 2016; 2, 7-12.

[100] Lin BJ, Chen WH. Sugarcane bagasse pyrolysis in a carbon dioxide atmosphere with conventional and microwave-assisted heating. Front Energy Res 2015;3:4. https://doi.org/10.3389/FENRG.2015.00004/BIBTEX.

[101] Du S, Gamliel DP, Valla JA, Bollas GM. The effect of ZSM-5 catalyst support in catalytic pyrolysis of biomass and compounds abundant in pyrolysis bio-oils. J Anal Appl Pyrolysis 2016;122:7–12. https://doi.org/10.1016/J.JAAP.2016.11.002.

[102] Zheng Y, Wang F, Yang X, Huang Y, Liu C, Zheng Z, et al. Study on aromatics production via the catalytic pyrolysis vapor upgrading of biomass using metal-loaded modified H-ZSM-5. J Anal Appl Pyrolysis 2017;126:169–79. https://doi.org/10.1016/J.JAAP.2017.06.011.

[103] Ren S, Lei H, Wang L, Bu Q, Chen S, Wu J, et al. Biofuel production and kinetics analysis for microwave pyrolysis of Douglas fir sawdust pellet. J Anal Appl Pyrolysis 2012;94:163–9. https://doi.org/10.1016/J.JAAP.2011.12.004.

[104] Chan KY, Van Zwieten L, Meszaros I, Downie A, Joseph S. Agronomic values of greenwaste biochar as a soil amendment. Aust J Soil Res 2007;45:629–34. https://doi.org/10.1071/SR07109.

[105] Shen Y, Zhao P, Shao Q, Ma D, Takahashi F, Yoshikawa K. In-situ catalytic conversion of tar using rice husk char-supported nickel-iron catalysts for biomass pyrolysis/gasification. Appl Catal B Environ 2014;152–153:140–51. https://doi.org/10.1016/J.APCATB.2014.01.032.

[106] Nguyen HKD, Pham V V., Do HT. Preparation of Ni/biochar Catalyst for Hydrotreating of Bio-Oil from Microalgae Biomass. Catal Letters 2016;146:2381–91. https://doi.org/10.1007/S10562-016-1873-8/TABLES/5.

[107] Su Y, Liu L, Zhang S, Xu D, Du H, Cheng Y, et al. A green route for pyrolysis poly-generation of typical high ash biomass, rice husk: Effects on simultaneous production of carbonic oxide-rich syngas, phenol-abundant bio-oil, high-adsorption porous carbon and amorphous silicon dioxide. Bioresour Technol 2020;295:122243. https://doi.org/10.1016/J.BIORTECH.2019.122243.

[108] Gao J, Liu Y, Li X, Yang M, Wang J, Chen Y. A promising and cost-effective biochar adsorbent derived from jujube pit for the removal of Pb(II) from aqueous solution. Sci Reports 2020 101 2020;10:1–13. https://doi.org/10.1038/s41598-020-64191-1.

[109] Removal of hexavalent chromium by biochar derived from Azadirachta indica leaves: Batch and column studies | Elsevier Enhanced Reader n.d. https://reader.elsevier.com/reader/sd/pii/S0045653521020701?token=1BE1D94333FEF8715536590B10B3FF7AD0476301F55A36CD90BA4CE1C2BB30C9329CA766FCEB2D920DF1577DB04DBABA&originRegion=eu-west-1&originCreation=20211109122352 (accessed November 9, 2021).

[110] Barman SR, Das P, Mukhopadhayay A. Biochar from waste Sterculia foetida and its application as adsorbent for the treatment of PAH compounds: Batch and optimization. Fuel 2021;306:121623. https://doi.org/10.1016/J.FUEL.2021.121623.

TH-3101_166107009

[111] Khoshnood Motlagh E, Asasian-Kolur N, Sharifian S. A comparative study on rice husk and rice straw as bioresources for production of carbonaceous adsorbent and silica. Biomass Convers Biorefinery 2020:1–10. https://doi.org/10.1007/S13399-020-01145-7/TABLES/1.

[112] Park JY, Mo Gu Y, Park SY, Hwang ET, Sang B-I, Chun J, et al. Two-Stage Continuous Process for the Extraction of Silica from Rice Husk Using Attrition Ball Milling and Alkaline Leaching Methods. Sustainability; 2021; 13, https://doi.org/10.3390/SU13137350.

[113] Ajeel SA, Sukkar KA, Zedin NK. Extraction of high purity amorphous silica from rice husk by chemical process. IOP Conf Ser Mater Sci Eng 2020;881:012096. https://doi.org/10.1088/1757-899X/881/1/012096.

[114] El-Sakhawy M, Adel AM, Diab MA, Al-Shemy M. Facile methods for the preparation of micro- and mesoporous amorphous silica from rice husk. Biomass Convers Biorefinery 2020:1–10. https://doi.org/10.1007/S13399-020-01112-2/FIGURES/5.

[115] Kim S, Park JY, Gu YM, Jang I-S, Park H, Kyeong D, et al. Eco-friendly and facile synthesis of size-controlled spherical silica particles from rice husk. Nanoscale Adv 2021. https://doi.org/10.1039/D1NA00668A.

[116] Ellis-Terrell C, Wei R, McKnight R, Huang X, Lin K. Thermal stability of superhydrophobic and oleophobic silica nanoparticle spray coating. Mater Today Commun 2020;25:101370. https://doi.org/10.1016/J.MTCOMM.2020.101370.

[117] Song H, Tang M, Lei X, Feng Z, Cheng F. Preparation of Ultrafine Fly Ash-Based Superhydrophobic Composite Coating and Its Application to Foam Concrete. Polymers; 2020; 12. https://doi.org/10.3390/POLYM12102187.

[118] Li J, Yan L, Zhao Y, Zha F, Wang Q, Lei Z. One-step fabrication of robust fabrics with both-faced superhydrophobicity for the separation and capture of oil from water. Phys Chem Chem Phys 2015;17:6451–7. https://doi.org/10.1039/C5CP00154D.

TH-3101_166107009

[119] Jang EH, Pack SP, Kim I, Chung S. A systematic study of hexavalent chromium adsorption and removal from aqueous environments using chemically functionalized amorphous and mesoporous silica nanoparticles. Sci Reports 2020 101 2020;10:1–20. https://doi.org/10.1038/s41598-020-61505-1.

[120] Vanithakumari SC, Jena G, Sofia S, Thinaharan C, George RP, Philip J. Fabrication of superhydrophobic titanium surfaces with superior antibacterial properties using graphene oxide and silanized silica nanoparticles. Surf Coatings Technol 2020;400:126074. https://doi.org/10.1016/J.SURFCOAT.2020.126074.

[121] Li J, Ding Z, Li Y, Miao J, Wang W, Nundlall K, et al. Reactive oxygen species-sensitive thioketal-linked mesoporous silica nanoparticles as drug carrier for effective antibacterial activity. Mater Des 2020;195:109021. https://doi.org/10.1016/J.MATDES.2020.109021.

[122] Silica from rice husk ash. Nat India 2011. https://doi.org/10.1038/NINDIA.2011.168.

[123] Singh S, Chakraborty JP, Mondal MK. Pyrolysis of torrefied biomass: Optimization of process parameters using response surface methodology, characterization, and comparison of properties of pyrolysis oil from raw biomass. J Clean Prod 2020;272:122517. https://doi.org/10.1016/J.JCLEPRO.2020.122517.

[124] Te WZ, Muhanin KNM, Chu YM, Selvarajoo A, Singh A, Ahmed SF, et al. Optimization of Pyrolysis Parameters for Production of Biochar From Banana Peels: Evaluation of Biochar Application on the Growth of Ipomoea aquatica. Front Energy Res 2021;8:406. https://doi.org/10.3389/FENRG.2020.637846/BIBTEX.

[125] Optimization of Bark Fast Pyrolysis for the Production of Phenol-Rich Bio-oil | Ren | BioResources n.d. https://ojs.cnr.ncsu.edu/index.php/BioRes/article/view/BioRes_08_4_Ren_Bark_Fast_Pyrolysis/2438 (accessed August 2, 2022).

[126] Hafeez S, Pallari E, Manos G, Constantinou A. Catalytic Conversion and Chemical Recovery. Plast to Energy Fuel, Chem Sustain Implic 2019:147–72. https://doi.org/10.1016/B978-0-12-813140-4.00006-6.

[127] Sluiter A, Hames B, Ruiz R, Scarlata C, Sluiter J, Templeton D, et al. Determination of structural carbohydrates and lignin in biomass. Lab Anal Proced 2008;1617:1–16.

[128] A. Sluiter R. Ruiz, C. Scarlata, J. Sluiter, and D. Templeton BH. Determination of Ash in Biomass Laboratory Analytical Procedure Lab Anal Proceed 2008.

[129] Denny K. S. Ng, Raymond R. Tan, Dominic C. Y. Foo, Mahmoud M. El-Halwagi. Process Design Strategies for Biomass Conversion Systems.Wiley; 2016.

[130] Antony J. Full Factorial Designs. Des Exp Eng Sci 2014:63–85. https://doi.org/10.1016/B978-0-08-099417-8.00006-7.

[131] Regmi P, Garcia Moscoso JL, Kumar S, Cao X, Mao J, Schafran G. Removal of copper and cadmium from aqueous solution using switchgrass biochar produced via hydrothermal carbonization process. J Environ Manage 2012;109:61–9. https://doi.org/10.1016/j.jenvman.2012.04.047.

[132] Bojić D, Momčilović M, Milenković D, Mitrović J, Banković P, Velinov N, et al. Characterization of a low cost Lagenaria vulgaris based carbon for ranitidine removal from aqueous solutions. Arab J Chem 2017;10:956–64. https://doi.org/10.1016/j.arabjc.2014.12.018.

[133] Álvarez-Torrellas S, Muñoz M, Zazo JA, Casas JA, García J. Synthesis of high surface area carbon adsorbents prepared from pine sawdust-Onopordum acanthium L. for nonsteroidal anti-inflammatory drugs adsorption. J Environ Manage 2016;183:294–305. https://doi.org/10.1016/j.jenvman.2016.08.077.

[134] Baccar R, Sarrà M, Bouzid J, Feki M, Blánquez P. Removal of pharmaceutical compounds by activated carbon prepared from agricultural by-product. Chem Eng J 2012;211–212:310–7. https://doi.org/10.1016/j.cej.2012.09.099.

[135] Vijayaraghavan K, Padmesh TVN, Palanivelu K, Velan M. Biosorption of nickel(II) ions onto Sargassum wightii: Application of two-parameter and three-parameter isotherm models. J Hazard Mater 2006;133:304–8. https://doi.org/10.1016/j.jhazmat.2005.10.016.

[136] TAN H, WANG S. Experimental study of the effect of acid-washing pretreatment on biomass pyrolysis. Journal of Fuel Chemistry and Technology. 2009;37;668–72. https://doi.org/10.1016/S1872-5813(10)60014-X.

[137] Naik S, Goud V V., Rout PK, Jacobson K, Dalai AK. Characterization of Canadian biomass for alternative renewable fuel. Renewable energy; 2010; 38; 1624-1631.https://doi.org/ 10.1016/j.renene.2009.08.033

[138] Uzunov I, Uzunova S, Angelova D, Gigova A. Effects of the pyrolysis process on the oil sorption capacity of rice husk. J Anal Appl Pyrolysis 2012;98:166–76.

[139] Ali M, Tindyala MA. Thermoanalytical studies on acid-treated rice husk and production of some silicon based ceramics from carbonised rice husk. J Asian Ceram Soc 2015;3:311–6. https://doi.org/10.1016/j.jascer.2015.06.003.

[140] Pütün E, Uzun BB, Pütün AE. Fixed-bed catalytic pyrolysis of cotton-seed cake: effects of pyrolysis temperature, natural zeolite content and sweeping gas flow rate. Bioresour Technol 2006;97:701–10.

[141] Onay O. Influence of pyrolysis temperature and heating rate on the production of bio-oil and char from safflower seed by pyrolysis, using a well-swept fixed-bed reactor. Fuel Process Technol 2007;88:523–31.

[142] Sun XF, Xu F, Sun RC, Fowler P, Baird MS. Characteristics of degraded cellulose obtained from steam-exploded wheat straw. Carbohydr Res 2005;340:97–106.

[143] de Souza Lima MM, Borsali R. Rodlike cellulose microcrystals: structure, properties, and applications. Macromol Rapid Commun 2004;25:771–87.

[144] Roy R, Ray S. Effect of various pretreatments on energy recovery from waste biomass. Energy Sources, Part A Recover Util Environ Eff 2019.

https://doi.org/10.1080/15567036.2019.1680767.

[145] Zhang S, Zhu S, Zhang H, Chen T, Xiong Y. Catalytic fast pyrolysis of rice husk: Effect of coupling leaching with torrefaction pretreatment. J Anal Appl Pyrolysis 2018;133:91–6. https://doi.org/10.1016/J.JAAP.2018.04.016.

[146] Cen K, Chen D, Wang J, Cai Y, Wang L. Effects of Water Washing and Torrefaction Pretreatments on Corn Stalk Pyrolysis: Combined Study Using TG-FTIR and a Fixed Bed Reactor. Energy & Fuels; 2016; 30;12;10627-10634. https://doi.org/10.1021/acs.energyfuels.6b02813.

[147] Açikalin K, Karaca F, Bolat E. Pyrolysis of pistachio shell: Effects of pyrolysis conditions and analysis of products. Fuel 2012;95:169–77. https://doi.org/10.1016/j.fuel.2011.09.037.

[148] Mushtaq F, Abdullah TAT, Mat R, Ani FN. Optimization and characterization of bio-oil produced by microwave assisted pyrolysis of oil palm shell waste biomass with microwave absorber. Bioresour Technol 2015;190:442–50. https://doi.org/10.1016/j.biortech.2015.02.055.

[149] Pütün AE, Özcan A, Pütün E. Pyrolysis of hazelnut shells in a fixed-bed tubular reactor: yields and structural analysis of bio-oil. J Anal Appl Pyrolysis 1999;52:33–49.

[150] Zhang S, Chen T, Xiong Y. Effect of washing pretreatment with aqueous fraction of bio-oil on pyrolysis characteristic of rice husk and preparation of amorphous silica. Waste and Biomass Valorization 2018;9:861–9.

[151] Dhanavath KN, Bankupalli S, Sugali CS, Perupogu V, V Nandury S, Bhargava S, et al. Optimization of process parameters for slow pyrolysis of neem press seed cake for liquid and char production. J Environ Chem Eng 2019;7. https://doi.org/10.1016/j.jece.2019.102905.

[152] Liu RH, Shen CJ, Wu HJ, Deng CJ, Liu SY. Characterisation of bio-oil from fast pyrolysis of rice husk in a fluidised bed reactor. J Energy Inst 2011;84:73–9. https://doi.org/10.1179/014426011X12968328625397.

[153] Kader EA, Hussein HS, Hussien NH, Diwani G El. Effect of Extractive Solvents on Bio-oil Production From Microalgae via Hydrothermal Liquefaction. Chemical and Process Engineering Research. 2015;38.

[154] Özçimen D, Karaosmanoğlu F. Production and characterization of bio-oil and biochar from rapeseed cake. Renew Energy 2004;29:779–87. https://doi.org/10.1016/j.renene.2003.09.006.

[155] IR Spectrum Table & Chart | Sigma-Aldrich n.d. https://www.sigmaaldrich.com/technical-documents/articles/biology/ir-spectrum-table.html (accessed June 20, 2020).

[156] Pütün AE, Özean A, Pütün E. Pyrolysis of hazelnut shells in a fixed-bed tubular reactor: Yields and structural analysis of bio-oil. J Anal Appl Pyrolysis 1999;52:33–49. https://doi.org/10.1016/S0165-2370(99)00044-3.

[157] How to Identify Carbonyls, Alkenes, Alkynes, and Aromatics in the IR Spectrum n.d. https://www.dummies.com/education/science/chemistry/how-to-identify-carbonyls-alkenes-alkynes-and-aromatics-in-the-ir-spectrum/ (accessed June 20, 2020).

[158] Dibutyl phthalate - SpectraBase n.d. https://spectrabase.com/compound/EHIlsyqcXGf#L16hYvm4Krd (accessed June 19, 2020).

[159] 4-Ethyl-2-methoxyphenol | C9H12O2 - PubChem n.d. https://pubchem.ncbi.nlm.nih.gov/compound/4-Ethyl-2-methoxyphenol#section=FTIR-Spectra (accessed June 19, 2020).

[160] Phthalic acid - FTIR Spectrum - SpectraBase n.d. https://spectrabase.com/spectrum/DG0j01hu3E5 (accessed June 20, 2020).

[161] Abnisa F, Mohd W, Wan A, Sahu JN. Optimization and Modeling of Bio-oil Production from Palm Shell by Pyrolysis Using Response Surface Methodology. Int Conf Appl Energy (ICAE 2010) 2010:1465–75.

[162] Wannapeera J, Worasuwannarak N, Pipatmanomai S. Product yields and

characteristics of rice husk, rice straw and corncob during fast pyrolysis in a drop-tube/fixed-bed reactor. Songklanakarin Journal of Science and Technology 2008; 30; 393-404.

[163] Yang H, Yan R, Chen H, Lee DH, Zheng C. Characteristics of hemicellulose, cellulose and lignin pyrolysis. Fuel 2007;86:1781–8. https://doi.org/10.1016/j.fuel.2006.12.013.

[164] Zanatta ER, Reinehr TO, Awadallak JA, Kleinübing SJ, dos Santos JBO, Bariccatti RA, et al. Kinetic studies of thermal decomposition of sugarcane bagasse and cassava bagasse. J Therm Anal Calorim 2016;125:437–45.

[165] Speight JG. Upgrading by Gasification. Heavy Oil Recover. Upgrad., Elsevier; 2019, p. 559–614. https://doi.org/10.1016/b978-0-12-813025-4.00013-1.

[166] Kadlimatti HM, Raj Mohan B, Saidutta MB. Bio-oil from microwave assisted pyrolysis of food waste-optimization using response surface methodology. Biomass and Bioenergy 2019;123:25–33. https://doi.org/10.1016/J.BIOMBIOE.2019.01.014.

[167] Shen Y, Ma D, Ge X. CO2-looping in biomass pyrolysis or gasification. Sustain Energy Fuels 2017;1:1700–29. https://doi.org/10.1039/c7se00279c.

[168] Pilon G, Lavoie J-M. Biomass char production at low severity conditions under CO 2 and N 2 environments. Energy and Sustainability; 2011;143. https://doi.org/10.2495/ESUS11.

[169] Borugadda VB, Goud V V. Synthesis of Waste Cooking Oil Epoxide as a Bio-Lubricant Base Stock: Characterization and Optimization Study. J Bioprocess Eng Biorefinery 2014;3:57–72. https://doi.org/10.1166/jbeb.2014.1077.

[170] Cronje KJ, Chetty K, Carsky M, Sahu JN, Meikap BC. Desalination. Elsevier Scientific Pub. Co; 2011.

[171] Cheng F, Li X. Preparation and Application of Biochar-Based Catalysts for Biofuel Production. Catal 2018, Vol 8, Page 346 2018;8:346. https://doi.org/10.3390/CATAL8090346.

[172] Doukeh R, Bombos D, Bombos M, Oprescu E-E, Dumitrascu G, Vasilievici G, et al. Catalytic hydrotreating of bio-oil and evaluation of main noxious emissions of gaseous phase. Sci Reports 2021 111 2021;11:1–13. https://doi.org/10.1038/s41598-021-85244-z.

[173] Janković B, Manić N, Stojiljković D. The gaseous products characterization of the pyrolysis process of various agricultural residues using TGA–DSC–MS techniques. J Therm Anal Calorim 2020;139:3091–106. https://doi.org/10.1007/S10973-019-08733-4/FIGURES/9.

[174] Kwon EE, Cho S-H, Kim S. Synergetic Sustainability Enhancement via Utilization of Carbon Dioxide as Carbon Neutral Chemical Feedstock in the Thermo-Chemical Processing of Biomass. Environ Sci Technol 2015;49:5028–34. https://doi.org/10.1021/es505744n.

[175] Kan T, Strezov V, Evans TJ. Lignocellulosic biomass pyrolysis: A review of product properties and effects of pyrolysis parameters. Renew Sustain Energy Rev 2016;57:1126–40. https://doi.org/10.1016/j.rser.2015.12.185.

[176] Yang M, Luo B, Shao J, Zeng K, Zhang X, Yang H, et al. The influence of CO2 on biomass fast pyrolysis at medium temperatures. J Renew Sustain Energy 2018;10:013108. https://doi.org/10.1063/1.5005013.

[177] Yavari S, Malakahmad A, Sapari NB, Yavari S. Sorption properties optimization of agricultural wastes-derived biochars using response surface methodology. Process Saf Environ Prot 2017;109:509–19. https://doi.org/10.1016/j.psep.2017.05.002.

[178] Jamaluddin MA, Ismail K, Mohd Ishak MA, Ab Ghani Z, Abdullah MF, Safian MTU, et al. Microwave-assisted pyrolysis of palm kernel shell: Optimization using response surface methodology (RSM). Renew Energy 2013;55:357–65. https://doi.org/10.1016/j.renene.2012.12.042.

[179] Menya E, Olupot PW, Storz H, Lubwama M, Kiros Y, John MJ. Optimization of pyrolysis conditions for char production from rice husks and its characterization as a precursor for production of activated carbon. Biomass

TH-3101_166107009

Convers Biorefinery 2020;10:57–72. https://doi.org/10.1007/S13399-019-00399-0.

[180] Titiladunayo IF, McDonald AG, Fapetu OP. Effect of temperature on biochar product yield from selected lignocellulosic biomass in a pyrolysis process. Waste and Biomass Valorization 2012;3:311–8. https://doi.org/10.1007/s12649-012-9118-6.

[181] Angin D. Effect of pyrolysis temperature and heating rate on biochar obtained from pyrolysis of safflower seed press cake. Bioresour Technol 2013;128:593–7. https://doi.org/10.1016/j.biortech.2012.10.150.

[182] Lee XJ, Lee LY, Hiew BYZ, Gan S, Thangalazhy-Gopakumar S, Ng HK. Valorisation of oil palm wastes into high yield and energy content biochars via slow pyrolysis: Multivariate process optimisation and combustion kinetic studies. Mater Sci Energy Technol 2020;3:601–10. https://doi.org/10.1016/j.mset.2020.06.006.

[183] Mohammed, I. Y., Abakr, Y. A., Kazi, F. K., Yusuf, S., Alshareef, I., and Chin, S. A , Pyrolysis of Napier Grass in a Fixed Bed Reactor: Effect of Operating Conditions on Product Yields and Characteristic BioResources 2015; 10; 6467-6478.

[184] Yavari S, Malakahmad A, Sapari NB. Effects of production conditions on yield and physicochemical properties of biochars produced from rice husk and oil palm empty fruit bunches. Environ Sci Pollut Res 2016 2318 2016;23:17928–40. https://doi.org/10.1007/S11356-016-6943-3.

[185] Wang Q, Li K, Guo Z, Fang M, Luo Z, Cen K. Effects of CO2 atmosphere on slow pyrolysis of high-ash lignite. Carbon Resour Convers 2018;1:94–103. https://doi.org/10.1016/J.CRCON.2018.04.002.

[186] Tomczyk A, Sokołowska Z, Boguta P. Biochar physicochemical properties: pyrolysis temperature and feedstock kind effects. Rev Environ Sci Biotechnol 2020;19:191–215. https://doi.org/10.1007/s11157-020-09523-3.

[187] Yang M, Luo B, Shao J, Zeng K, Zhang X, Yang H, et al. The influence of CO2

on biomass fast pyrolysis at medium temperatures. J Renew Sustain Energy 2018;10. https://doi.org/10.1063/1.5005013.

[188] Cao X, Harris W. Properties of dairy-manure-derived biochar pertinent to its potential use in remediation. Bioresour Technol 2010;101:5222–8. https://doi.org/10.1016/j.biortech.2010.02.052.

[189] Shinogi Y, Kanri Y. Pyrolysis of plant, animal and human waste: Physical and chemical characterization of the pyrolytic products. Bioresour Technol 2003;90:241–7. https://doi.org/10.1016/S0960-8524(03)00147-0.

[190] Jindo K, Mizumoto H, Sawada Y, Sanchez-Monedero MA, Sonoki T. Physical and chemical characterization of biochars derived from different agricultural residues. Biogeosciences 2014;11:6613–21. https://doi.org/10.5194/bg-11-6613-2014.

[191] Lee JW, Kidder M, Evans BR, Paik S, Buchanan III AC, Garten CT, et al. Characterization of Biochars Produced from Cornstovers for Soil Amendment. Environ Sci Technol 2010;44:7970–4. https://doi.org/10.1021/es101337x.

[192] Claoston N, Samsuri AW, Ahmad Husni MH, Mohd Amran MS. Effects of pyrolysis temperature on the physicochemical properties of empty fruit bunch and rice husk biochars. Waste Manag Res 2014;32:331–9. https://doi.org/10.1177/0734242X14525822.

[193] Shen Y. Rice Husk-Derived Activated Carbons for Adsorption of Phenolic Compounds in Water. Glob Challenges 2018;2:1800043. https://doi.org/10.1002/gch2.201800043.

[194] Sharizal Sirrajudin M, Abdus Salam M, bin Ahmad A, - al, Mardalena M, Syarif S, et al. Characteristics of activated carbon resulted from pyrolysis of the oil palm fronds powder. IOP Conf Ser Mater Sci Eng 2018;309:012072. https://doi.org/10.1088/1757-899X/309/1/012072.

[195] Shen Z, Zhang Y, McMillan O, Jin F, Al-Tabbaa A. Characteristics and mechanisms of nickel adsorption on biochars produced from wheat straw pellets and rice husk. Environ Sci Pollut Res 2017;24:12809–19.

https://doi.org/10.1007/s11356-017-8847-2.

[196] Paethanom A, Yoshikawa K. Influence of Pyrolysis Temperature on Rice Husk Char Characteristics and Its Tar Adsorption Capability. Energies 2012;5:4941–51. https://doi.org/10.3390/en5124941.

[197] Zhang Y, Ma Z, Zhang Q, Wang J, Ma Q, Yang Y, et al. Comparison of the Physicochemical Characteristics of Bio-char Pyrolyzed from Moso Bamboo and Rice Husk with Different Pyrolysis Temperatures. BioResources 2017;12:4652–69.

[198] Kawamoto H. Lignin pyrolysis reactions. J Wood Sci 2017;63:117–32. https://doi.org/10.1007/s10086-016-1606-z.

[199] Mondal S, Sinha K, Aikat K, Halder G. Adsorption thermodynamics and kinetics of ranitidine hydrochloride onto superheated steam activated carbon derived from mung bean husk. J Environ Chem Eng 2015;3:187–95. https://doi.org/10.1016/j.jece.2014.11.021.

[200] Cardoso NF, Pinto RB, Lima EC, Calvete T, Amavisca C V., Royer B, et al. Removal of remazol black B textile dye from aqueous solution by adsorption. Desalination 2011;269:92–103. https://doi.org/10.1016/j.desal.2010.10.047.

[201] Mojoudi N, Mirghaffari N, Soleimani M, Shariatmadari H, Belver C, Bedia J. Phenol adsorption on high microporous activated carbons prepared from oily sludge: equilibrium, kinetic and thermodynamic studies. Sci Rep 2019;9:1–12. https://doi.org/10.1038/s41598-019-55794-4.

[202] Karagöz S, Tay T, Ucar S, Erdem M. Activated carbons from waste biomass by sulfuric acid activation and their use on methylene blue adsorption. Bioresour Technol 2008;99:6214–22. https://doi.org/10.1016/j.biortech.2007.12.019.

[203] Fierro V, Torné-Fernández V, Montané D, Celzard A. Adsorption of phenol onto activated carbons having different textural and surface properties. Microporous Mesoporous Mater 2008;111:276–84. https://doi.org/10.1016/j.micromeso.2007.08.002.

[204] Kumari P, Meena A. Application of enzyme-mediated cellulose nanofibers from lemongrass waste for the controlled release of anticancer drugs. Environ Sci Pollut Res 2020:1–13. https://doi.org/10.1007/s11356-020-08358-3.

[205] Nayak PP, Datta AK. Synthesis of SiO 2-Nanoparticles from Rice Husk Ash and its Comparison with Commercial Amorphous Silica through Material Characterization n.d. https://doi.org/10.1007/s12633-020-00509-y.

[206] Gu S, Zhou J, Yu C, Luo Z, Wang Q, Shi Z. A novel two-staged thermal synthesis method of generating nanosilica from rice husk via pre-pyrolysis combined with calcination. Ind Crops Prod 2015;65:1–6. https://doi.org/10.1016/J.INDCROP.2014.11.045.

[207] Jesionowski T, Krysztafkiewicz A. Preparation of the hydrophilic/hydrophobic silica particles. Colloids Surfaces A Physicochem Eng Asp 2002;207:49–58. https://doi.org/10.1016/S0927-7757(02)00137-1.

[208] Raval N, Maheshwari R, Kalyane D, Youngren-Ortiz SR, Chougule MB, Tekade RK. Importance of Physicochemical Characterization of Nanoparticles in Pharmaceutical Product Development. Basic Fundam Drug Deliv 2019:369–400. https://doi.org/10.1016/B978-0-12-817909-3.00010-8.

[209] Du Plessis PW, Ojumu T V., Petrik LF. Waste Minimization Protocols for the Process of Synthesizing Zeolites from South African Coal Fly Ash. Mater 2013, Vol 6, Pages 1688-1703 2013;6:1688–703. https://doi.org/10.3390/MA6051688.

[210] Liu J, Janjua ZA, Roe M, Xu F, Turnbull B, Choi KS, et al. Super-Hydrophobic/Icephobic Coatings Based on Silica Nanoparticles Modified by Self-Assembled Monolayers. Nanomater 2016, Vol 6, Page 232 2016;6:232. https://doi.org/10.3390/NANO6120232.

[211] Kraka E, Cremer D. Characterization of CF Bonds with Multiple-Bond Character: Bond Lengths, Stretching Force Constants, and Bond Dissociation Energies. ChemPhysChem 2009;10:686–98. https://doi.org/10.1002/CPHC.200800699.

TH-3101_166107009

[212] Li J, Yan L, Zhao Y, Zha F, Wang Q, Lei Z. One-step fabrication of robust fabrics with both-faced superhydrophobicity for the separation and capture of oil from water. Phys Chem Chem Phys 2015;17:6451–7. https://doi.org/10.1039/C5CP00154D.

[213] Li C, Zhang J, Han J, Yao B. A numerical solution to the effects of surface roughness on water–coal contact angle. Sci Reports 2021 111 2021;11:1–12. https://doi.org/10.1038/s41598-020-80729-9.

[214] Gadhave R V., Dhawale P V., Sorate CS. Surface Modification of Cellulose with Silanes for Adhesive Application: Review. Open J Polym Chem 2021;11:11–30. https://doi.org/10.4236/OJPCHEM.2021.112002.

Indian Institute of Technology Guwahati

List of Publications

भारतीय प्रौद्योगिकी संस्थान गुवाहाटी • Indian Institute of Technology Guwahati •

List of Publications

Journal Publications:

[1] **S. Das**, V. V. Goud, Characterization of a low-cost adsorbent derived from agro-waste for ranitidine removal, Mater. Sci. Energy Technol. 3 (2020) 879–888. https://doi.org/10.1016/j.mset.2020.10.009.

[2] **S. Das**, V. V. Goud, RSM-optimized slow pyrolysis of rice husk for bio-oil production and its upgradation, Energy. (2021) 120161. https://doi.org/10.1016/j.energy.2021.120161.

[3] **S. Das**, V. V. Goud, Bio-char assisted upgradation of pyrolytic oil via slow pyrolysis of rice husk under a carbon-dioxide environment, Biomass Conversion and Biorefinery (2022) https://doi.org/10.1007/s13399-022-03482-1.

[4] **S. Das**, V. V. Goud, Optimal production of bio-char with maximum carbon content under both inert (N2) and reactive (CO2) environment employing RSM, Environmental Progress & Sustainable Energy. (2022) https://doi.org/10.1002/ep.13924.

[5] **S. Das**, V. V. Goud, Rice husk derived biogenic silica coated cotton as an effective, sustainable oil-water separation platform. (Submitted)

TH-3101_166107009

Book Chapters:

[1] **S. Das**, A.S. Reshad, N. Bhuyan, D. Sut, P. Tiwari, V. V. Goud, R. Kataki, Utilization of nonedible oilseeds in a biorefinery approach with special emphasis on rubber seeds, Waste Biorefinery. (2020) 311–336. https://doi.org/10.1016/B978-0-12-818228-4.00012-5.

[2] P.G. Suryawanshi, **S. Das**, V.B. Borugadda, V. V Goud, A.K. Dalai, Process Improvements and Techno-Economic Feasibility of Hydrothermal Liquefaction and Pyrolysis of Biomass for Biocrude Oil Production, Biorefinery Altern. Resour. Target. Green Fuels Platf. Chem. (2020) 221–248. https://doi.org/10.1007/978-981-15-1804-1_10.

[3] **S. Das**, N. D. Devi, A. Chaudhuri, V. V. Goud, Renewable fuels recovery from Anaerobic Digestate, Anaerobic Digestate Management : **Submitted**

Conference Presentations:

[1] **S. Das**, V. V. Goud, Utilization of agricultural residue for the production of bio-oil, International Conference on Renewable and Alternate Energy (ICRAE-2018), Assam Science and Technology University, 4-6 December, 2018, Assam.

[2] **S. Das**, V. V. Goud, Co-pyrolysis of agricultural residue and spent algae for the production of bio-oil, International Conference on Advanced Materials, Energy and Environmental Sustainability (ICAMEES-2018), 14-15 December, University of Petroleum and Energy Studies (UPES), Dehradun, India.

[3] **S. Das**, V. V. Goud, Utilization of Agricultural waste for the production of Bio-oil and Bio-char presented, Third ISEES International Conference on Sustainable

Energy and Environmental Challenges (III SEEC-2018), 18-21 December, 2018 IIT, Roorkee, India.

[4] **S. Das**, V. V. Goud, Optimization of slow pyrolysis for the production of bio-oil and its characterization, Reflux (2019), 28-29 September, 2019, IIT Guwahati, India.

[5] **S. Das**, V. V. Goud, Utilization of spent micro algal biomass for the production of bio-oil employing slow pyrolysis process, International Conference on Future Aspects of Sustainable Technologies (FAST-2019), 11-12 November, 2019, CIT Kokrajhar.

Indian Institute of Technology Guwahati